UNIVERSITÉ DE MONTRÉAL

MODEL PREDICTIVE CONTROL OF BUILDING SYSTEMS FOR ENERGY FLEXIBILITY

KUN ZHANG

DÉPARTEMENT DE GÉNIE MÉCANIQUE

ÉCOLE POLYTECHNIQUE DE MONTRÉAL

THÈSE PRÉSENTÉE EN VUE DE L'OBTENTION

DU DIPLÔME DE PHILOSOPHIAE DOCTOR (Ph. D.)

(GÉNIE MÉCANIQUE)

OCTOBRE 2018

UNIVERSITÉ DE MONTRÉAL

ÉCOLE POLYTECHNIQUE DE MONTRÉAL

Cette thèse intitulée :

MODEL PREDICTIVE CONTROL OF BUILDING SYSTEMS FOR ENERGY FLEXIBILITY

présentée par : ZHANG Kun

en vue de l'obtention du diplôme de : Philosophiae Doctor

a été dûment acceptée par le jury d'examen constitué de :

M. CIMMINO Massimo, Ph. D., président

M. KUMMERT Michaël, Ph. D., membre et directeur de recherche

M. ANJOS Miguel F., Ph. D., membre

M. ZMEUREANU Radu G., Ph. D., membre externe

ACKNOWLEDGEMENTS

My greatest thanks go to my supervisor Prof. Michaël Kummert. I am really grateful for your guidance, support, suggestions and invaluable time throughout the different projects in my graduate studies. Thank you for your confidence to let me work within the IEA Annex 67 project and present my work at different conferences and meetings across the world. Those opportunities have broadened my horizons in the research field. Your encouragement, positive feedback and kind personality have made this journey enjoyable.

I wish to extend my gratitude to Prof. Michel Bernier. Thank you for your valuable advice on my work and for giving me the opportunities to work as your teaching assistant through those years. I am also appreciative to Dr. Massimo Cimmino for his recommendation for my future career. The casual talks we had in and outside the office were delightful.

I would like to thank the past and present members of the Bee(r) Lab: Katherine D'Avignon, Benoit Delcroix, Humberto Quintana, Samuel Letellier-Duchesne, Behzad B. Bafrouei, Camille Beurcq, Alex Laferrière, Louis Leroy, Walid Lallam, Adam Neale, Houaida Saidi. Thank you for your help on the technical and nontechnical issues I have encountered. You made the lab life and the time away from home more pleasant.

I also acknowledge the following entities for their funding support: NSERC, SNEBRN, Sumaran, and Stelpro. I could not carry out this research without their generous contributions.

At last, a special thank you to my family and friends for your love and always being there, actually or virtually.

谢谢你们。Merci à tous!

RÉSUMÉ

Les besoins énergétiques des bâtiments contribuent de manière significative à la demande de pointe du réseau électrique. Cependant, les bâtiments, par leur capacité de stockage de l'énergie, peuvent fournir des services de flexibilité énergétique au réseau. La Gestion de la Demande de Puissance (GDP) du bâtiment est considérée comme une solution pratique pour réduire les demandes de pointe du réseau. Cette approche est moins coûteuse et plus écologique que d'utiliser la réserve de puissance ou que d'investir dans de nouvelles infrastructures. La GDP peut également jouer un rôle plus important au niveau de l'équilibrage de charge, lorsque le réseau intègre des sources d'énergie renouvelables, qui sont intermittentes et variables.

Cette thèse étudie le potentiel de flexibilité énergétique des bâtiments vis-à-vis du réseau électrique par le biais de la simulation. Une méthodologie générale pour caractériser la flexibilité énergétique des bâtiments, ainsi qu'un ensemble d'indicateurs sont proposés. La méthodologie est testée sur un modèle détaillé de maison canadienne type, calibré avec des données mensuelles et horaires mesurées. La calibration permet de représenter fidèlement la consommation d'énergie selon les critères de la directive 14 de l'ASHRAE, ainsi que les variations dynamiques des conditions thermiques intérieures, ce qui est nécessaire pour l'étude des stratégies de commande.

Les résultats des simulations, basés sur ce modèle calibré, montrent que la flexibilité énergétique fournie par la masse thermique du bâtiment est importante, même pour les bâtiments résidentiels à faible masse thermique. La quantité d'énergie flexible dépend cependant des conditions météorologiques, de l'heure du jour, de la durée de la GDP et de l'occupation du bâtiment.

La flexibilité énergétique est également fortement liée à la stratégie de commande du système de chauffage et climatisation. Une méthode de contrôle avancée est étudiée : la Commande Prédictive basée sur un Modèle (CPM). Avant d'appliquer cette méthode à la flexibilité énergétique, un cadre général de CPM est proposé. Les erreurs de modélisation, l'estimation de l'état et l'identification des paramètres y sont discutées en détail. Ce cadre est ensuite appliqué à deux types de modèles de contrôleurs différents : un modèle détaillé et un modèle simplifié du bâtiment étudié.

Les résultats montrent que la CPM peut améliorer la flexibilité énergétique par rapport à une stratégie de Commande Basée sur les Règles (CBR). La flexibilité énergétique obtenue par une

CPM avec modèle détaillé est la plus élevée. Cette énergie est deux à trois fois supérieure à celle obtenue par une stratégie CBR, selon l'heure de l'évènement de la GDP. L'énergie flexible obtenue par une MPC avec modèle simplifié est moindre que celle avec modèle détaillé. Mais son coût de calcul est beaucoup moins cher. Il est similaire à celui de la méthode CBR : de l’ordre de quelques secondes. D’autre part, l'effet de rebond des méthodes CPM est plus prononcé, ce qui génère une efficacité flexible inférieure à celle de la stratégie CBR.

ABSTRACT

Energy needs from buildings contribute a large share to the peak demand of the electric grid. Meanwhile, buildings can also provide energy flexibility services to the grid with their related assets, e.g. energy storage. Demand Response (DR) of building systems has been considered a feasible solution to shift loads, or to reduce the peak demands. This approach is less costly and more environmentally-friendly than operating reserve power, or investing in extra power plants. DR can play a more important role for load balancing when the grid integrates with renewable energy sources, which are intermittent and variable.

This thesis investigates the energy flexibility potential in buildings for the grid through simulation studies. A general methodology to characterize the building energy flexibility is proposed along with a set of indicators. The methodology is applied to a detailed building model of a typical Canadian home, which is calibrated with monthly and hourly measured data. The calibration evaluates not only the energy use required by the ASHRAE guideline 14, but also the dynamic indoor conditions, which is important to study control strategies.

Simulation results, based on the calibrated model, show that the energy flexibility provided by the building thermal mass is significant, even for typical Canadian residential buildings with a low thermal mass. The amount of flexible energy however depends on the weather condition, time of day, duration of the DR event and occupancy scenario of the building.

The control strategy of the space conditioning system has also a high impact on the energy flexibility. An advanced control method called Model Predictive Control (MPC) is investigated. Prior to applying the MPC method on energy flexibility study, a general supervisory MPC framework is presented. Common issues associated with modelling errors, state estimation, and parameter identification are discussed in detail. The framework is then applied to two different types of controller models: a detailed model and a simplified model of the studied building respectively.

The MPC method is shown to be able to increase the building flexibility as compared to the Rule-Based Control (RBC) strategy. MPC with the detailed model delivers the highest flexible energy, twice or three times of the RBC method depending on the time of the DR event. MPC with the simplified model presents less flexible energy than that with the detailed model, but its

computation cost is also less expensive, in the same magnitude as the RBC method in seconds. On the other hand, the rebound effect of the MPC methods is more pronounced, resulting in lower flexible efficiency than RBC.

TABLE OF CONTENTS

LIST OF TABLES

LIST OF FIGURES

LIST OF SYMBOLS AND ABBREVIATIONS

Symbols

A, B, C, D, K	State-space representation matrices [-]
C	Thermal capacitance [J/kg-K]
e	Error [-]
E	Energy [kWh]
f	Coefficient factor [-]
J	Objective function value
k	Thermal conductivity [W/m-K]
m	Flowrate [kg/h]
N	Number of measurements [-]
P	Power [kW]
Q	Heat flow rate [W]
R	Thermal resistance [m^2K/W]
t	Time [s]
T	Temperature [°C]
U	Controlled input
U_p	Thermal conductance [W/K]
UA	Heat transfer coefficient [W/K]
W	Uncontrolled inputs
x, X	Inputs
y	Values (simulated or measured)
$\bar{y}$	Average values

Y	Outputs

Greek symbols

α	Coefficient of solar radiation [-]
ρ	Density [kg/m^3]
ε	Effectiveness of heat recovery ventilation system [-]
η	Flexible energy efficiency [-]

Subscripts

a, amb	Ambient
b	Basement
c	Continuous
d	Discrete
dr	Demand response
f	Flexible
g	Ground
ig	Internal gains
$ineq$	Inequality
inf	Infiltration
h	Heating
l	Living room
m	Measurement
min	Minimum

max	Maximum
p	Prediction
rb	Rebound
ref	Reference
s	Sleeping room
sa	Supply air
sg	Solar gains

Abbreviations

ACH	Air Changes per Hour
AIM	Alberta infiltration model
ANN	Artificial Neural Network
ARMA	Autoregressive Moving Average
ARMAX	ARMA with exogenous terms
ARX	Autoregressive with Exogenous terms
ASHRAE	American Society of Heating, Refrigeration and Air-conditioning Engineers
BCVTB	Building Controls Virtual Test Bed
BPS	Building Performance Simulation
CBR	Commande Basée sur les Règles
CCHT	Canadian Centre for Housing Technology
COP	Coefficient of Performance
CPM	Commande Prédictive basée sur un Modèle
CVRMSE	Coefficient of Variation of the Root Mean Squared Error

CWEC	Canadian Weather for Energy Calculation
DR	Demand Response
DHW	Domestic Hot Water
DSM	Demand Side Management
EBC	Energy in Buildings and Communities
ECM	Energy Conservation Measures
EPBD	Energy Performance of Building Directive
FEMP	Federal Energy Management Program
GDP	Gestion de la Demande de Puissance
GPS	Generalized Pattern Search algorithm
HRV	Heat Recovery Ventilator
HVAC	Heating, Ventilation and Air Conditioning
IEA	International Energy Agency
IESO	Independent Electricity System Operator
IoT	Internet of Things
IPMVP	International Performance Measurement and Verification Protocol
ISO	Independent System Operator
KPI	Key Performance Indicators
LEED	Leadership in Energy and Environmental Design
LTE	Laboratoire des technologies de l'énergie
MBE	Mean Bias Error
MPC	Model Predictive Control
M&V	Monitoring and Verification
NMBE	Normalized Mean Bias Error

PID	Proportional-Integral-Derivative
PSO	Particle Swarm Optimization
PV	Photovoltaic
RMSE	Root Mean Squared Error
RBC	Rule-Based Control
RC	Resistance and Capacitance
RES	Renewable Energy Sources
RR	Reset Ratio
SRI	Smart Readiness Indicator
TOU	Time of Use
USGBC	United States Green Building Council
VAV	Variable Air Volume

LIST OF APPENDICES

CHAPTER 1 INTRODUCTION

1.1 Context

The electric grid generally experiences on-peak and off-peak times on a daily basis, which are highly correlated with human activities. The blue curve in Figure 1.1 shows the power demand of Ontario's utility Independent Electricity System Operator (IESO) in four consecutive days from December 27 to December 30, 2017, where two peaks can be observed each day in this winter month (IESO, 2016). This shape of daily demand profile with a morning peak, an afternoon dip, and another evening peak is very typical. When a large amount of generation from photovoltaic (PV) panels adds to the grid on a sunny day, the system curve displays an even more obvious "belly" appearance in the midday and a steep rise after the sunset, portraying the silhouette of a duck. This phenomenon of grid demand profile is also known as "duck curve" (Denholm, O'Connell, Brinkman, & Jorgenson, 2015).

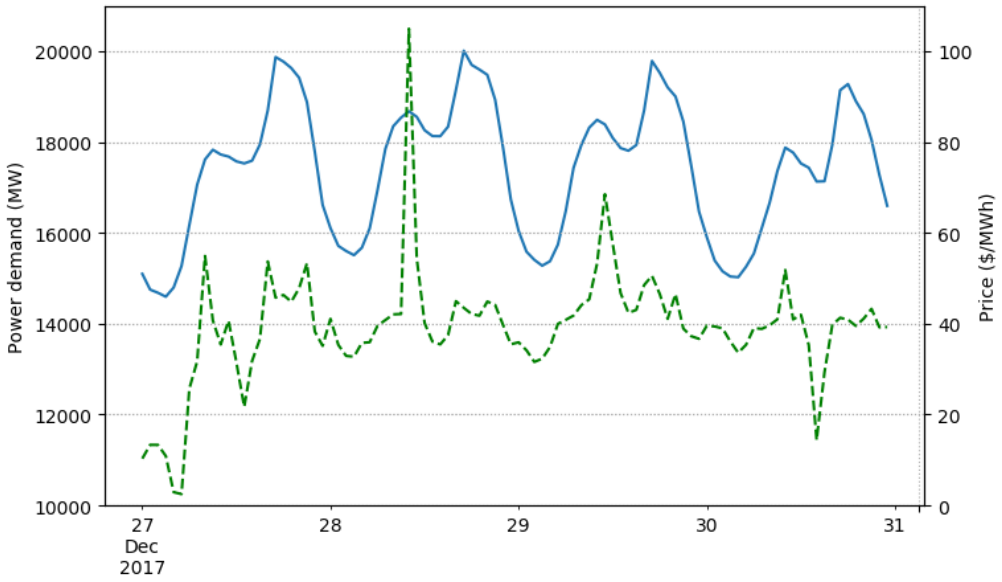

Figure 1.1: IESO daily power demand

The grid also experiences seasonal critical peak periods, i.e. the annual highest peak demand hours. For instance, the critical peak hours for IESO annually occur in summer due to air conditioning loads; while for Hydro-Quebec, the utility company in Quebec, the critical peak hours happen in winter because of space heating demands. Figure 1.2 shows the annual critical

peak durations on January 17 in the year of 2009 for Hydro-Quebec. It can be seen that the highest peak demand occurred in the morning at around 7 AM.

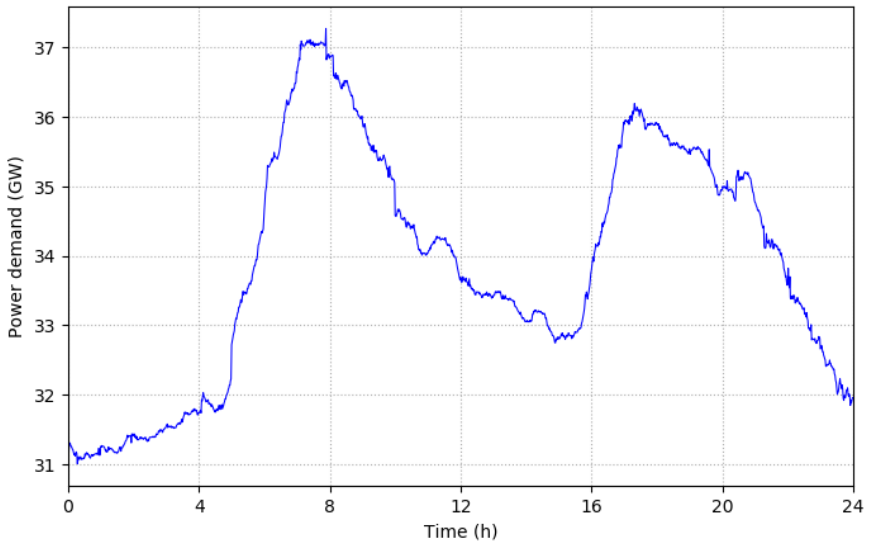

Figure 1.2: Hydro-Quebec seasonal critical peak demand

The grid has traditionally been regulated to control the supply to meet demand variations, where grid reliability or resilience requires balancing demand and supply. Historically, the balancing has been technically achieved from the supply side: operating reserve generators when there is supply shortage; or curtailing generation during oversupply. The last issue has been a growing occurrence for grids integrated with Renewable Energy Sources (RES), for example, for the Californian utility California Independent System Operator (California ISO, 2017) and also for the German grid (Schwarz & Cai, 2017).

Another approach for flattening the demand curve is through Demand Response (DR), where consumers adjust their electricity usage during a certain amount of time in response to grid signals. The signals can be time-based rates, penalties, contracts or other forms of financial tools. Considering the electricity as a commodity, it can be bought and sold like stocks in spot markets. Energy policy researchers have been studying this topic, which is outside of the scope of this work.

DR has been proven less costly and more environment-friendly than operating reserve power or investing in extra plants when the capacity is insufficient for the peak demand (Davito, Tai, & Uhlaner, 2010). It can play a more significant role for the load balancing when the RES are

integrated to the grid, where the variable generation power and dependence on climate conditions of the renewables add more challenges to the grid balance.

On the consumption side, the power demand of Heating, Ventilation, and Air Conditioning (HVAC) systems in buildings contributes significantly to the grid peak power demand. In Ontario, the summer peak demand is dominated by residential air conditioning with almost 22% of the peak demand (Hydro One, 2003). In Quebec, it is estimated that residential electric heating accounts for 30% of the winter peak, with a market share of 70% (Kummert, Leduc, & Moreau, 2011). Buildings can, therefore, play an important role in DR. The magnitude and flexibility of buildings' energy demand can actually become a key asset for DR if well managed (Li, Dane, Finck, & Zeiler, 2017).

DR programs have been successfully implemented in practice to shift the peak power demand of buildings from critical periods to off-peak time (Palensky & Dietrich, 2011). For instance, the utility could turn off heat pumps or electric water heating systems in buildings during peak time through direct load control. In Ontario, a DR program in residential HVAC systems has been promoted through voluntary participation. The device installed in homes receives signals from the grid to cycle down the air conditioner during peak hours. The participants benefit by paying less for on-peak electricity. Hydro-Quebec also tested several experimental DR programs with its employees' homes (Fournier, Leduc, & Sansregret, 2018; Laurencelle & Moreau, 2018).

Besides the "direct control" program discussed above, another "indirect control" approach may be more practical, where buildings can actively respond to grid signals rather than being passively controlled by the grid directly.

With the effort of grid modernization or "smart grid", demand-response buildings can help facilitate and optimize grid operations, resources, and infrastructure. This possibility of demand response of buildings is provided by the temporal elasticity of building energy demand, or more concretely, the energy flexibility of buildings.

The energy flexibility of a building is defined broadly as "the ability to manage its demand and (energy) generation according to its local climate conditions, user needs and energy network requirements" by the Annex 67 of the International Energy Agency (IEA) Energy in Buildings and Communities Programme (EBC) (Jensen, Marszal-Pomianowska, et al., 2017).

The flexibility of buildings is largely contributed by energy storage systems (e.g. thermal mass, hot water tanks, ice storage, phase change materials, battery) or energy generation systems (e.g. photovoltaic panels, solar thermal collectors, wind turbines) in or around buildings, or fuel switch if more than one type of fuel is available to supply the building energy needs.

This new terminology is closely related to more established terms like load shifting or load shedding, but it is a more general concept and can be applied to broader circumstances, especially for future smart grid and intelligent buildings, where two-way communications between the grid and buildings would become a common practice. It can act as a label for buildings similar to the energy performance certificate practice carried out in many countries. A position paper published by the Annex 67 more thoroughly explained the context and functionality of energy flexible buildings (Jensen, Henrik, et al., 2017).

A closely related project called “Smart Readiness Indicator (SRI)” for buildings has been launched by the European Energy Performance of Building Directive (EPBD) since 2017, where flexibility is one of the impact criteria for the smartness of buildings. Based on eight different criteria, a single score is given to the assessed building classifying its smart readiness (Vito NV, 2018). The United States Green Building Council (USGBC) and New Building Institute have also initiated a project called GridOptimal in mid-2018. The two institutes aim at creating a rating system with standardized metrics and guidance for building-grid interactions, somewhat similar to the well-established Leadership in Energy and Environmental Design (LEED) program of USGBC (New Buildings Institute, 2018).

In summary, the new operating conditions (e.g. RES integration, oversupply risk) of the electric grid require novel concepts and methodologies to tackle the associated problems. With the advancement of internet and communication technologies, buildings, with its embedded energy flexibility, can contribute significantly to the process of grid modernization, as well as the indispensable part of the smart grid.

1.2 Objectives

The overall goal of the dissertation is to study the potential of building energy flexibility for the grid through simulation studies. It aims at investigating how the advanced control strategy Model Predictive Control (MPC) can contribute to the flexibility potential which is highly impacted by

the HVAC control method. The thesis further aims at proposing a general methodology with simple indicators to quantify the amount of energy flexibility.

More specifically, the objectives of the work can be summarized into the following items:

- Constructing reliable models of the studied building system in order to apply MPC strategy as modelling is the first part of the proposed control approach;
- Proposing a general MPC framework which works for different purposes including energy flexibility;
- Investigating a general method with universal Key Performance Indicators (KPIs) to quantify the energy flexibility including using different control strategies;
- Applying the defined MPC framework for energy flexibility simulation and quantifying the flexibility potential according to the investigated KPIs.

1.3 Structure

Based on the aforementioned objectives, the structure of the thesis is illustrated in the following diagram.

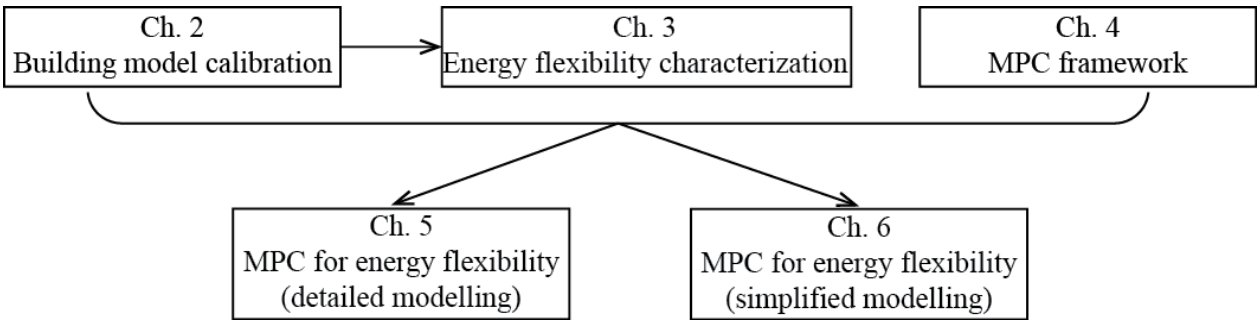

Figure 1.3: Structure of the thesis

Chapter 1 is an overview of the thesis which illustrates the background and objective of the study.

Chapter 2 presents the construction and calibration process for a detailed building model. This simulated building is the basis of the thesis; therefore this chapter is devoted to detailing the modelling and calibrating results. The calibrated model is further used to investigate the general methodology to quantify building energy flexibility and to test the proposed KPIs in Chapter 3. The detailed building model is also employed to identify simplified models in Chapter 5 and used

as the model for MPC in Chapter 6. The arrows in Figure 1.3 visualizes the connections among the chapters.

Based on the calibrated model of Chapter 2, **Chapter 3** illustrates a methodology with KPIs to quantify the energy flexibility of building thermal mass. A brief sensitivity analysis is conducted for the methodology.

Chapter 4 introduces a general supervisory MPC framework which can be regarded as a tutorial for building energy modellers to try MPC strategy on their own modelled system.

Chapter 5 and 6 test two different MPC implementation methods: one uses a simplified building model while the other the calibrated detailed model. The energy flexibility results are reported and analyzed based on these two MPC methods.

Chapter 7 concludes the thesis and provides recommendations for future work.

References and Appendices follow Chapter 7.

1.4 Contributions

The original contributions of this thesis include the following:

- A detailed building model based on measured data has been calibrated, where both yearly results and dynamic characteristics have been analyzed. The calibration method with associated sensitivity analysis could be referenced by other researchers to calibrate their own models.
- A general model predictive control framework applied to buildings has been proposed with detailed and step-by-step guidance. The mathematics and jargons from control theory have been kept to a minimum with examples only for buildings. It is especially beneficial for building mechanical engineers who are not familiar with but intend to understand control theory and applications on building systems. Although this framework has only been applied to a single building in this thesis, it can be extended to more complex building systems such as high-rise buildings or district thermal networks.
- A general method to quantify energy flexibility potential of buildings has been verified and modified metrics have been tested based on a case study. The method and metrics have also been proved to be applicable to MPC strategy.

- A comparative study of two different MPC implementation methods has been conducted. The potential of MPC to facilitate building energy flexibility has been presented and compared with the rule-based control strategy. This simulation study has laid a theoretical foundation for further real-life experiments.

CHAPTER 2 DETAILED BUILDING MODEL

This chapter describes a detailed building model calibrated based on measurements. To apply model predictive control, we first need a mathematical model of the controlled system. Buildings, in our case, can be modelled in different approaches as well as using various software programs. This calibrated model is further used to test the energy flexibility of the case building, as well as to identify simplified building models and apply MPC.

2.1 Introduction

2.1.1 A literature review of calibrated building simulation

Calibrating building models using real-world data such as utility bills has been a practice since the 1980s (Reddy, 2006). The initiation of Demand Side Management (DSM) to reduce the energy consumption of buildings led to utility bill analysis and identification of Energy Conservation Measures (ECMs) for building retrofits. The calibrated simulation was thus adopted as a useful technique for the ECM identification as well as for Monitoring and Verification (M&V).

Calibrated simulation can also be utilized for other purposes, where a review paper summarized six different applications of the approach, including fault detection and diagnosis, load control measures and supervisory control from over 30 papers (Reddy, 2006). The paper discussed the problems of the calibrated simulation, for example, the lack of a generic methodology or procedure for the calibration practice. This review paper is part of the results of the American Society of Heating, Refrigeration and Air-conditioning Engineers (ASHRAE) Research Project 1051 “Procedures for Reconciling Computer-Calculated Results with Measured Energy Data”. Besides the literature review, the research project also proposed a methodology which can be divided into four main steps: gathering data, blind coarse bounded grid search, guided refined search and uncertainty analysis. For the statistical criteria, the research team proposed a goodness-of-fit index based on ASHRAE guideline 14, which was often referenced in the literature for the calibration criteria of results (ASHRAE, 2014). It also discussed in detail about the sensitivity analysis to identify strong and weak parameters based on the Chi-square test (Reddy, Maor, & Panjapornpon, 2007a). After presenting their calibration method, they applied

the method to three case study office buildings: two synthetic and one actual and summarized the lessons learned on how to implement the proposed calibration method (Reddy, Maor, & Panjapornpon, 2007b). A fourth paper from the same project presented the calibration using an analytic optimization approach (Sun & Reddy, 2006).

Following the same idea, a thesis calibrated a mixed-use university building. The principal difference was that the thesis adopted a stochastic Latin Hypercube Sampling method instead of mid-point Latin Hypercube Monte Carlo method proposed in the ASHRAE project (Johnson, 2017).

Another important review paper on calibration was written by Coakley, Raftery, & Keane (2014). They presented a thorough review of approaches used to model development and calibration and commented on the problems and advantages of different methods. Furthermore, they assessed various analytical and statistical tools utilized by practitioners. A similar review paper also presented common calibration methodologies (Fabrizio & Monetti, 2015).

It should be noted that the aforementioned studies discussed building model calibration solely from the perspective of energy use. In other words, only monthly energy use from utility bills or hourly energy data from metering or auditing were used for calibration, without considering the indoor conditions calibration. This approach is in accordance with the purpose of ASHRAE guideline 14, where the calibrated simulation is just one approach to quantify energy and demand savings of buildings. Similarly, most case studies in the literature calibrated only the energy consumption predicted by the building energy models.

Outside of the calibration purpose for energy and demand savings, early studies in the PASSYS project had reported calibration practice with a focus on indoor temperature prediction (Clarke, Strachan, & Pernot, 1993). The pioneered project was intended to show the replicated potential of passive solar techniques based on the calibrated model. Another paper from the project also proposed a method to compare simulation results with measurements using residual analysis (Palomo, Marco, & Madsem, 1997), which were not adopted by the ASHRAE guideline.

A recent study presented both energy and space temperature calibration (Royapoor & Roskilly, 2015). However, only the monthly average temperature calculated from hourly values were compared and the transient phenomenon of temperature variation in a certain zone was not

discussed between the simulation and measurements. Another study also only reported monthly zone temperature error in their calibration study (Coakley, Raftery, & Molloy, 2012).

An evidence-based methodology was proposed for the calibrating process, which recommended that available evidence under clearly defined priorities should be used as the model inputs (Raftery, Keane, & O'Donnell, 2011). To achieve this, a version control programme could be utilized to facilitate and document the iterative process. The method adopted in our study is based on existing evidence and documents for model inputs selections, which is close to the approach in that study, although not quite the same.

With widespread building management systems, communicative devices such as meters and sensors installed, and the increasing popularity of smart buildings and Internet of Things (IoT), buildings are experiencing an explosion of operation data. The availability of building operation data will only become helpful for the calibration studies as well as to extend the current practice and research to a new level.

2.1.2 Objective

The purpose of this chapter is to calibrate a whole building performance model using measured data. The calibrated model should satisfy the calibration criteria in terms of energy use as well as for indoor conditions. The model should be able to capture the dynamic behaviour of space temperature variations in the building zones, which is especially important to investigate control strategies for the energy flexibility.

2.1.3 Case study building

This dissertation selects the Canadian Centre for Housing Technology (CCHT) houses as an example for discussion and illustration. They are among the several houses that have been studied in the course of this research project.

The CCHT houses are twin houses, composed of a test house and a reference house (see Figure 2.1). They were built in 1998 in Ottawa as an experimental platform to assess the energy performance of new technologies related to building envelope and HVAC devices (Swinton, Moussa, & Marchand, 2001).

Figure 2.1: Canadian Centre for Housing Technology (CCHT) twin houses

The houses are common North-American wood-frame buildings with brick facing, constructed according to the Canadian standard R-2000 (Natural Resources Canada, 2012). The houses have two floors above ground, a basement, an unfinished attic, and an attached garage. The liveable area is approximately 210 m^2 excluding the basement. Table 2.1 summarizes the brief characteristics of the houses with key parameter values from a CCHT research publication (Manning, Swinton, Szadkowski, Gusdorf, & Ruest, 2007).

Table 2.1: Brief characteristics of CCHT houses

Feature	**Details**
Liveable area	210 m^2 (2 storeys)
Insulation	Walls: R=3.5 m^2K/W; Rim joists: R=3.5 m^2K/W; Attic: R=8.6 m^2K/W
Basement	Poured concrete, full basement Floor: concrete slab, no insulation Walls: R=3.5 m^2K/W in a framed wall
Windows	Low-e coated, argon filled windows Area: 35 m^2 total, 16.2 m^2 south facing
Exposed floor over garage	R=4.4 m^2K/W with heated/cooled plenum air space between insulation and sub-floor
Airtightness	1.5 h^{-1} @ 50 Pa

In the houses, home automation systems are installed to simulate occupant behaviour by activating appliances, lights and water valves etc. according to predefined schedules.

Incandescent bulbs are installed and controlled to account for sensible internal gains due to occupants. Both houses are fully instrumented and a data acquisition system tracks more than 20 meters and 250 sensors.

2.1.4 Available measurement data

The validation datasets were historic data recorded for the reference house for the year 2002 – 2003. Table 2.2 summarizes the duration and frequency of the available data. They were provided by National Research Council Canada responsible for operating the facility. The measurement accuracy, however, is unclear due to the replacement of measuring devices and staff in charge. Therefore, the measurement error is not further discussed in this work.

Table 2.2: Summary of available measurements

Dataset	Duration	Frequency	Data
1	Nov 2002 – Oct 2003 (1 year)	Daily	Energy use: appliances, occupants, lighting, ventilation, heating and cooling;
2	Nov 2002 – Oct 2003 (1 year)	Daily	Outdoor dry bulb temperature, global horizontal solar radiation;
3	Jan, Mar, Aug, Oct 2003 (4 months)	Hourly	Outdoor dry bulb temperature, outdoor relative humidity, global horizontal solar radiation;
4	Jan, Mar, Aug, Oct 2003 (4 months)	Hourly	Indoor dry bulb temperature, indoor relative humidity.

A preliminary data processing was carried out and some missing data points were filled for the furnace gas and electric use measurement. The most significant problem was found in the weather data: the daily temperature means of Dataset 3 show significant differences with the available daily means from Dataset 2 in Table 2.2. Therefore, external weather data files for 2002 and 2003 were obtained for reference from WhiteBox Technologies for the Ottawa airport (WhiteBox Technologies, 2018).

Figure 2.2 shows the comparison of daily average ambient temperature between WhiteBox Technologies and the hourly measured values. We can see that the two data sets match quite well. To quantify the differences in the ambient temperature data, the heating and cooling degree days were calculated for both sets of data (when available) using a base temperature of 21 °C. The difference between the two datasets is less than 0.5 %.

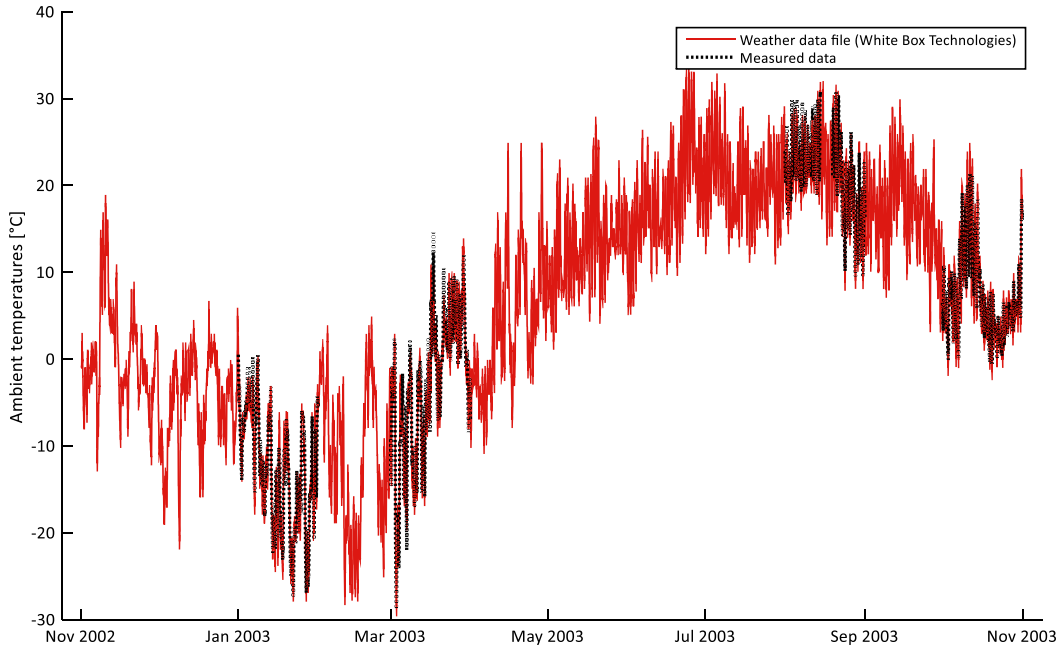

Figure 2.2: Daily average ambient temperature - weather data file vs. measured values

The agreement with hourly data is not perfect, but the daily averages are consistent with the recorded ones for all days. The match for solar radiation is not as good, as shown in Figure 2.3.

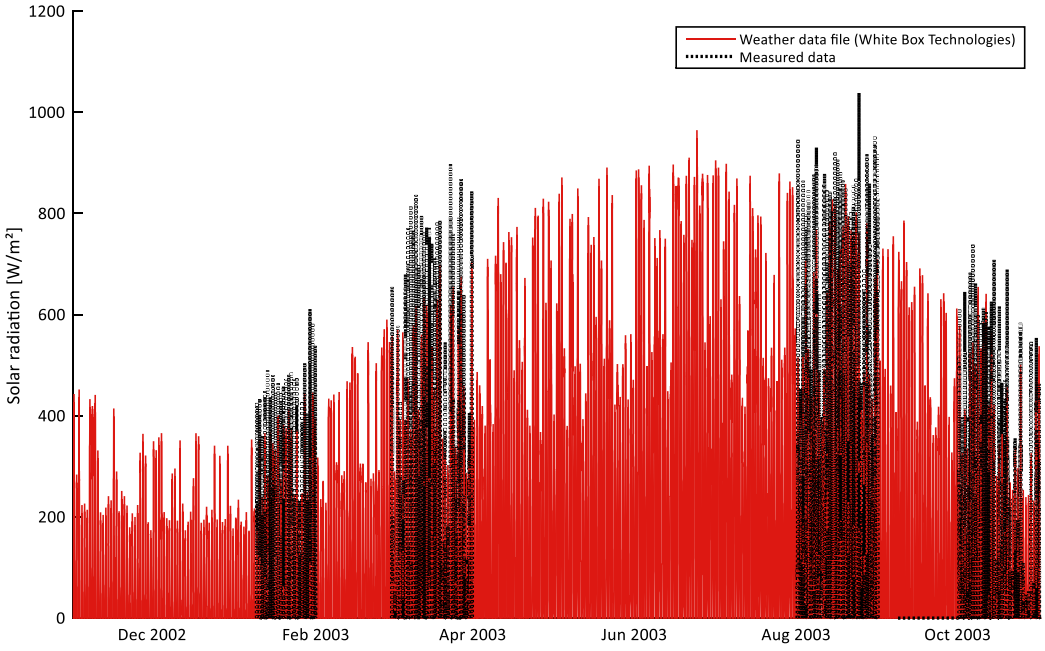

Figure 2.3: Global horizontal solar radiation - weather data file vs. measured values

Solar radiation in the weather file is estimated from satellite measurements, so the accuracy can be expected to be lower. Solar radiation is also more complex to measure, so on-site

measurements could also present some inconsistencies. The total global horizontal solar radiation (integrated over the periods when measurements are available) is 93 % of the measured value.

Figure 2.4 shows a 10-day period in summer where the agreement between both sets of data is very good. The satellite-based estimation is less accurate for cloudy days but provides a reasonable estimate of daily solar gains.

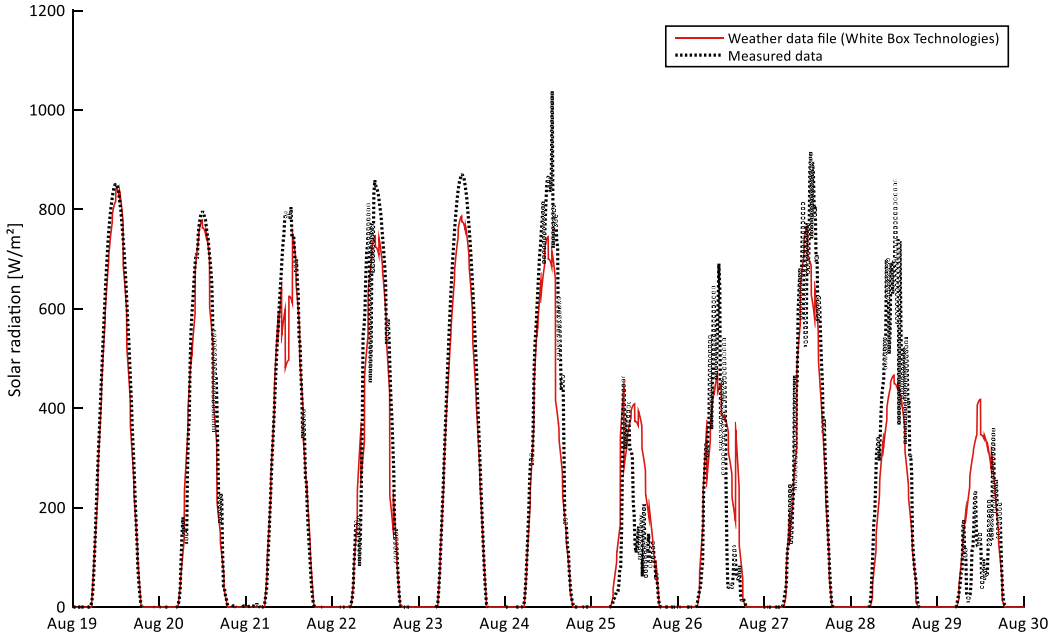

Figure 2.4: Global horizontal solar radiation - weather data file vs. measured values (August)

Figure 2.5, on the other hand, shows a period in March where the weather data file consistently underestimates solar radiation for 8 days and then shows variations that bear little resemblance to the measured data.

Given the above analysis, a hybrid weather data file was adopted. The measured solar radiation was used when available while the outdoor dry bulb temperature was from WhiteBox Technologies since the difference is minor. This means that the differences shown in the above figures for solar radiation have been cancelled in the simulation. The solar radiation in the WhiteBox Technologies weather data for the other months cannot be verified, and it probably represents a relatively crude estimate of the actual solar radiation at the CCHT site. This may import considerable uncertainties to the calibration accuracy given that large south-facing windows are installed in the houses.

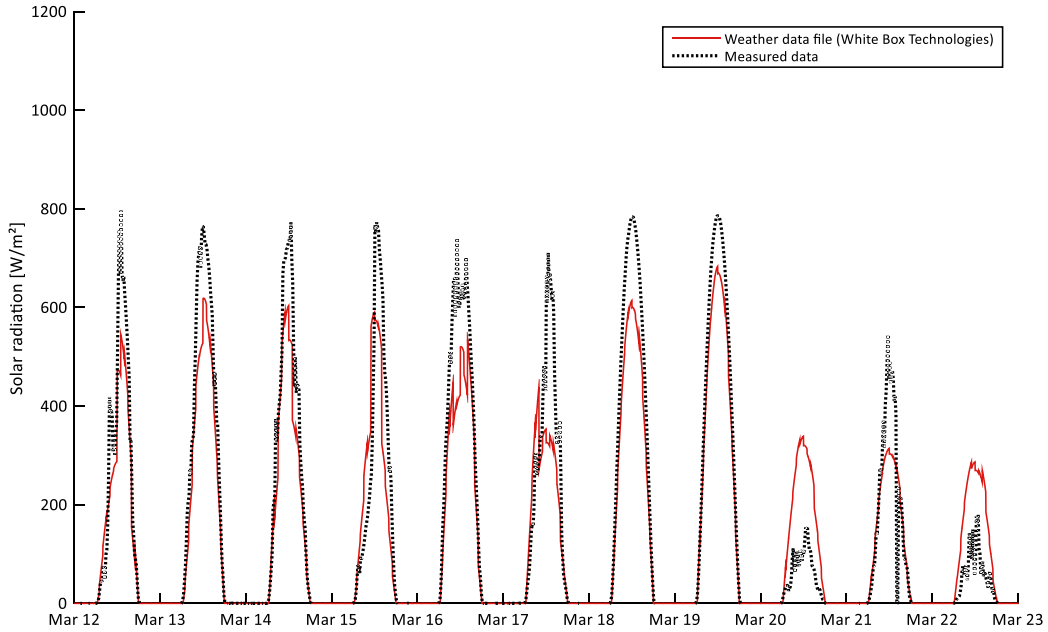

Figure 2.5: Global horizontal solar radiation - weather data file vs. measured values (March)

2.2 Methodology

2.2.1 Calibration criteria

In the literature, three guidelines were mentioned for calibration criteria: the International Performance Measurement and Verification Protocol (IPMVP), the U.S. Federal Energy Management Program (FEMP) M & V guidelines and ASHRAE guideline 14-2014 (ASHRAE, 2014). The last two guidelines propose consistent criteria, which are employed as the calibration criteria in this study. The equations below explain the procedure to calculate the two main indicators Normalized Mean Bias Error (NMBE) and Coefficient of Variation of the Root Mean Squared Error (CVRMSE).

The Root Mean Squared Error (RMSE) is an absolute value in the variable units (e.g. kWh for energy use). In the equations below, y denotes the simulation value while y_m the measured value. $\bar{y}_m$ denotes the average value of the N measurements.

$$RMSE = \sqrt{\sum \frac{(y - y_m)^2}{N - 1}} \tag{2.1}$$

The RMSE can be normalized by dividing it by the average value of the measured variable and expressed in %. This is usually referred to as the Coefficient of Variation of the RMSE (CVRMSE):

$$CVRMSE = \frac{\sqrt{\sum \frac{(y - y_m)^2}{N - 1}}}{\bar{y}_m} \times 100\% \quad (2.2)$$

The RMSE is an unsigned value, so it does not indicate whether a model has a bias error. The Mean Bias Error can be used for that purpose. It is again a value expressed in the same units as the variable:

$$MBE = \frac{\sum(y - y_m)}{N - 1} \quad (2.3)$$

The MBE can be normalized by dividing the value by the average of measured values, as for the CVRMSE. This gives the Normalized Mean Bias Error (NBME), expressed in %:

$$NMBE = \frac{\sum(y - y_m)}{(N - 1) \times \bar{y}_m} \times 100\% \quad (2.4)$$

The first three columns of Table 2.3 summarizes the recommended calibration criteria by the ASHRAE guideline 14 to assess the uncertainty of the model. It only provides targets for the monthly and hourly calibration but not for daily calibration. It is reasonable to estimate that the targets for daily values would be between the targets for monthly values and for hourly values as shown in the last column of Table 2.3.

Table 2.3: Criteria of calibrated building energy models

Indicators	**Monthly**	**Hourly**	**Daily**
NMBE	5%	10%	5%~10%
CVRMSE	15%	30%	15%~30%

2.2.2 Model inputs assumptions

The CCHT houses, unlike most calibration case studies, have rich reported information in relative reports and research papers; however, the presence of conflicting information is not

uncommon. The obtained data for internal gains, for example, are significantly different from the theoretical schedules presented in CCHT documents.

The method for selection and assumptions of the model inputs are based on the following steps:

- literature review: a thorough literature review is conducted to collect all reported information available about the houses. The information is then categorized in tables in order to identify the most possible value for each input. For instance, the value occurring most frequently is ranked as more trustworthy;
- on-site visits and meetings with colleagues from Natural Resources Canada: photos of houses and HVAC systems have been taken during the visits; a large part of the data and documents have been verified with on-site project managers;
- email verification: emails are exchanged for further verification during the course of the calibration process;
- engineering judgment: experience from engineering practice is the last resort to assume certain inputs for unconfirmed information.

Finally, when the uncertainty of input parameters is high or the input information unavailable, for example, the soil properties used for basement modelling is unknown, some alternative values are explored within boundaries to improve the model performance.

The iterative process of calibration is manually conducted. The optimization method is not employed because the model of the initial version has a good performance basis before the calibration. Optimization may pose a risk to overfit the model to the data. When simulation results of the model reach within the set criteria, no further improvement is explored to reduce the gaps between the simulation and the measurements.

A sensitivity analysis of some key input assumptions is further carried out after the calibration.

2.3 Detailed modelling in TRNSYS

In this work, TRNSYS was employed to model the building system based on first principles (Thermal Energy System Specialists LLC, 2018). This software has been certified based on ASHRAE standard 140 (ASHRAE, 2014) and accepted for certifications such as LEED and

ASHRAE standard 90. The sections below explain the essential components of the whole building model.

2.3.1 Zones and constructions

Figure 2.6 presents the sketch of floor plans with room separations. Type 56 (TrnBuild), a multi-zone building module in TRNSYS, uses the concept of thermal zones by assuming a homogeneous air temperature across a zone. Therefore, zoning scenarios in a Type 56 model may not be identical to the real world room separations. In the final model, a 3-zone scenario was used by regarding each floor as a thermal zone with open doors: the first floor, the second floor, and the basement. The garage and attic are always included as two separate zones in the model to account for the thermal interaction between conditioned and unconditioned zones.

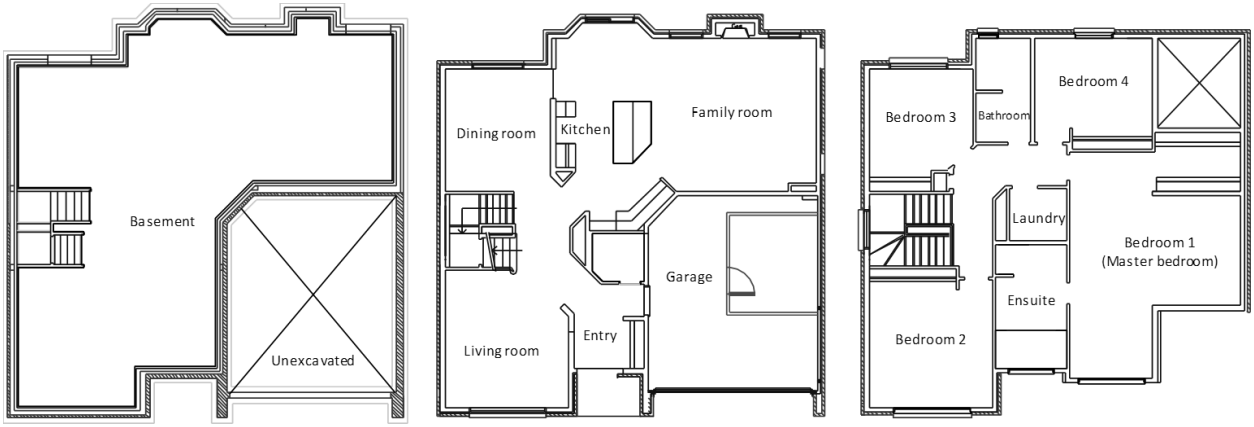

Figure 2.6: Floor plans of the CCHT houses

Type 56 requires data of construction properties including conductivity, specific capacity and density of layers composed of the building structures as well as the geometry of enclosed spaces. This information was taken from the as-built engineering drawings of the houses.

Equivalent layers of the wood studs were calculated using thermal properties from the literature. In particular, the thermal conductivity for insulation batts is assumed to be 0.046 W/m-K (ASHRAE Fundamentals 2009 Chapter 18), which leads to thermal resistance RSI values for the walls that are significantly lower than the “nominal” values mentioned on the as-built drawings. For example, nominal RSI value of the insulation layer mentioned in the drawings is 3.85 m²-K/W; the actual RSI value for the insulation layer, with a thickness of 140 mm and a conductivity of 0.046 W/m-K is 3.04 m²-K/W or 79 % of the nominal value.

The window type in the model uses an equivalent window, which assumes an identical window type with overall U-value 1.73 W/m²-K for all the windows in the house. The window area is then assigned for each window in the zones.

2.3.2 Basement

Basement is an important part in the residential house modelling, as it introduces a significant uncertainty in the heat transfer between the building and the ground. Type 1244 (Thornton et al., 2018) was adopted in the whole building model for the interaction between the ground and building parts in contact with it (e.g. basement and garage slab). This type requires physical parameters of soil and the environment (e.g. soil density, soil specific heat, and the day of minimum surface temperature), as well as geometry information and heat transfer rates from the building to the surrounding ground.

Type 1244 uses a 3D array to map the geometry of the built volume and the defined surrounding space. It divides the given building geometry and maximum distances beyond the building in multiple 3D cells. The elements of the array do not necessarily represent volumes of the same size. The closer to the boundaries, the smaller. The contents of the array indicate the volume to be inside of one of the building zones, above or in the ground.

The CCHT house has two building zones: the garage slab, and the basement. Considering all the detailed dimensions for the basement, the resulting array has $60 \times 51 \times 15$ cells along the three dimensions (x, y, z). The first horizontal layer (x, y) of the array is shown in Figure 2.7, where the global shape of the house (see in Figure 2.6) can be recognized. The yellow color represents the basement and the red color represents the floor in contact with the garage. The z-axis is represented as successive layers in the text file.

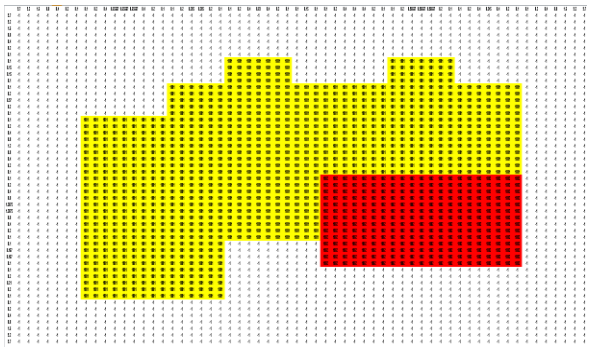

Figure 2.7: The first layer of the 3D ground model input file

Clay type soil parameters are taken in the model and are listed below. The uncertainty on most of these parameters is relatively high, so alternative values were explored in the calibration process. A brief sensitivity analysis can be found in section 2.4.3.

Table 2.4: Type 1244 (3D ground coupling) parameters

Parameter	Value	Units
Soil thermal conductivity	1.9 (values between 1 and 2.4 were explored)	W/(m-K)
Soil density	1930 (values between 1900 and 2400 were explored)	kg/m3
Soil specific heat	0.84	kJ/(kg-K)
Deep earth temperature	8.3 (values between 5.8 and 8.9 °C were explored)	°C
Amplitude of surface temperature	14.2 (value between 12 and 14.2 °C were explored)	°C
Day of minimum surface temperature	41	Day of the year
Soil surface mode	1	-
Soil surface emissivity	0.90	-
Soil surface absorptance	0.40	-

2.3.3 Infiltration and HRV

The infiltration model used in the study was the Alberta Infiltration Model (AIM-2). The AIM-2 (Walker & Wilson, 1998) model only applies to detached single-family buildings up to 3 storeys. It implements a simple natural ventilation algorithm with empirical functions for the superposition of wind and stack effect. Furnace, fireplace and Domestic Hot Water (DHW) flues are considered as separate leakage sites. The model differentiates houses with basements (or slab-on-grade) and crawlspaces. Parameters from the blower door test of the CCHT houses were used in the model.

A Heat Recovery Ventilation (HRV) unit was installed in the houses and Type 760 in TRNSYS was used to model this unit. Figure 2.8 shows the schematic of the ventilation system in the TRNSYS model. Part of the return air goes through the HRV and then mixes with the rest of the return air before entering the furnace system.

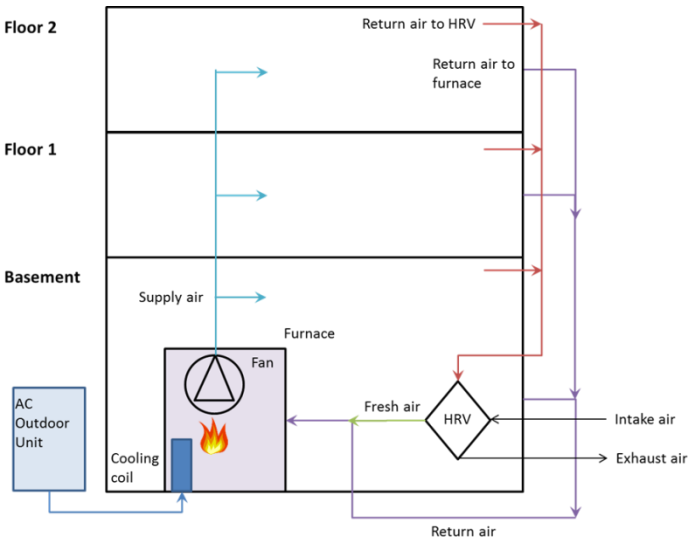

Figure 2.8: Diagram of a forced air system with HRV

Constant air volume to each zone was assumed in the model with total flowrate 65 cfm with the defined ratio to each zone. The HRV power is set to a constant value of 94.5 W. The effectiveness of the HRV is assumed to vary linearly with the ambient temperature. The 2 points at 0 °C and -25 °C are taken from the HVI ratings for Venmar AVS HE1.8 at the lowest flowrate (Venmar, 2018), where Venmar was the original system installed in the reference house. The rated values at the two points are respectively 84 % and 72 %. Note that the effectiveness is not extrapolated, i.e. 84 % is kept above 0 °C, and 72 % is kept under -25 °C. The following equation is implemented in the model:

$$\varepsilon_{HRV} = \min\left(0.84, max\left(0.72, 0.84 + T_{dbamb} \cdot \frac{0.12}{25}\right)\right) \quad (2.5)$$

Defrost is modelled in a simple way: if the ambient temperature is below -5 °C, the HRV switches to defrost mode for 12 min per hour, based on a fixed schedule. This means that the fresh air flowrate goes to zero and the fan power increases to 175 W. That heat is injected into the return air before the furnace.

2.3.4 Forced air system

As presented in Figure 2.8, the original system in the reference house is a forced air system, commonly seen in Canadian single-family homes. The conditioned air is supplied from the

basement to each zone through ducts with fresh air handled by the HRV system. The furnace uses gas as the main fuel source and shares the same blower fan with the air conditioner.

In the TRNSYS model, the furnace is modelled with a constant efficiency of 80.2 % and a capacity of 17584.3 W (60000 Btu/h). The setpoint for the supply air temperature is unknown. It is set to a high value (60 °C) in the model so that the supply air temperature is limited by the furnace capacity. The supply air temperature actually never reaches 60 °C in the simulation because the flowrate is high enough.

The air-conditioner is modelled with TESS Type 921. A TRNSYS performance map has been created from the manufacturer data. The rated conditions are taken from the performance map:

- Total cooling capacity = 6.86 kW
- Sensible cooling capacity = 5.14 kW (sensible heat ratio of 75 %)
- Power use = 2.06 kW
- COP = 3.32

The power used by the condenser fan is assumed to be included in the data. The manufacturer data provides the motor horsepower 1/5 hp. Assuming a permanent split capacitor motor efficiency of 60 %, the actual power usage of the fan would be 250 W. This power is used in Type 921 but has no impact on performance as it is assumed to be included in the performance map.

The air handler flowrate and fan power are estimated as follows:

- Low speed (circulation): 450 L/s, 350 W
- 2nd highest speed (heating): 620 L/s, 530 W
- Highest speed (cooling): 680 L/s, 570 W

The power used for the furnace power vent motor is not explicitly taken into account (i.e. it is supposed to be included in the 530 W).

These 3 points are used to define a power curve for a variable speed fan. The control signal is adapted to the operation mode (circulation, heating, or cooling). In TRNSYS, this is implemented as follows:

Fan rated flowrate 2947.392 kg/h, fan rated power 2052 kJ/h

Fan power curve:

$$P = -1.056445 + 3.439614m - 1.383168m^2 \quad (2.6)$$

m is the flowrate in each mode and P is the power.

Fan control signal (speed ratio):

$$speedRatio = 0.661765 + furnaceOn \cdot 0.250000 + acOn \cdot 0.338235 \quad (2.7)$$

2.3.5 Internal gains and occupancy

The appliances, lighting and occupant simulators in the CCHT houses were operated according to a predefined schedule repeated daily. Note that the occupants were simulated using lightbulbs, so there were no humidity gains. This experimental setting reduced the complexity of the calibration study associated with the accessory energy use. In the calibrated model, the schedule with measured power consumptions for all equipment was imported as external data into the model. Therefore, there are no differences between simulation results and measurements for the appliance yearly energy use.

For internal gains due to lighting, appliance, and occupants, they are split between convective and radiative parts according to standard ratios from the ASHRAE handbook fundamentals (American Society of Heating, Refrigerating and Air-Conditioning Engineers, 2017). The ratios of the internal gains that are actually released in the room are also referred from the handbook, e.g. for the dryer, most of the electricity (70%) is used to heat the exhausted air, which means only 30% becomes internal gains.

2.4 Calibration results

Since the calibration is an iterative process, different versions of TRNSYS models of the whole house were simulated with different parameters and inputs. All simulations during the process were run for 2 full years (2002 and 2003) with a time step of 5 minutes. The results reported here is the final version of the model, and results from November 2002 to October 2003 are used for comparison and analysis.

2.4.1 Energy use results

Yearly results

Table 2.5: Annual energy use, measured and simulated

Item	Meas. values	Model version r205		Comments
	MJ	MJ	% diff.	
Lighting and appliances	11577	11577	0.0%	Model inputs including lights and receptacles, fridge, stove, dishwasher, clothes washer, dryer
Furnace fan	12910	12375	-4.1%	Fan power at different speeds is model input, differences caused by operating hours in different modes
HRV fans	3054	3090	1.2%	Fan power is model input, differences caused by operating hours in defrost mode
DHW blower	203	203	0.2%	Blower power when operating is model input, differences caused by operating hours
Air conditioner	5759	5729	-0.5%	Includes compressor power and outdoor fan power. Performance map is an input
Furnace gas	65701	65558	-0.2%	Furnace steady-state efficiency is model input (80 %), differences caused by load differences
DHW gas	25569	25630	0.2%	Differences can be attributed to mains water temperature
Total electricity	33503	32973	-1.6%	Differences mostly come from furnace air-handler power, somewhat compensated by other categories
Total gas	91270	91188	-0.1%	Relatively similar differences for furnace and DHW (both slightly overestimated)
Total energy	124773	124162	-0.5%	Obtained by summing gas and electricity MJ, without equivalence factors

Table 2.5 summarizes the annual energy use for each category with the second column showing the measured energy use. The third column lists the simulated energy use with the number *r205* indicating the model version accepted as the calibrated model. Note that this number in the figures and tables below means the same final model version.

We can see that the error on total energy use (gas and electricity combined) is as low as 0.5 %. This includes lighting and appliances, which are model inputs and account for 10 % of the total

energy use. The relative error on annual energy use for heating and cooling are both less than 1 %. These differences could be even reduced by fine-tuning some of the parameters, but this was not attempted given the relatively high uncertainty on some key parameters e.g. Air Changes per Hour (ACH) @ 50 Pa. A discussion on the impact of some key parameters is presented in section 2.4.3.

Monthly results

Figure 2.9 presents the monthly energy use for heating (furnace gas) and cooling (air-conditioner electricity). Both values are expressed in MJ/day. It should be noted that the negative bars for cooling do not denote negative electricity use. The negative sign is only used as per the TRNSYS convention.

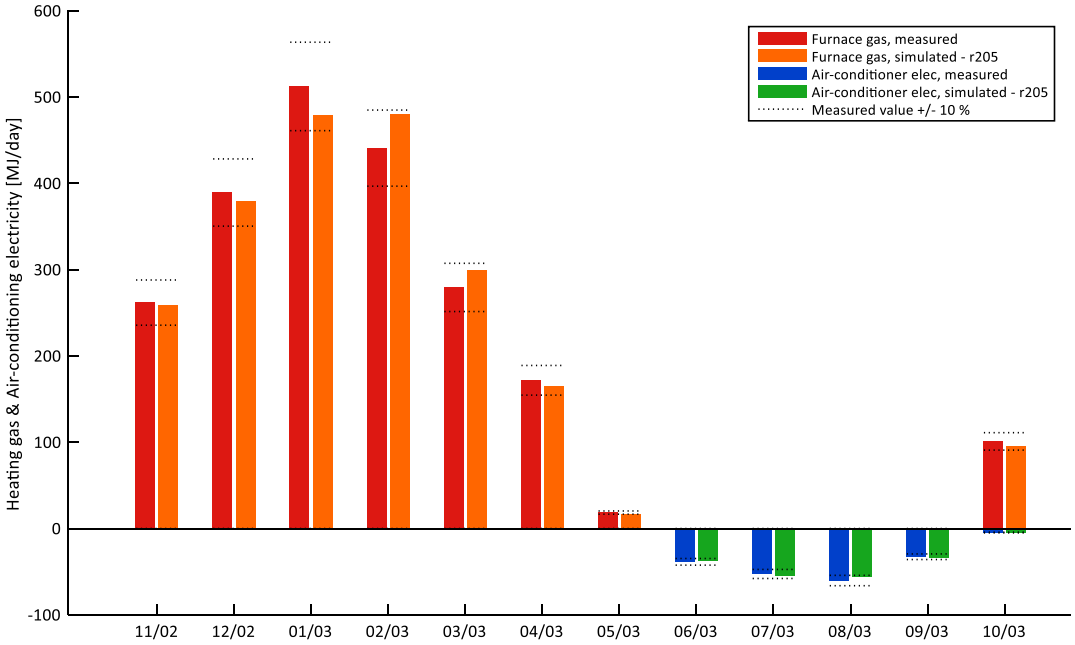

Figure 2.9: Monthly furnace gas and air-conditioner electricity use

We can find that the energy use differences of each month are within 10%. Larger differences are observed for January (underestimation) and for February and March (overestimation). The overestimation in February could be related to low solar radiation in the data file. The profile of the undisturbed ground surface temperature could also have an impact. The underestimation in October could be related to start-up problems or slight setpoint differences at the beginning of a new heating season.

The $CV(RMSE)$ of monthly energy use of the model are:

$$\text{Furnace gas use: } CV(RMSE) = 7.9\,\%$$

$$\text{Air-conditioner electricity: } CV(RMSE) = 6.2\,\%$$

Both results indicate a good performance of the calibrated model, well under the ASHRAE target of 15 %. Note that the results here only count the heating season for furnace gas use and cooling season for air conditioner electricity use. The $NMBE$ values of the model are also well under the ASHRAE target of 5% as shown below:

$$\text{Furnace gas use: } NMBE = -0.1\,\%$$

$$\text{Air-conditioner electricity: } NMBE = -0.6\,\%$$

Daily results

Given that our measurements have daily energy use data for a full year, we compared the simulated daily energy use with the measurements, although daily results comparison are not required by the ASHRAE guideline. Figure 2.10 shows the daily values for furnace gas use and air-conditioner electricity use, while Figure 2.11 shows the daily errors for the same variables.

Both values are in very good agreement. The day-to-day variability of heating and cooling demands seems to be well captured by the model. Figure 2.11 also identifies the data points that were interpolated in the experimental data. Some of the largest differences occur during interpolated days, which would seem to indicate that the procedure used to fill in missing daily values is at least partly responsible for these larger discrepancies. Some relatively large errors are still present during the non-interpolated days, and the model seems to consistently overestimate the heating load in late February / early March. However, most of the large errors are all within 20% of the absolute values for that particular day.

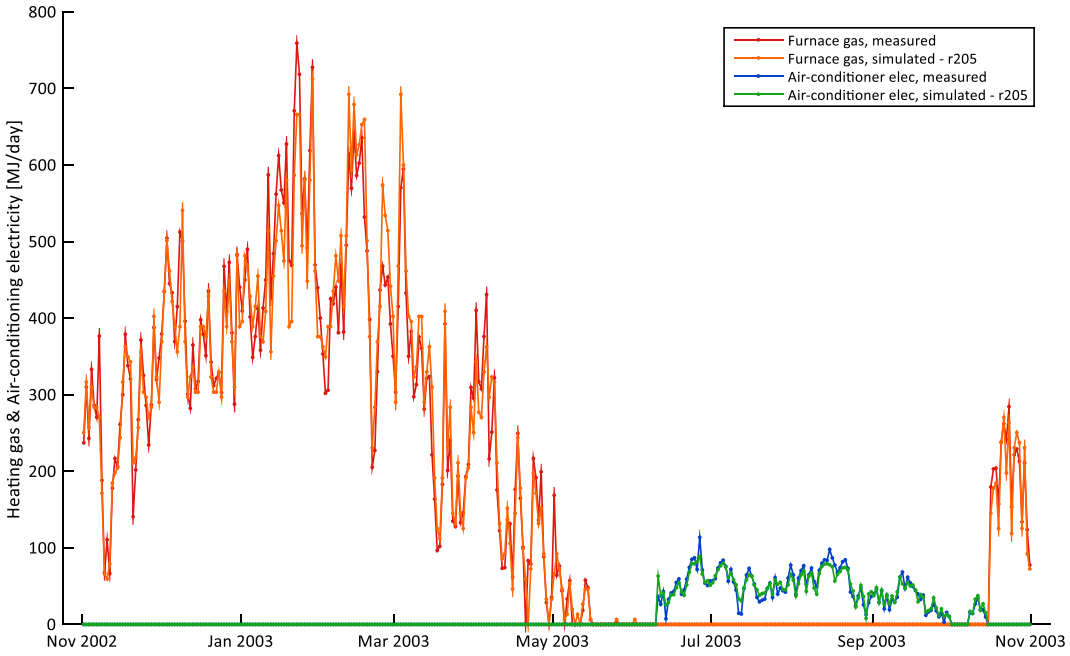

Figure 2.10: Daily furnace gas and air-conditioner electricity use

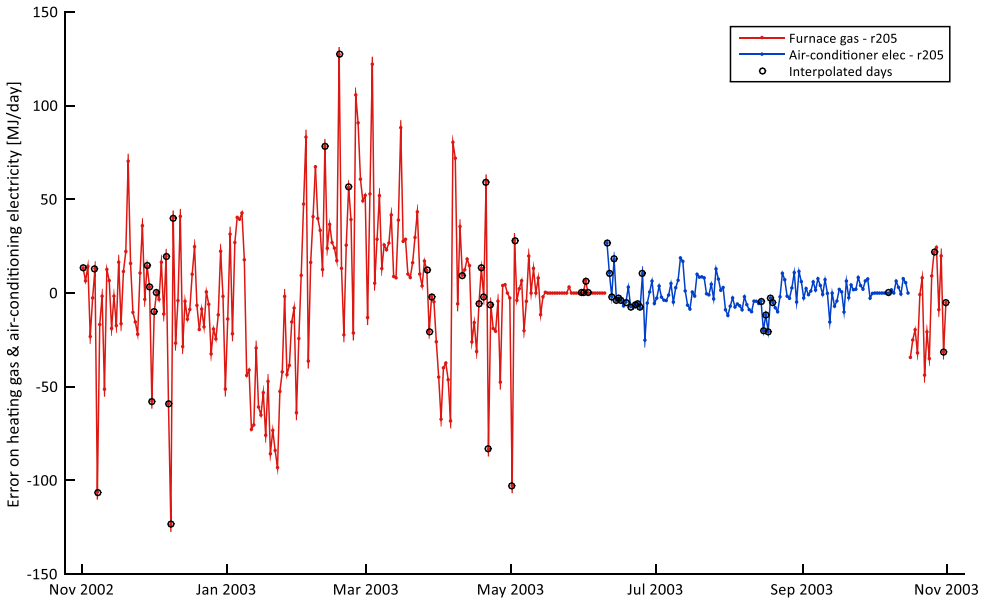

Figure 2.11: Daily error on furnace gas and air-conditioner electricity use

Table 2.6 shows the daily performance indicators and the ASHRAE targets. All performance indicators for daily energy use are well within the ASHRAE targets for hourly values and in most cases even within the targets for monthly values.

Table 2.6: ASHRAE goodness-of-fit indicators for daily energy use

	Model r205	**ASHRAE target (hourly)**	**ASHRAE target (monthly)**
Daily $CV(RMSE)$ for furnace gas use	13.5 %	30 %	15 %
Daily $NMBE$ for furnace gas use	-0.2 %	10 %	5 %
Daily $CV(RMSE)$ for furnace gas use (Excluding interpolated days)	12.0 %	30 %	15 %
Daily $NMBE$ for furnace gas use (Excluding interpolated days)	0.0 %	10 %	5 %
Daily $CV(RMSE)$ for air-conditioner electricity use	16.9 %	30 %	15 %
Daily $NMBE$ for air-conditioner electricity use	-0.5 %	10 %	5 %

2.4.2 Dynamic results

Hourly values are available for the first floor, for selected periods. These values are plotted with hourly-averaged simulation results in Figure 2.12.

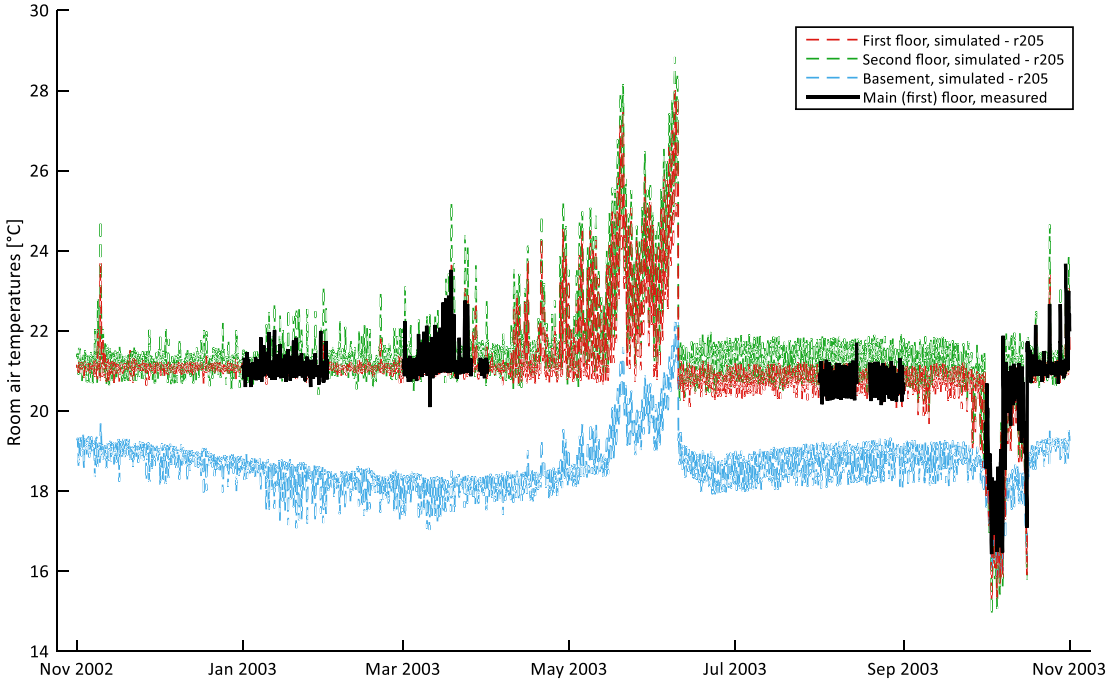

Figure 2.12: Room temperatures - hourly measured and simulated values

Hourly temperatures show significant variation within the margins of the controllers deadbands, due to the on/off nature of the heating and cooling control. The free-floating behaviour during

shoulder periods seems to be well reproduced by the model (early October 2003). The basement is significantly colder than the other floors, and this will be analyzed below.

The ASHRAE indicators can be calculated for the 4 months for which hourly measurements are available. The table below shows that the $CV(RMSE)$ for air-conditioner power usage is slightly above the ASHRAE target. Unfortunately, it is difficult to draw conclusions given that only one month of data (August) and a few days in October are available.

Table 2.7: ASHRAE goodness-of-fit indicators for hourly energy use

	Model r205	**ASHRAE target (hourly)**
Hourly $CV(RMSE)$ for furnace gas use	31.5 %	30 %
Hourly $NMBE$ for furnace gas use	-3.7 %	10 %
Hourly $CV(RMSE)$ for air-conditioner electricity use	38.7 %	30 %
Hourly $NMBE$ for air-conditioner electricity use	-2.3 %	10 %
Hourly $CV(RMSE)$ for room temperature	1.8 %	30 %
Hourly $NMBE$ for room temperature	-0.4 %	10 %

The next figures show more details on the dynamic behaviour, plotting the 5-min simulated values against hourly measured values for typical periods in winter and summer.

Figure 2.13 shows a typical cold winter week. The on/off furnace control leads to large oscillations around 21 °C for the main floor, while the second floor is generally slightly warmer and the basement is significantly colder (but with similar oscillations as their flowrate is controlled simultaneously). Even during very cold periods, the furnace rarely turns on for two consecutive time steps with the selected deadband. During periods with higher gains, the furnace sometimes remains off for several hours.

The average measured main floor temperature (hourly measurements are only available for two months) is 21.1 °C, while the average simulated 1st-floor temperature over the same period is 21.07 °C. The measured temperature corresponds to one point (thermostat location), while the simulated value models the volume average of the entire floor, so this good match hides differences such as the ones visible in Figure 2.13 during the high gain periods.

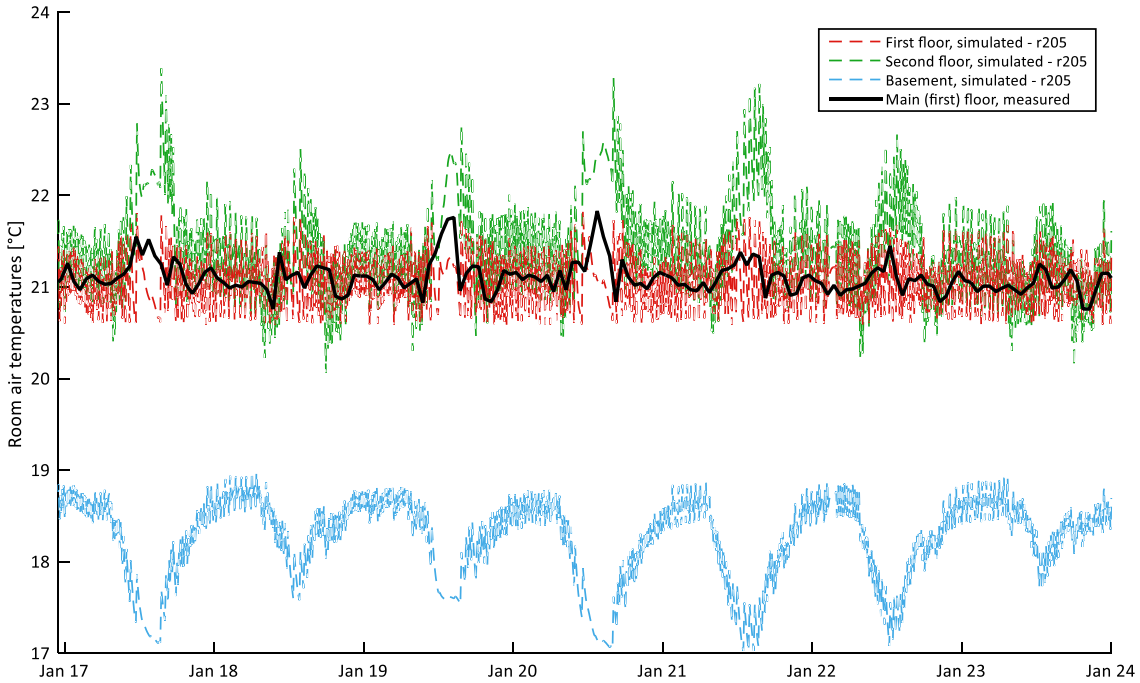

Figure 2.13: Hourly measured main floor temperature and simulated 5-min values – winter

Figure 2.14 shows a typical warm summer week. The air-conditioner is not oversized as the furnace is, so it operates for long periods, from 30 min to several hours. Off periods range from about one hour to a few hours at night. The average measured main floor temperature (over the period for which measurements are available) is 20.8 °C, and the simulated 1st-floor temperature for the same period has the same average value. Again, given the different nature of measured temperature (discrete thermostat sensor) and modelled temperature (volume average for the thermal zone), this agreement may hide short-term discrepancies.

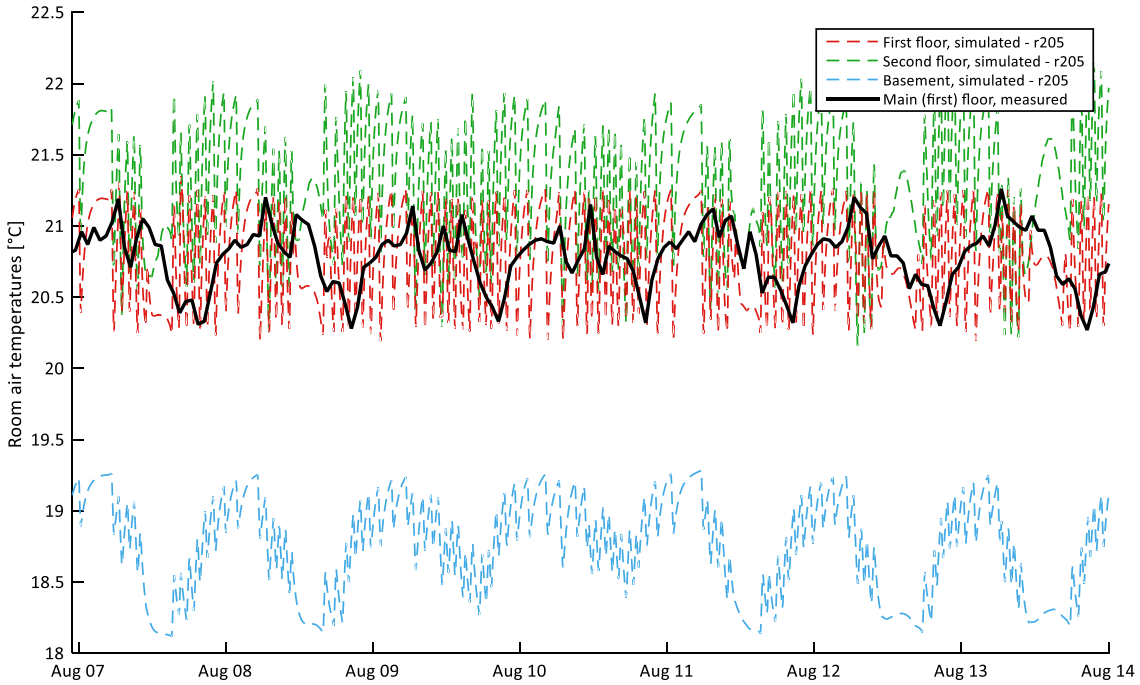

Figure 2.14: Hourly measured main floor temperature and simulated 5-min values – summer

2.4.3 Sensitivity analysis

Thermostatic control

In the absence of 5-min experimental data, it is difficult to assess the accuracy of the model in terms of the fine dynamic behaviour of the thermostat control. The following figures compare available hourly data with 5-min and hourly averaged simulation results, focusing on furnace gas input and air-conditioner power.

Figure 2.15 shows the furnace gas input power for January 21st and 22nd. During these very cold days, the furnace operates for most of the day. The average gas input over these 2 days is 7.9 kW, which is still far from the furnace rated input (17.6 kW), so the furnace cycles On and Off during the whole period. The variation in furnace use during periods with higher heat gains seems to be mostly captured by the model.

Figure 2.16 shows a similar graph for October 24 and 25, two relatively mild days. The model seems to capture the times when more or less heat is required by the house, except for a delay when heating starts again late at night on October 24. This seems to be related with the over-prediction of the room temperature during the day. Without 5-minute data and more accurate

weather data, it is difficult to investigate the exact cause of this difference, as some other days show the opposite behaviour (i.e. overheating during the day is under-predicted).

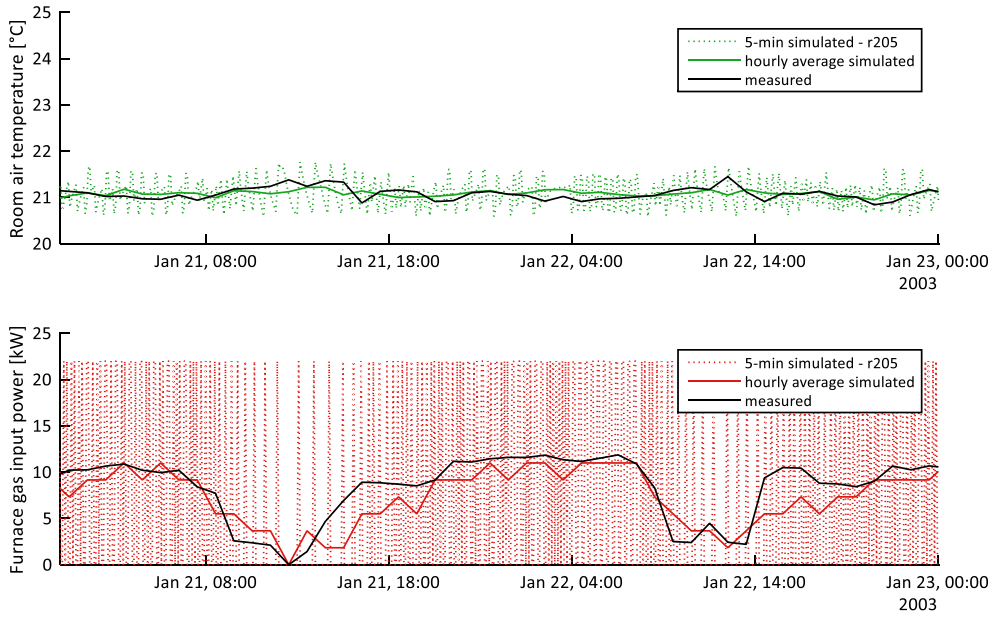

Figure 2.15: Furnace gas input and main floor temperature Jan 21 and 22

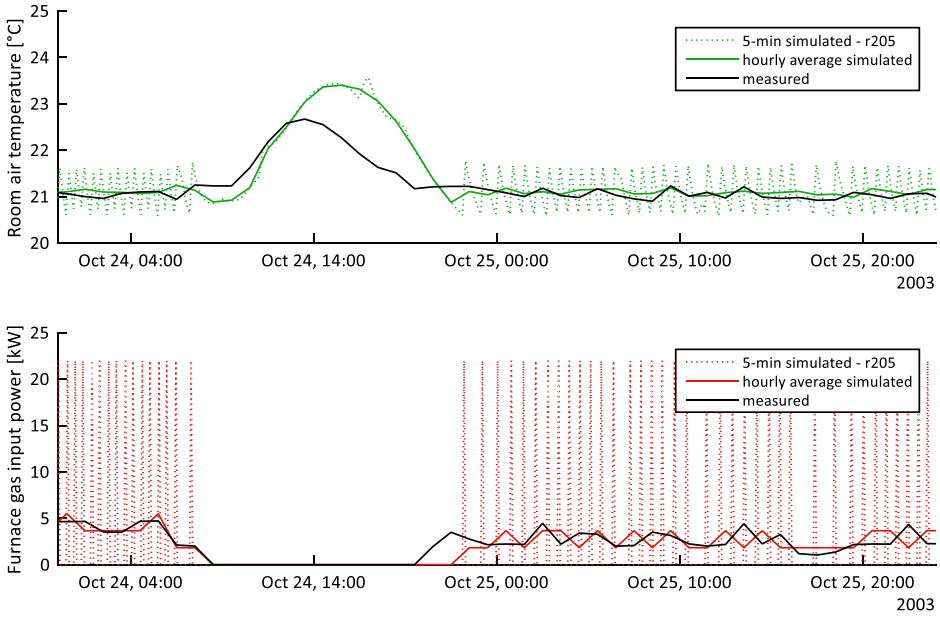

Figure 2.16: Furnace gas input and main floor temperature for October 24 and 25

Figure 2.17 shows the power used by the air-conditioner during two very warm days (August 12 and 13, 2003). The overall shape of the air-conditioner usage seems to be captured by the model,

except during very late night / very early morning periods, where the model shows more oscillations resulting from long On/Off cycles.

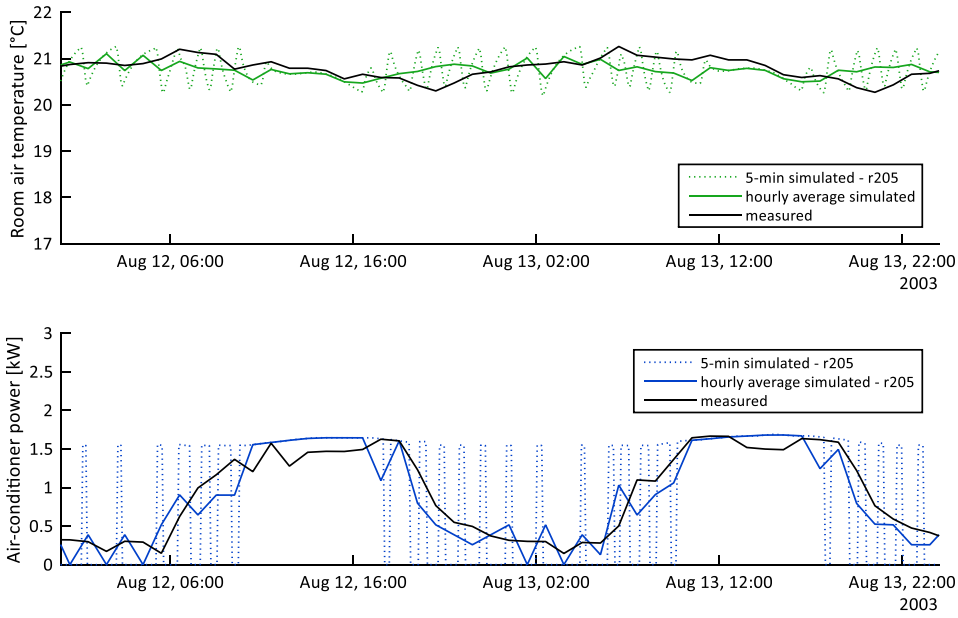

Figure 2.17: Air-conditioner power use - August 12 and 13

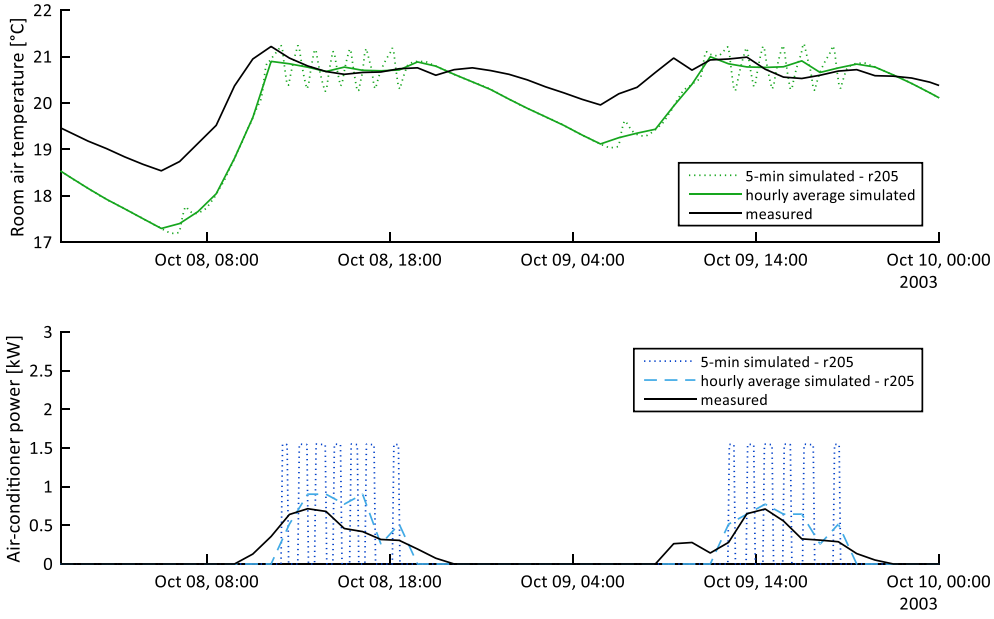

Figure 2.18: Air-conditioner power use - October 8 and 9

Figure 2.18 shows the air-conditioner power usage for milder days (October 8 and 9). Again, the model seems to have captured the dynamic behaviour of the building and HVAC system, although with one significant difference. The simulation starts the air-conditioner later in the

morning, which is probably related to the underestimation of the main floor temperature at night. Without 5-min data, it is difficult to analyze the exact cause of this difference. The internal mass could be underestimated by the model, although there is no evidence of such a difference in winter.

Model sensitivity to some key parameters

Table 2.8: Model sensitivity to key parameters

Model version	**Parameters**												**ASHRAE indicators**			
	ACH_{50}	k_{gnd}	ρ_{gnd}	$T_{avg,gnd}$	$Ampl_{gnd}$	day_{min}	ρ_{SHAD}	I_{SHAD}	T_{setH}	ΔT_H	T_{setC}	ΔT_C	$NMBE_H$	$NMBE_C$	$CV_{RMSE,H}$	$CV_{RMSE,C}$
	1/h	W/m-K	kg/m³	°C	°C	-	-	-	°C	°C	°C	°C	%	%	%	%
r201	1.25	1.9	1930	8.5	12	31	0.75	0.25	21	2	20.5	2	-1.0	-3.1	13.8	16.5
r202	1.25	1.9	1930	8.5	12	31	0.75	0.25	21.1	1	20.75	1	1.0	-6.4	13.8	18.1
r203	1.5	1.9	1930	9	12	31	0.5	0.2	21.1	1	20.75	1	1.0	0.2	13.7	17.0
r204	1.5	1.6	1930	8	12	31	0.5	0.2	21.1	1	20.75	1	0.8	-2.4	13.6	17.4
r205	1.5	1.6	1930	8.5	12	31	0.5	0.2	21.1	1	20.75	1	-0.2	-0.5	13.5	16.9
r206	1.5	1.6	1930	8	14	31	0.5	0.2	21.1	1	20.75	1	1.4	-1.0	13.8	17.0

Explanation of the parameters:

ACH_{50} : infiltration rate at 50 Pa

k_{gnd} : ground thermal conductivity

ρ_{gnd} : ground density

$T_{avg,gnd}$: average surface temperature

$Ampl_{gnd}$: amplitude of the surface temperature

day_{min} : day with minimum surface temperature

ρ_{SHAD} : $REFLISHADE$ and $REFLOSHADE$ in Type 56 (reflectivity of shading device)

I_{SHAD} : $ISHADE$ in Type 56 (fraction of incoming radiation that is intercepted)

T_{setH}: heating setpoint

ΔT_H: heating deadband

T_{setC}: cooling setpoint

ΔT_C: cooling deadband

Table 2.8 shows a brief summary of the impact of some key parameters on the ASHRAE hourly goodness-of-fit indicators. Only six different model versions are listed while the *r205* is the chosen final version as mentioned previously. The notation of C and H indicates cooling and heating respectively.

From the model version r201 to r202 shown in the table, the heating and cooling setpoint temperature were slightly changed with the deadband reduced from 2 °C to 1 °C. The $NMBE$ for the cooling energy is nearly doubled but the dynamic behaviour shows better performance. The setpoint temperature and deadband values were kept until the final version.

The air infiltration rate is a parameter impacting the space conditioning energy use significantly, yet the real value is difficult to measure; therefore, it is commonly regarded as a fine-tuning button for calibration studies. The calibration results show that reducing the infiltration rate decreases heating load; however, its impact on the cooling load is less significant because the driving temperature differences for infiltration and the energy impact of incoming air are lower in summer. During the process, several values for infiltration rate were tried out to reduce the calibration errors, but as we can see from Table 2.8, the final value 1.5 1/h @50 Pa was chosen, the same as reported in many papers (Manning et al., 2007; Swinton, Moussa, & Marchand,

2001; Zirnhelt, 2013). It was not further explored to make the errors smaller in case of over calibration, in line with the proposed calibration method.

The calibration results are also sensitive to the ground properties for the basement model, as mentioned in the section 2.3.2. The impact of the ground thermal conductivity, average ground surface temperature and amplitude are shown from the last four runs. Increasing the ground surface temperature decreases the heating load, but it also reduces the cooling load. Increasing the assumed temperature amplitude for the surface temperature, on the other hand, increases both the heating and cooling loads.

2.5 Discussions

This chapter introduced the case study building in the thesis, the CCHT houses. They were three-storey twin houses, selected to represent the typical single-family dwelling in Canada. The detailed whole building model was built in TRNSYS and the main TRNSYS modules such as the basement and HVAC system were presented. The model calibration was conducted with historic measured data; the calibration method and the analysis of the calibration results were also illustrated. The uncertainty on some key parameters and the lack of detailed (sub-hourly) measurements made this calibration study difficult; the results, however, showed a good agreement with measured values. They were well below the targets suggested by ASHRAE Guideline 14 for calibrated simulations for monthly values, and fairly close for hourly values.

Fine-tuning parameters of the model to reduce the energy use gap between simulation and measurements was not pursued in this study, because the initial goal was not only calibrating the energy use, but also the space temperatures. The dynamic results showed that the calibrated model could capture the temperature variations in the space quite well. This is particularly important for the study because the model will be used for control purpose in the following chapters.

The sensitivity analysis of the calibration study showed that several parameters affect energy usage quite significantly. For example, the ground conductivity is a parameter with a relatively high uncertainty and impacts both the heating and cooling load. The air infiltration rate, commonly used as a “tuning button”, impacts the heating load more than the cooling load. For

temperature variation in the zones, the heating and cooling setpoints and deadbands are critical parameters.

The literature on calibrated simulations mostly concerned about calibration of energy use. This chapter presented a study not only dealing with energy use but also indoor conditions calibration. The results and analysis presented may be helpful for other similar studies.

CHAPTER 3 ENERGY FLEXIBILITY CHARACTERIZATION

This chapter presents a general methodology to characterize energy flexibility in buildings. Definitions for Key Performance Indicators associated with the energy flexibility are explained in detail. The methodology and KPIs are applied to the calibrated building model described in the last chapter. Only simple Rule-Based Control (RBC) is investigated in this chapter.

3.1 Introduction

3.1.1 Literature review

Energy flexibility is essential to operate the electric grid, which needs long-term as well as short-term flexibility to meet variable electricity demand on the daily and seasonal basis (Aggarwal & Orvis, 2016). In this context, buildings, due to their large electricity demand and energy storage capability, can provide an energy flexibility service to the grid. Note that the very short timescale electrical storage in seconds used to stabilize grid frequency is not within the scope of this thesis (Ulbig, Borsche, & Andersson, 2014). The short-term flexibility contributed by buildings is in the magnitude of hours.

The term “energy flexibility” in buildings is not completely new but its formalization has been underpinned by the Annex 67 of the Internal Energy Agency Energy in Buildings and Communities Programme. The project “Energy Flexible Buildings” (2014-2019) is in the process of exploring a standard approach to evaluate the potential of building energy flexibility (IEA EBC Annex 67, 2014). The project is divided into three subtasks. The first subtask “Definitions and Context” solves the problem of scientific definitions for terms associated with energy flexible buildings. The second subtask “Analysis, Development, and Testing” intends to propose a generic approach to analyze the potential of energy flexibility in buildings through both simulations and experiments, and develop technologies applicable to real systems. The last subtask “Demonstration and User Perspective” investigates the acceptance of building users and operators and showcases the applicability of the developed technologies through demonstration projects.

Clauß, Finck, Vogler-finck, & Beagon (2017) reviewed most of the previous studies related to the energy flexibility and listed existing Key Performance Indicators in a wide range of studies,

like for PV or thermal storage systems. A more detailed report for the literature review is also included on the website of the Annex (Finck et al., 2018). Yin et al., (2016) investigated the DR potential for both residential and commercial buildings through global setpoint temperature adjustment using regression models which were adopted to reduce the computation intensity. They defined the DR potential as the percentage of the difference between baseload and DR load divided by the base load. They discussed the DR potential for individual customers as well as for the sub-station level of the grid. De Coninck & Helsen (2016) used an MPC approach to optimize energy cost based on dynamic imbalance price in Belgium. The energy flexibility was achieved by adjusting the temperature within the thermal comfort band (between 21.8 °C and 23.5 °C) as well as by thermal storage tank associated with the heat pump system.

Le Dréau & Heiselberg (2016) discussed the energy flexibility for two types of residential buildings in Denmark (a passive house and an old house built in the 1980s) as well as for two kinds of heating systems (radiators and underfloor heating). The adopted KPIs were the amount of thermal energy stored and the amount of energy discharged. The charged amount was always positive and the discharged always negative. Another indicator was the shifting efficiency, calculated as the absolute ratio of these two terms. A similar approach was taken to assess the energy flexibility for detached and terraced dwellings from 4 different ages in Belgium (Reynders, Diriken, & Saelens, 2015, 2017). The proposed KPIs were flexibility capacity and storage efficiency. As in the paper by Le Dréau and Heiselberg, the authors focused on the storage performance of the thermal mass and thus the storage capacity was always positive.

The methodology and KPIs proposed by the last two teams investigated the energy flexibility from the perspective of buildings. They looked at the building thermal mass as a storage medium and characterized how much energy the building could store or discharge in a DR event based on their indicators. And those indicators are not directly associated with the electric load of the grid. Therefore, those KPIs are difficult to interpret from the utility perspective. KPIs that quantify the flexibility of electric power and energy demand of buildings are assessed from the grid perspective in the present study.

3.1.2 Objective

The amount of building energy flexibility contributed by its thermal mass is impacted by how the HVAC system is controlled. An advanced control strategy like MPC could possibly provide

larger energy flexibility than a simple thermostatic modulation, but advanced control strategies are less common in real residential buildings.

The objective of this chapter is to characterize building energy flexibility in a quantitative way using a straightforward case. Specifically, we are going to investigate the energy flexibility through setpoint temperature modulation, which is fairly feasible to implement as a potential DR program on real buildings. Starting from a simple case is also helpful to define a general methodology and metrics to quantify the energy flexibility. When the methodology and metrics are ready, they can be applied or extended to more complex situations.

3.2 Methodology

3.2.1 KPIs

To quantify the energy flexibility contributed by the building thermal mass, we introduce the four following indices in the present study. Figure 3.1 presents a conceptual energy flexibility of buildings with a downward flexibility event happening from 8 am to 10 am, with E_f flexible energy; E_{rb} rebound energy; P_{fmax} maximum flexible power and t_{dr} duration of demand response event.

Note that this plot only presents the reactive response case; in other words, the system responds to the grid at the moment when the DR event starts. When one considers the anticipative capability of the building system like with a predictive controller, the shape of the curve becomes different. Chapter 5 will discuss the transformations of the KPIs.

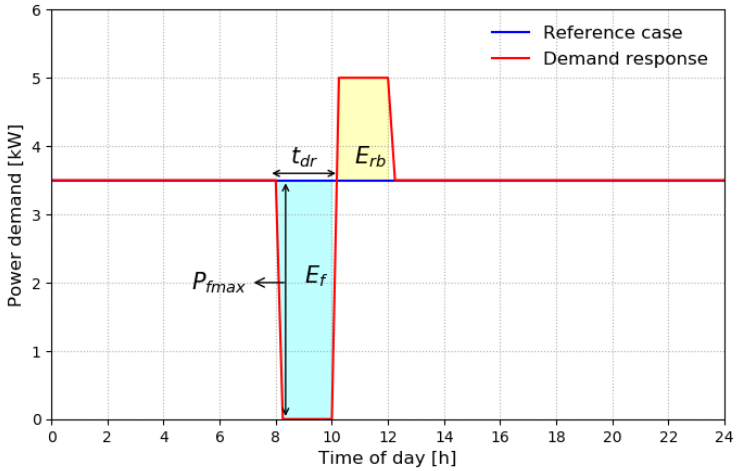

Figure 3.1: Flexible energy demand of buildings (downward flexibility)

Flexible energy E_f

The flexible energy quantifies the amount of energy that has been shifted compared with the reference scenario, either downward or upward. It indicates the decreased or increased energy usage during the DR event. The cyan shaded area shown in Figure 3.1 indicates the downward flexible energy amount during a DR event. A formal equation to calculate the flexible energy can be written as:

$$\boldsymbol{E_f} = \int_0^{t_{dr}} \left(P_{dr} - P_{ref}\right) dt \tag{3.1}$$

Note that P_{dr} and P_{ref} in the equation are *electric power*, not *thermal power*. This index also shows the amount of shifted power in average during the DR duration: the average shifted power equals E_f divided by the time of DR duration t_{dr}.

Rebound energy E_{rb}

After the DR event, there is a high possibility of energy rebound, positively or negatively. If we have saved energy during the peak (in the case of downward flexibility), we may immediately see power demand go up after the peak. Similarly, if we have increased energy use during the demand valley (in the case of upward flexibility), the energy need may ramp down after the event because part of the excess energy can be stored. The rebound energy E_{rb} is used to denote this

amount of energy rebounded after the DR event (as shown by the yellow shaded area in Figure 3.1).

$$\boldsymbol{E_{rb}} = \int_{t_{dr}}^{t_\infty} \left(P_{dr} - P_{ref}\right) dt \tag{3.2}$$

Note that the upper bound for the integration in Equation (3.2) is infinite, but we take it as 48 hours in the calculation. In all our simulation results, we have confirmed that no rebound effect lasts longer than this horizon; therefore, 48 hours is effectively infinite for our study. It may, however, be different in other situations.

Flexible energy efficiency $\boldsymbol{\eta}$

The DR action does not necessarily save energy consumption for electricity users. The flexible energy efficiency is introduced to quantify the energy consumption change. Similarly, a cost efficiency could also be introduced to consider the price change, for instance, time-of-use or dynamic electricity price. This study intends to be general and not to address the price signals.

$$\boldsymbol{\eta} = \left|\frac{E_f}{E_{rb}}\right| \times 100\% \tag{3.3}$$

Maximum flexible power $\boldsymbol{P_{fmax}}$

This indicator is helpful to identify the maximum potential for power change during a DR event against the reference case. Eq. (3.4) is separated into the downward and upward cases instead of using absolute values to take into consideration that the rebound phenomenon may occur during the DR event.

$$\boldsymbol{P_{fmax}} = \begin{cases} \max\limits_{t_{dr}} \left(P_{ref} - P_{dr}\right) \\ \max\limits_{t_{dr}} \left(P_{dr} - P_{ref}\right) \end{cases} \quad \text{for} \begin{matrix} \text{downward} \\ \text{upward} \end{matrix} \tag{3.4}$$

3.2.2 Implementation

The simple RBC setpoint control during a DR event to be implemented is

- Decreasing the reference setpoint by 2 °C for 2 hours in the downward flexibility;

- Increasing the reference setpoint by 2 °C for 2 hours in the upward flexibility.

The same control strategy has also been adopted by (Le Dréau & Heiselberg, 2016; Reynders et al., 2017). Note that this 2 °C change happens in one-time step (15 minutes in our case). The reference setpoint case represents a typical setpoint profile as shown in Table 3.1.

Table 3.1: Reference setpoint scenario

Zone	Reference setpoint	DR event
First floor	21 °C	2 °C change
Second floor	21 °C	2 °C change
Basement	17 °C	Not modified

To investigate the general energy flexibility of buildings, we assume the DR event can occur at any hour of the year. We focus on the heating season starting from October 15th to April 29th (altogether 196 days); in other words, the DR event happens at 4704 different hours (196 × 24 hr.). To assure independent DR events, one simulation corresponds to only one event.

The validated building model presented in Chapter 2 was used with CWEC weather file for Montreal, Canada in this section (Numerical Logics, 1999). The electric baseboard heating system was modelled using the idealized heating in TRNSYS Type 56. The setpoint control was thus idealized in the simulation that the setpoint can be perfectly reached given the available heating capacity. There is neither a cycling effect of on/off control nor errors related to Proportional-Integral-Derivative (PID) control such as overshooting. Matlab was used to run the simulation in batches for different DR events in different scenarios.

3.3 Results of a single DR event

The temperature and power change during a 2-h downward flexibility event on a typical day is shown in the left figure of Figure 3.2. In this case, the setpoint temperatures for the first floor and second floor both drop 2 °C from 7 am to 9 am during the DR event (the black dashed curve in Figure 3.2 presents the setpoint change for the second floor; the modulation for the first floor is the same).

We can observe that the total power demand decreases drastically when the setpoint suddenly drops by 2 °C. The heating system is shut off during the first hour and then turned on with

minimum power to maintain the setpoint. In result, the zone temperature of the second floor drops by 1 °C after 1 hour and remains at the setpoint for the second hour of the event. When the event ends and the setpoints go back to normal, we then observe a power rebound (shown by the magenta curve). This consequence is expected since this is a simple thermostatic control and no strategy is implemented to counteract the rebound effect.

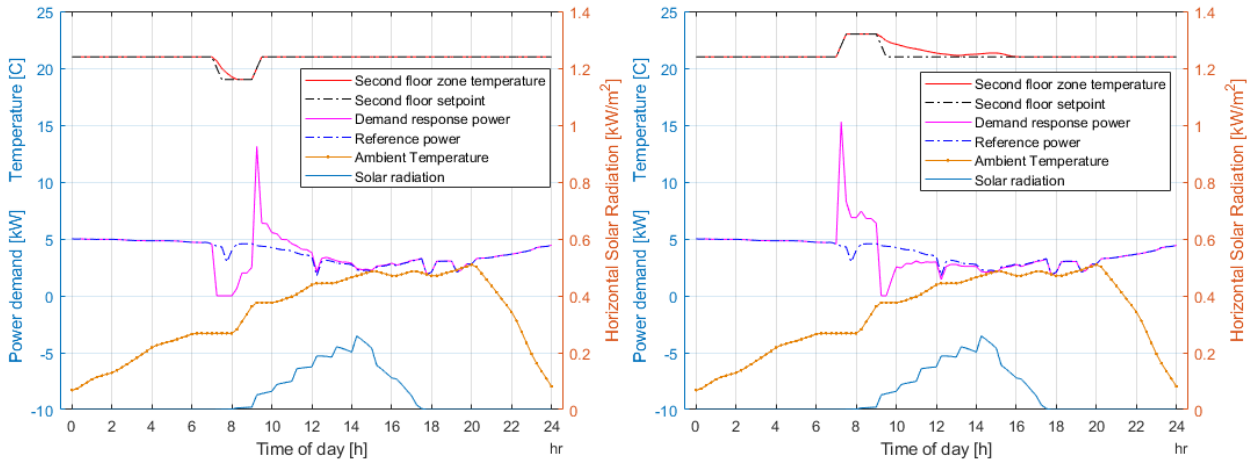

Figure 3.2: Temperature and power profiles in a DR event (left: downward; right: upward)

The blue curve shows the total power demand in the reference scenario, whose setpoint temperature remains at 21 °C all the time. On this day, the reference power demand stays relatively stable. It decreases slightly when the ambient temperature goes up and the building absorbs the solar radiation during the daytime.

The flexible energy E_f for this DR event is the difference between the sum of the power use for the demand response and the total reference power use from 7 am to 9 am, i.e., the difference between the magenta and blue curves. This is the real power change profile of the conceptual line as presented in Figure 3.2. Similarly, the rebound energy is the difference of the same two terms but the integration period starts after the event (from 9 am on) and lasts for the next 48 hours. From Figure 3.2, we can see that the rebound effect is strong during the first half an hour and lasts for about 3 hours.

The right figure of Figure 3.2 shows the upward flexibility event occurring at the same time of the same day as in the left figure. Contrary to the downward flexibility, the upward flexibility event increases the setpoint temperatures by 2 °C. We can observe an immediate power increase in response to this action. This phenomenon occurs because we allow the setpoint increase by

2 °C in one-time step in the simulation and the heating capacity also suffices for this change (note that the setpoint temperatures shown in these two figures are average values over one time step). This sudden peak in power demand could be reduced if it was a concern (as for the power rebound effect in the downward flexibility). For example, the setpoint temperature could be increased linearly over a few time steps.

When the DR event ends, we see that the zone temperature of the demand response case (the red curve) drops slowly and its power demand remains almost 0 for a while. This is because the thermal mass has stored heat during the event. The power demand then goes back to the same level as the reference case after about 5 hours.

3.4 Sensitivity analysis

The building energy flexibility and the associated KPIs proposed in the study are performance-based; therefore many parameters could impact the results. The building construction (insulation level, airtightness, thermal mass etc.) is a common parameter discussed in the literature as mentioned above. This chapter investigates the energy flexibility of one typical housing archetype and the studied parameters include weather, DR duration t_{dr}, setpoint change scale and setpoint profiles representing different occupancy profiles.

3.4.1 Weather impact

Figure 3.3 presents the downward flexible energy E_f for 2-h DR events happening every hour for the whole heating season (note the negative values in the y axis). As in Figure 3.2, each independent DR event lasts for 2 hours with 2 °C modulation of setpoint temperatures for the first and second floor (the big blue dot in Figure 3.3 presents the flexible energy of the single event in Figure 3.2). Each data point in the figure represents one simulation result, and all the data points were sorted out by the hour of the day as well as their correspondent months. The transparent boxes are the same as in boxplots with the top edge indicating the 75th percentiles and the bottom edge indicating the 25th percentiles.

The blue curve in the middle shows the median value of the flexible energy. We can observe that the amount of energy which can be shifted is highly correlated to the hour of the day. During the night time, the shifted energy is much more significant than that of daytime with maximum value

three times the minimum. This is because the building experiences higher ambient temperature generally during the day and can have solar gains as well. This daily cycle of temperature results in lower energy demand in the reference case and therefore reduced DR potential.

The colours of the data points indicate the months. Among the 7 months investigated, it is clear that the coldest months (January and December) have higher flexibility than the shoulder months (like March, April, and October). The small values of flexible energy that spread out in the top part of the figure mostly fall in the three shoulder months. This seasonal trend is the same as explained for the daily phenomenon in that the reference case has lower energy demand, therefore the DR has also lower potential to shift the energy demand.

Figure 3.4 shows the upward energy flexibility in the same format as shown in Figure 3.3, in which the big blue dot indicates the flexible energy of the single event in Figure 3.2. We find a similar daily and seasonal trend for the upward flexibility due to the same reasons as discussed above. The spread of E_f values shows a strong daily variation, but the median upward flexible energy is approximately constant (and close to the available heating capacity). This shows that the thermal mass capacity of the studied building is large enough to store the heating energy provided during the 2-h DR event.

The maximum power shift P_{fmax} displays the same trends as the flexible energy for both cases and figures are not shown in the study.

Based on our discussion above, we conclude that the potential of buildings to shift heating power demand is higher during colder weather. This is beneficial for the utility, which experiences a higher demand during these periods. The ability to use more power by buildings is also higher in colder weather but the weather impact on the median values is not as significant. The building could still have the potential to use more energy when the grid would experience a significant solar power input during the day.

Figure 3.5 presents the downward flexible efficiency. We find a near-constant median efficiency of around 1.2. This means that the rebound energy is almost always 20% less than the saved energy (the several zero points represent cases when both the flexible energy and rebound energy are 0). The upward flexible efficiency shows similar results as the downward one as shown in Figure 3.6. This confirms that the DR strategy in our study is not energy inefficient.

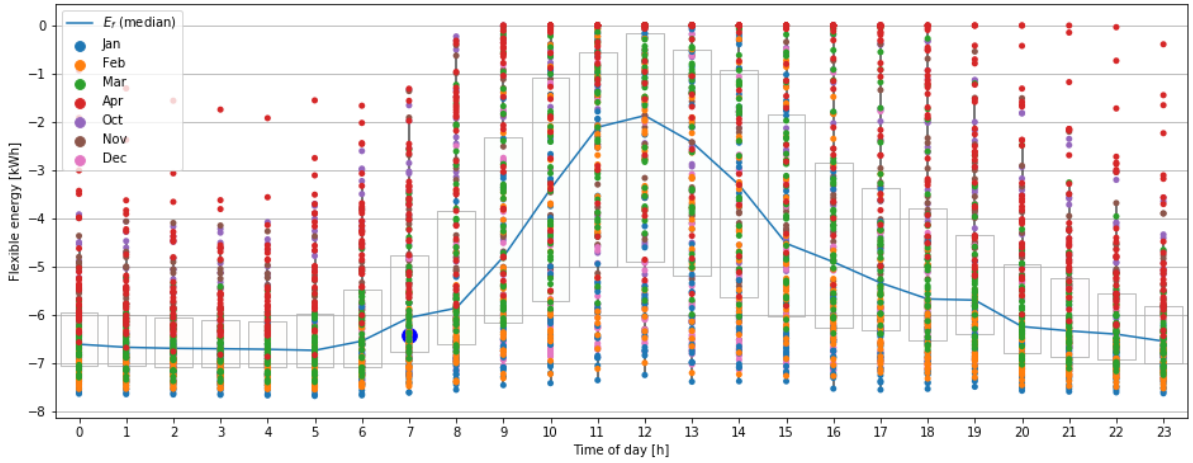

Figure 3.3: Downward flexible energy of the heating season

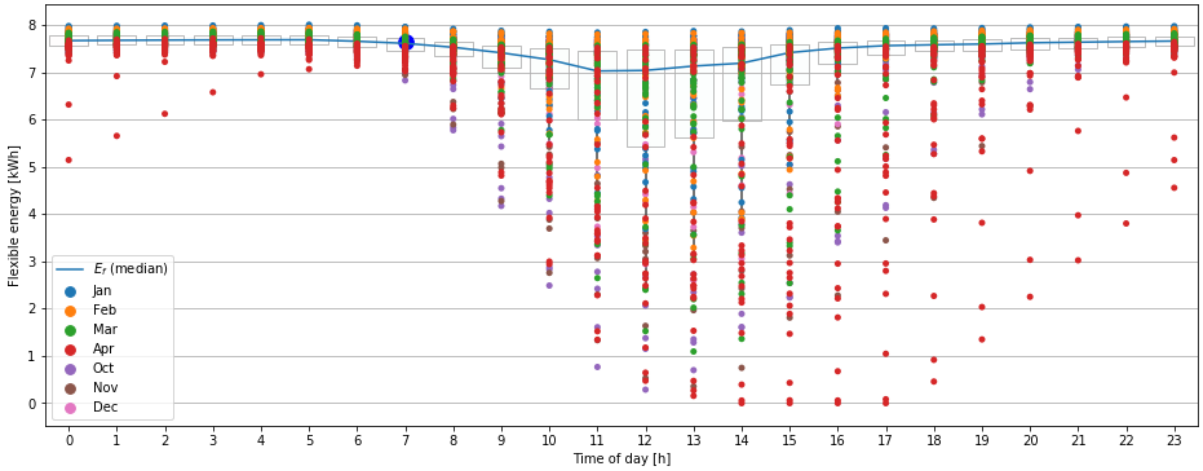

Figure 3.4: Upward flexible energy of the heating season

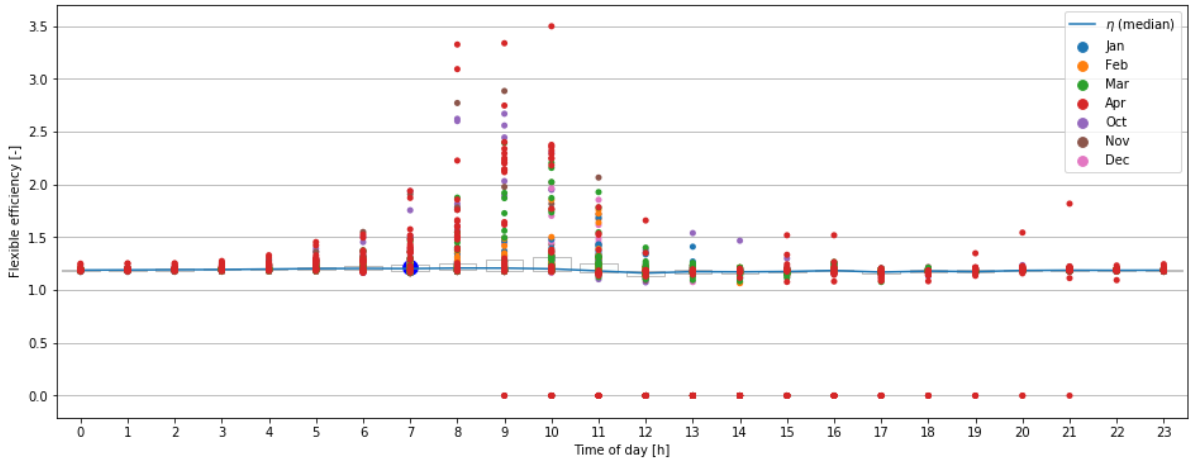

Figure 3.5: Downward flexible efficiency of the heating season

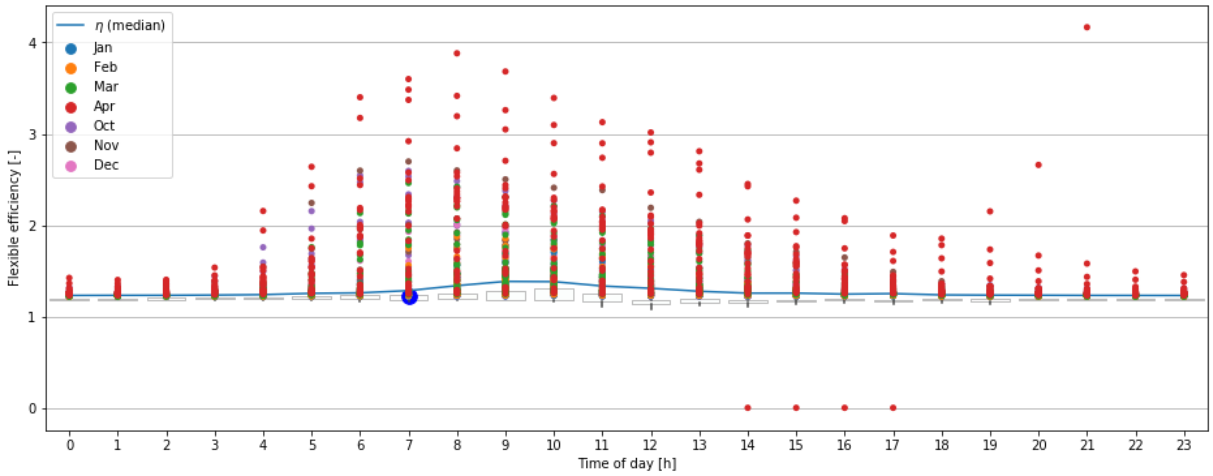

Figure 3.6: Upward flexible efficiency of the heating season

3.4.2 DR duration

The DR duration t_{dr} discussed in the above scenarios is 2 hours. This parameter depends on the utility requirements and is related to the impact of DR strategies on thermal comfort (a drop of 2 °C may be acceptable for one hour but not for 6 hours). Different DR durations were compared to assess the impact of this parameter and to investigate whether an optimal value exists.

Figure 3.7 shows the upward and downward flexible energy amount E_f as a function of the DR duration t_{dr}. For the two scenarios at each duration, each box in the figure presents the results from 4704 simulations. We can see an increasing trend from the median values (the red lines inside the boxes) that the longer the duration, the larger the flexible energy. The top edge of the

box indicates the 75th percentiles of the results excluding the outliers accounting for around 0.7% of the results (not displayed in the plot), while the bottom edge indicates the 25th percentiles. We can see that more data points are concentrated around the median values for the upward flexibility than the downward flexibility, which means the upward flexible energy reports steadier values and is less likely to be impacted by other factors than the downward flexibility. This result is consistent with the results from Figure 3.3 and Figure 3.4.

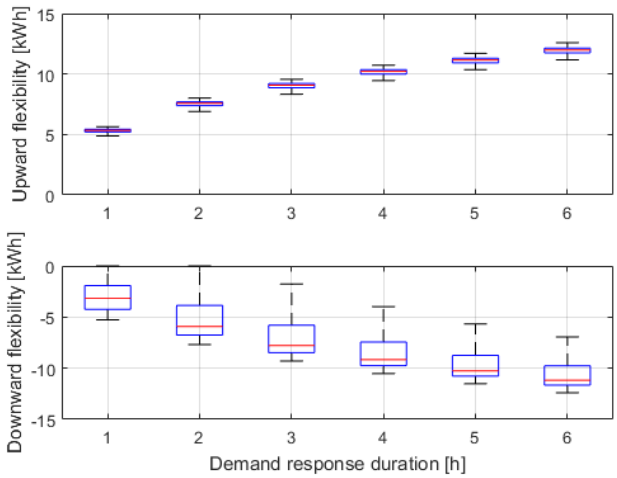

Figure 3.7: Flexible energy as a function of DR duration

Figure 3.8 presents boxplots for the rebound energy E_{rb} in a similar style to Figure 3.7. The upper plot shows the rebound energy for the upward flexibility; therefore it is a negative value. The lower plot shows the opposite. We can also observe an increasing trend for the rebound energy as the DR duration increases. However, its increase slows down when the duration becomes longer. This observation is clearer in Figure 3.9, which shows the median flexible efficiency η as a function of DR duration.

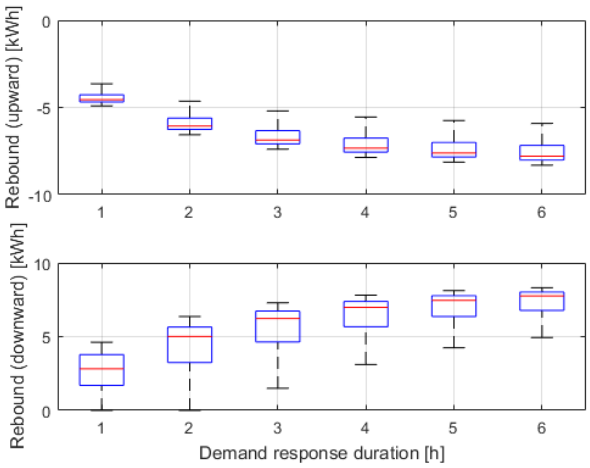

Figure 3.8: Rebound energy as a function of DR duration

We can see from Figure 3.9 that the median efficiency is always larger than 1 for both scenarios, which means that the amount of flexible energy E_f is always larger than the rebound energy E_{rb}. For instance, when the DR duration is 2 hours, the downward efficiency is close to 1.2, which signifies that this DR event saves around 20% of energy use. This result is consistent with what we discussed in the last section (Weather impact).

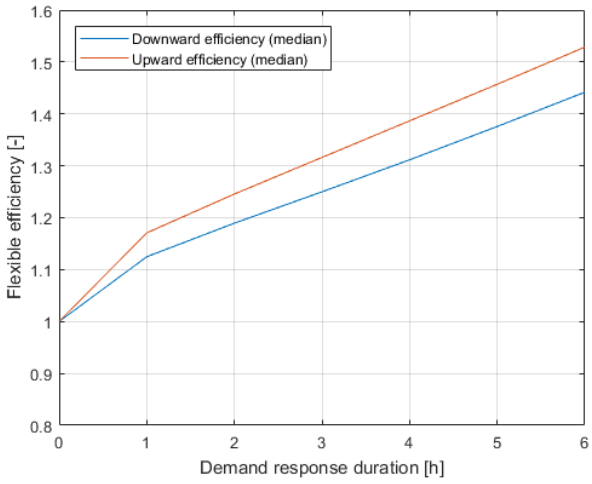

Figure 3.9: Median flexible efficiency as a function of DR duration

Although the DR duration does impact the flexible energy E_f and rebound energy E_{rb}, it has a negligible impact on the maximum flexible power P_{fmax} as shown in Figure 3.10. In our case, the heating system has no time delay to respond to the demand no matter when the event begins. Thus, the power shift ability can almost always reach its maximum at the beginning of the event.

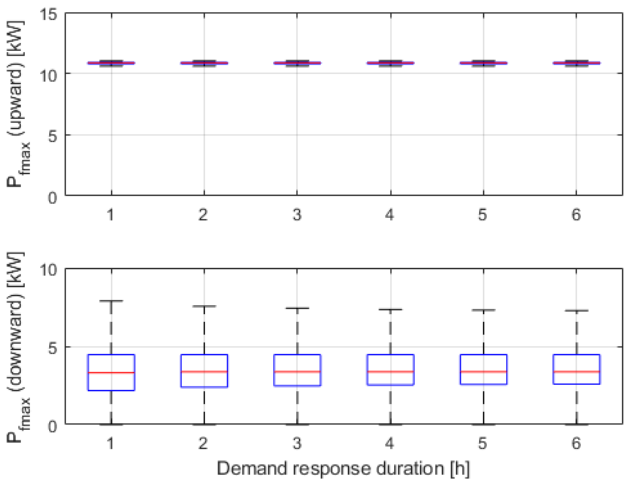

Figure 3.10: Maximum flexible power vs. DR duration

Based on the above analysis for the four indicators, we conclude that the flexible energy increases as the DR duration increases; so does the rebound energy and flexible efficiency. However, the increase of the flexible energy slows down when the duration is longer. And the long duration of DR events could lead to thermal comfort compromise; therefore, 2 to 3 hours could be an optimal DR duration.

3.4.3 Setpoint temperature change

In the previous simulations, the setpoint temperature change is always 2 °C, upward or downward. This section investigates the impact of that parameter for a DR event duration of 2 hours.

The top two plots in Figure 3.11 show respectively the downward and upward flexible energy as a function of setpoint temperature change. We can see that when the setpoint drops by 2 °C, the median downward flexible energy amount is about 1.5 times that obtained with a 1 °C decrease. When the setpoint increases by 2 °C, the median upward flexible energy is about twice as large as with an increase of 1 °C. The flexible efficiency, however, remains almost the same for both cases, as can be seen from the middle two plots. This shows that the rebound effect remains relatively similar no matter how the setpoint temperature is modulated during the DR event.

The lower two figures show that the maximum power reduction capability does not change much for the two setpoint changes, while the maximum power increasing capability for the 2 °C change is twice that for 1 °C.

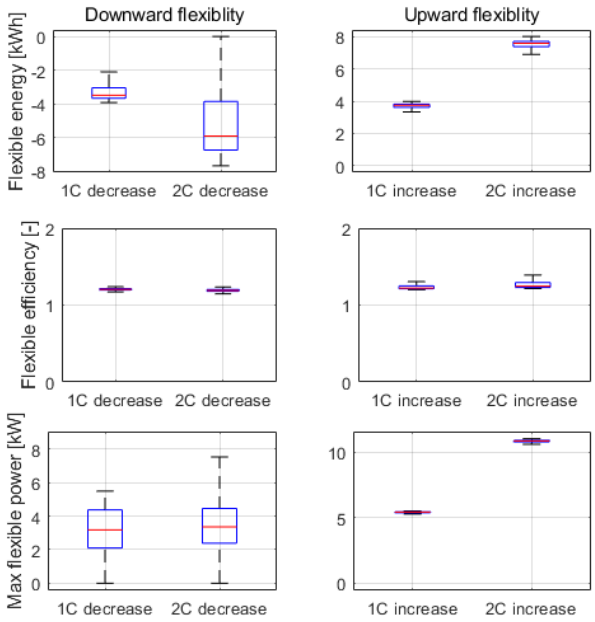

Figure 3.11: Setpoint temperature change

In summary, we find that a 2 °C increase of setpoint is more effective than 1 °C increase for the upward flexibility. For downward flexibility, 2 °C drop of setpoint gives a higher flexible energy but the improvement over a 1 °C increase is not as large as for the upward flexibility. This conclusion is interesting if a 2 °C drop is deemed unacceptable for thermal comfort, although it should be noted that the temperature will not reach the lower setpoint very quickly for shorter DR durations.

3.4.4 Occupancy (constant setpoint vs. setback)

For all the simulations above, we used a constant setpoint profile for the reference case. This scenario is not uncommon in reality if the installed thermostat is not programmable. If the reference setpoint profile includes a setback, we would expect different results. The studied setback scenario is summarized in Table 3.2, which represents a typical setback profile in Canadian households.

For the downward DR event, we impose a 2 °C decrease during the event. For the upward DR event, we assume an upper limit of 23 °C, the same as the constant setpoint case. This means 6 °C increase for both zones when they are unoccupied, 2°C increase when the first floor is occupied and 4 °C increase when the second floor is occupied. In the same way, the basement is not modified for DR events. Note that the DR duration always remains 2 hours for this case.

Table 3.2: Reference setback profile

Zone	Temperature	Time
	Occupied / unoccupied	Occupied
First floor	21 / 17 °C	06:00~08:00, 16:00~22:00
Second floor	19 / 17 °C	22:00~06:00
Basement	17 °C	/

Figure 3.12 summarizes the simulation results for the setback profile as a reference case. Compared with the constant setpoint reference case, we can see that the median downward flexible energy of the setback case is around 33% smaller (4 kWh vs. 6 kWh). Both reference cases have very similar maximum and minimum values for the flexible energy, but the values are more widely spread out for the setback case (therefore lower median value). Contrarily, the upward flexible energy of the setback case is much larger, almost twice of the constant case. The difference of the maximum flexible energy is even more pronounced with the setback case reaching 21 kWh and the constant case around 8 kWh.

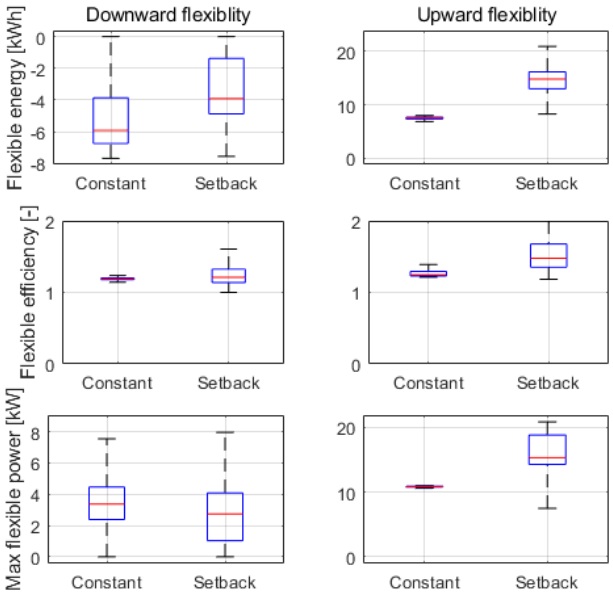

Figure 3.12: Setback setpoint scenario

The maximum flexible power shows a similar situation as the flexible energy, but the differences between the two cases are smaller. This is expected since the setpoint increases are much larger for the setback case when the zones are not occupied, while for the downward flexibility, the setpoint decrease will not produce much flexibility during the setback periods.

The flexible efficiency does not show much difference for both upward and downward flexibility for the two reference cases.

3.5 Discussions

This chapter assessed the energy flexibility of an electrically heated Canadian house during the heating season. Energy flexibility is defined as the ability of a building to modify their energy demand compared to “normal” operation.

The energy flexibility was categorized into two scenarios: downward and upward flexibility. The former scenario is similar to load shifting, which shows the ability of buildings to reduce power demand during peak periods. The upward flexibility denotes the ability to use more energy when the power demand is low for the grid. Energy flexibility at the individual building level results from the use of energy storage and on-site generation. This study focused on the use of thermal mass, through modifications in the building heating setpoint to respond to Demand Response events.

To quantify the amount of energy flexibility, the chapter investigated four key performance indicators, which are flexible energy, rebound energy, flexible efficiency and maximum flexible power. Each indicator applies for both flexibility scenarios (upward and downward). Numerous simulations were carried out based on a validated TRNSYS model of a typical Canadian house modified to use electric baseboard heating, and the indicators were then computed.

Results show that the energy flexibility potential of using thermal mass is significant. The studied house shows a median decrease in the energy use by 6 kWh and a median increase of 7.5 kWh for 2-h DR events. The flexibility depends on the time of the DR event, as it is affected by weather and building operation. The flexible energy amount is higher during colder weather because the normal operation of the house has a higher energy demand during these periods. In addition, the maximum flexible power is also very promising, especially for the upward flexibility.

An analysis of the rebound effect after the demand response event shows that the rebound energy is never higher than the shifted energy. The median energy savings associated with the DR event are about 20%.

A sensitivity analysis of the indicators was conducted. Results show that an optimal duration of the event is around 2 or 3 hours considering both the amount of energy flexibility and the thermal comfort in the building. A setpoint modulation of 2 °C as a control strategy during a downward DR event is probably acceptable most of the time because the thermal mass will prevent the building from actually reaching the lower setpoint. The impact of the reference scenario (constant setpoint or setback) is relatively mild on downward flexibility but strong on upward flexibility, the setback scenario providing a higher upward energy flexibility than the constant setpoint case.

The discussions about the method to characterize energy flexibility of buildings and associated KPIs as well as the sensitivity analysis in this chapter are beneficial to investigate more complex scenarios like applying MPC strategy to increase energy flexibility.

CHAPTER 4 MODEL PREDICTIVE CONTROL FRAMEWORK

The chapter details a supervisory model predictive control framework. Several scenarios associated with the framework are discussed such as modelling errors, state estimation, and parameter identification. This framework is further employed in the next two chapters to investigate its potential for energy flexibility.

4.1 Introduction

4.1.1 Literature review

Model Predictive Control (MPC) has been practically applied and theoretically investigated in chemical engineering since the 1960s (Morari & Lee, 1999) and it has drawn increasing interest lately in building engineering field (Coffey, 2013). The idea of MPC proposed for building supervisory control can be dated back as early as in 1988 (Kelly, 1988); however, it did not witness steady growing research projects until the last decade.

This phenomenon follows with a rapid increase of research publications of MPC for buildings, and it attracts attention from control researchers as well (Privara et al., 2013). The popularity of MPC is supported by the urgent needs of advanced control strategies in current engineering projects or potential challenges confronted buildings in the near future. For instance, for high performance buildings or net-zero energy buildings, integration of on-site renewable energy generation, energy management in the community scale, and interaction with smart grid such as demand response, MPC can play a vital role to achieve those goals (Coffey, Haghighat, Morofsky, & Kutrowski, 2010; Henze, 2013).

Prior to the MPC application in the building field, James Braun and his team worked on related optimal control for demand limiting since 1990. Their first work investigated optimal control of a cooling system in a commercial building (Braun, 1990). To model the thermal zones of the building, a simple discrete-time polynomial model proposed by (Seem et al. 1989) was adopted. Parameters were identified with data generated from a detailed TRNSYS model by minimizing least squares errors. The components of the cooling plant were modelled using empirical regression equations. The simulation results found the optimal setpoint profile for zone temperature, mode of operation for air handlers and supply air temperature setpoint trajectory.

Following these papers, a review of the state-of-the-art load control studies was conducted with the conclusion that both computer simulation and field test at that time were in a preliminary stage with few findings (Braun, 2003).

Another type of simplified model for the demand control purpose was also investigated (Braun & Chaturvedi, 2002). The new model was based on an RC network, whose parameters were identified using measured data. The RC network model was applied on two following papers (Lee & Braun, 2006b, 2008b), where the building was modelled by a 10^{th}-order RC network model. In those two papers, a constant cooling rate was optimized to maintain the zone temperature within the thermal comfort boundary during peak time. When the target cooling load was reached, the setpoint temperature would increase to limit the cooling load below the target. The target cooling load was further adjusted so that the zone temperature reached the upper bound of thermal comfort at the end of the occupied time. In such a way, an optimal setpoint profile was acquired. The optimal precooling starting time was also investigated.

Experimental work was conducted to validate the simulation outcomes (Lee & Braun, 2006a, 2008b). Results showed 30% reductions in peak cooling loads with a little thermal uncomfortableness in the morning due to precooling. Another experiment was carried out with less aggressive setpoint changing, leading to better thermal comfort.

To investigate the manipulation of setpoint temperature trajectory, Braun & Lee (2006) proposed a simple algorithm to obtain the optimal setpoint profile based on a first-order building model. A relation was proposed between the setpoint and 3 variables: effective time constant which can be estimated using experiment; demand-limiting duration which can be obtained or set up; and the cooling starting time. Since the first two variables are known constants, the setpoint temperature only changes with cooling starting time. This simple algorithm was applied to a small commercial building in different regions of California, USA. It should be noted that the setpoint temperature was assumed to equal zone temperature in the research, which might be an issue. Another questionable assumption was the zero air thermal mass in each zone.

Following the same idea, three heuristic methods for optimal setpoint trajectory were proposed (Lee & Braun, 2006b, 2008a). The first two methods “semi-analytical” and “exponential setpoint equation-based semi-analytical” were based on the same first-order RC network model mentioned above and the same assumption that setpoint temperature equals zone temperature,

while the third method “load weighted-averaging” was based on a data-driven black-box model. The main difference among these three methods was the requirement of input data. Companion papers assessed the application of the three methods on different sizes of commercial buildings (Lee & Braun, 2006c, 2008a). All three methods showed promising peak demand reduction capabilities, while the last method provided a slightly better performance with an easier implementation.

The heuristic method has also been studied by (J. A. Candanedo, Dehkordi, Saberi-Derakhtenjani, & Athienitis, 2015), which focused on the transition period between two constant temperature setpoints specifically. The two constant temperature setpoints were assumed to be known in advance due to the fact that the thermal comfort must be within a minimum and maximum temperature range. Global Optimization Toolbox in Matlab was used to find the sequence of the intermediate setpoints yielding the smallest load. A general formulation of the setpoint trajectory was proposed, which was expressed by a single “curvature” parameter. The parameter was a function of another two parameters: building time constant and user-required transition time. The former may be not easy to estimate. This approach was more suitable for a programmable thermostat given that several parameters must be known or set up in advance such as the temperature oscillation boundary and transition time periods. Note that it was not a predictive controller.

Most studies in demand limiting control in the literature focused on space cooling in commercial buildings. The heating system in residential buildings was considered through several studies by the team from the Laboratoire des technologies de l’énergie (LTE) at Hydro-Quebec.

Using TRNSYS simulation, Leduc, Daoud, & Le Bel (2011) studied three main load control strategies: setback, preheating and power limitation. A useful concept Reset Ratio (RR) was proposed to quantify the power rebound effect after the load control strategy because the possible demand rebound may cause new peaks. This indicator was also adopted in the paper by (J. A. Candanedo et al., 2015). Fournier & Leduc (2014) tested the setpoint modulation strategy in the twin houses test bench built at the LTE sites. Date, Athienitis, & Fournier (2015) studied different temperature profiles considering different levels of thermal mass, both theoretically and experimentally. It was found that floor coverings would impact the demand response strategy because floor coverings would increase the thermal mass, and one or two-hour temperature ramp

could reduce the peak demand up to 10% to 20% by simply replacing the night setback temperature profile.

The Henze team from the University of Colorado at Boulder investigated MPC on ice storage tank and building thermal mass in a variety of studies (Henze et al., 2005; Henze, Felsmann, & Knabe, 2004). MPC application on window operation for mixed natural and mechanical ventilation was also studied in an office building by the team (Corbin, Henze, & May-Ostendorp, 2013; May-Ostendorp, Henze, Corbin, Rajagopalan, & Felsmann, 2011).

MPC applications on Variable Air Volume (VAV) systems were studied by (Nassif, Kajl, & Sabourin, 2005a, 2005b; Wang & Jin, 2000). Other systems were also discussed in the Model Predictive Control in Buildings workshop in Canada in 2011 and related papers were published later such as thermally activated building system with ground coupled heat pump (Sourbron, Verhelst, & Helsen, 2012) and chiller and cooling tower system (Y. Ma, Borrelli, Hencey, Packard, & Bortoff, 2009).

Plenty of industrial and academic MPC tools and techniques have been developed, e.g., the MPC toolbox in Matlab is very powerful (Bemporad, Morari, & Ricker, 2015). Nonetheless, the developed theories and methods, techniques and tools, as well as practical experiences were meant for their own contexts, which are not necessarily suitable for the building industry. The applicability of the existing MPC theory cannot be easily extended to the building engineering domain.

Offset-free tracking is a common topic in the MPC control theory, where the objective of the MPC controller is to track the given reference signal as close as possible. Certain performance indicators or design parameters are used to quantify the controller performance, such as overshoot percentage and settling time. For the case of room temperature in buildings, this assumption of tracking reference signal (setpoint temperature) may not be suitable, because the thermal comfort can allow setpoint ranges instead of a constant value. System stability composes of a big section of the MPC discussion when formulating the prediction, which may be minor for the room temperature regulation (Camacho & Bordons, 2007; Rawlings & Mayne, 2012; Rossiter, 2003).

Another important area in the control domain is the discussion of disturbances. A common assumption is to incorporate a term of white Gaussian noise in the equation of input, output or

both, to compensate for measurement errors. However, for building control, the foremost disturbance comes from weather and/or building users, which cannot usually be assumed to be white noise. The daily and seasonal variations of weather and occupants have a strong impact on the building thermal behaviour.

4.1.2 Objective

To address the gap from MPC theory to the application on buildings, the aim of this chapter is to describe a simple approach to apply MPC on building simulations. It introduces the MPC concept and illustrates what MPC is and how it works for supervisory control. It demonstrates how to implement the MPC technique step by step from the perspective of building energy modellers. Simple examples are given herein with results analysis. This may be helpful for building energy modellers who are interested in this topic but not familiar with it.

Three scenarios are discussed in this work, i.e., MPC without model mismatch, MPC with online parameter identification and MPC with state estimation. The study also investigates the optimization results in detail for each scenario. Examples corresponding to each scenario are explained. Complex applications can be implemented based on the proposed approach and given examples.

4.2 Methodology

4.2.1 Supervisory control

Many MPC frameworks in the literature dedicated to local control (J. Candanedo, Dehkordi, & Lopez, 2013), where the MPC controller interacts directly with actuators or HVAC systems. This is a common approach in the control studies, for example, the offset-free tracking discussed in Section 4.1 takes such an approach.

In this work, we present a simple scheme of MPC for supervisory control. In this method, the MPC works at the supervisory level, where it computes the optimal signal for the local controllers or actuators. Figure 4.1 shows an example of thermostatic temperature control with supervisory control. At the top level, the supervisory MPC computes the optimal setpoint based on its own model predictions, and then sends the control sequence to the thermostat. The thermostat compares the feedback temperature from the zone and decides whether or not

activates the HVAC system by its own control logic. In such a way, the existing local controller does not need to be replaced.

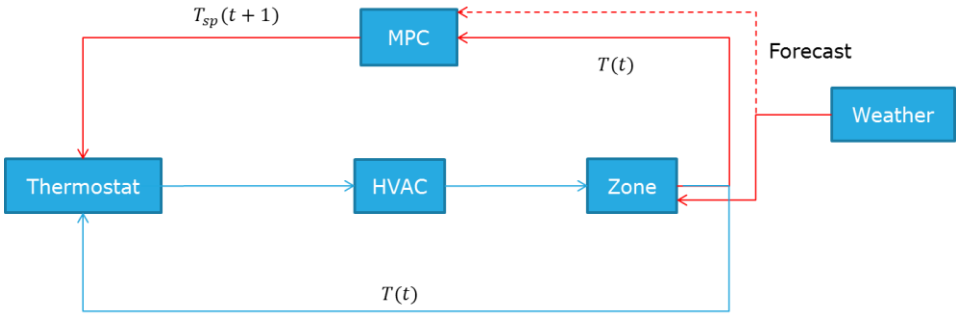

Figure 4.1: MPC scheme for supervisory control

In summary, the difference between local and supervisory control depends on where the reference signal comes from. In the supervisory control, the reference signal comes from the high-level MPC, while in the local control the reference signal is user-defined. For the implementation of the supervisory MPC in reality, the optimal reference signal can have the option to be overridden by users if necessary.

4.2.2 MPC implementation

There are many different ways to implement MPC in building simulation tools. This work adopts the method of co-simulation: the virtual buildings implemented in a Building Performance Simulation (BPS) tool with the MPC controller in another environment. This work uses co-simulation between TRNSYS and Matlab; but the BPS tool can be other programs such as EnergyPlus, ESP-r etc.

The co-simulation, in this case, allows the two programs to communicate with each other iteratively, which mimics the online control fashion in the real world. The Matlab component Type 155 from the TRNSYS library is useful for this realization (using BCVTB (Wetter, 2011) is another way), where at each time step or defined duration of time steps the controller in Matlab sends an optimal control signal to TRNSYS, while the latter sends feedback signal instantly to the former.

4.2.3 Example building and control context

To explain the procedure simply, we use an example building and a representative context to develop the idea of the study. We consider a 2-zone building inspired by the two BESTEST suite cases: Case 900 and Case 600 (Henninger & Witte, 2004). Case 900, a heavy-weight room, represents Zone 1. Case 600, a light-weight room adjacent to Zone 1, represents Zone 2. Figure 4.2 displays a sketch of the two-zone building. The window areas of both zones are reduced to 4 square meters and the internal gains for Zone 2 is modified to 200 Watts.

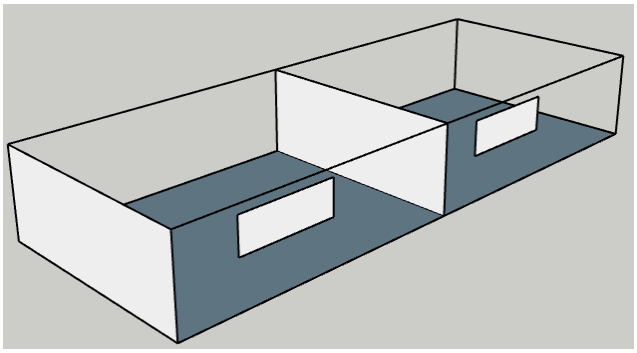

Figure 4.2: Sketch of an example 2-zone building

The control objective is to minimize energy consumption with time-of-use power price and the control signal is the optimal setpoint temperature for the thermostat in the Zone 1. We suppose Zone 2 is uncontrolled for the ease of explanation for state estimation later. Peak periods are assumed to be 5:30~9:30 and 16:30~20:30 with off-peak times for the rest hours. The two yellow bars in Figure 4.5 represent the two peak periods when its power price is twice the off-peak price.

We use the CWEC weather data file for Montreal (Numerical Logics, 1999), where space heating is dominated. Assuming this is a residential building with actively occupied time from 6:30 to 8:00 and from 16:30 to 22:00, when the thermal comfort range in winter is assumed to be 20~23 °C. When the building is not occupied during the rest hours of the day, the thermal comfort range is 18~25 °C. The green dash-dotted curves in Figure 4.5 represent the comfort ranges at different hours of a day. Note that the weather and occupancy forecast is not addressed in this chapter, which may deserve investigation separately. In this work, the disturbance from the weather and occupancy is assumed to be known. In a real-world implementation, the weather forecast can be obtained from the Internet conveniently.

4.3 MPC without model mismatch

The work of modelling accounts for half of the workload for MPC and model mismatch is often referred as one of the reasons when analyzing the imperfection of the model-based optimal controllers in the past studies (Morari & Lee, 1999). This argument can be reasonable because real systems are often much more complicated than models, which makes it difficult to consider all the nonlinearities and uncertainties associated with the physical system.

For this reason, we first investigate an MPC without model mismatch. This can be easily realized in computer simulation by using an identical model for the controlled system and the controller. In such a way, we can assess the controller performance by excluding the impact of modelling errors. It indicates the best performance the controller can deliver under perfect circumstances. It is also beneficial to investigate issues such as the optimization accuracy which may occur to certain algorithms. In addition, it helps to test the effectiveness of our MPC approach before beginning to analyze potential errors or mistakes.

4.3.1 Modelling

To have the same model in TRNSYS and Matlab, we consider a lumped-capacitance building model of second order, where each zone is represented by 1 node. Type 660 in TRNSYS is such a model ready for use. To simplify the illustration, the moisture balance of each zone is not considered; therefore only heat balance is treated here. However, the moisture equations can be added to the model in the same fashion if needed.

To neglect the moisture impact, we set all parameters and variables of absolute humidity identical in TRNSYS to keep moisture constant. We then need to develop a lumped-capacitance model for the controller in Matlab. The governing heat balance equation for each zone can be written as:

$$C_{p1}\dot{T}_1 = UA_1(T_a - T_1) + m_{sa1}c_{pa1}(T_{sa1} - T_1) + m_{inf1}\,c_{pa1}(T_a - T_1) + U_p(T_2 - T_1) + Q_{sg1} + Q_{ig1} + Q_{h1} \quad (4.1)$$

$$C_{p2}\dot{T}_2 = UA_2(T_a - T_2) + m_{sa2}c_{pa2}(T_{sa2} - T_2) + m_{inf2}\,c_{pa2}(T_a - T_2) + U_p(T_1 - T_2) + Q_{sg2} + Q_{ig2} + Q_{h2} \quad (4.2)$$

The left side of the two equations are thermal storage in each zone; the right side are respectively heat loss through building envelope, ventilation heat injection, infiltration heat loss, solar gains, internal gains, heat transfer between two zones, and heating rate from the heating system. If we present the model in Resistance-Capacitance (RC) network, the diagram can be drawn as below.

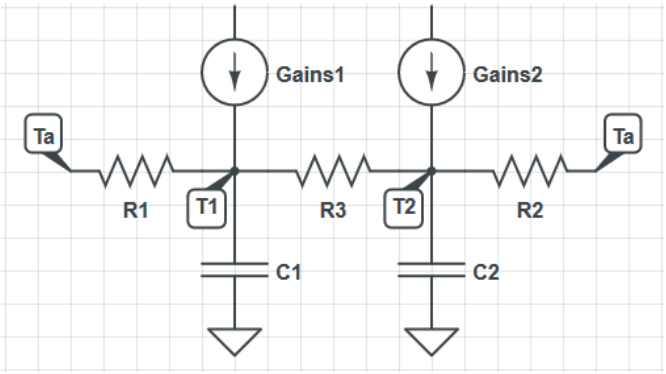

Figure 4.3: RC network of the lumped-capacitance model

The thermal capacities and overall heat loss coefficients are assumed constant in our system. The specific air capacity c_{pa} is a property of air and suppose the ventilation flowrate m_{sa} is known. Regard the two zone temperatures as the states $T(t) = \begin{bmatrix} T_1(t) \\ T_2(t) \end{bmatrix}$, Q_h the controlled input $u(t)$, T_{sa}, T_a, Q_{sg} and Q_{ig} the uncontrolled but measured inputs. Suppose the output that we are interested in is $T_1(t)$, then we can rewrite the equations using state space representation:

$$\begin{cases} \dot{T}(t) = A_c T(t) + B_c u(t) + E_c w(t) \\ y = C_c T(t) \end{cases} \tag{4.3}$$

$$A_c = \begin{bmatrix} \dfrac{UA_1 + m_{sa1}c_{pa1} + m_{inf1}\,c_{pa1} + U_p}{C_{p1}} & \dfrac{U_p}{C_{p1}} \\ \dfrac{U_p}{C_{p2}} & \dfrac{UA_2 + m_{sa2}c_{pa2} + m_{inf2}c_{pa2} + U_p}{C_{p2}} \end{bmatrix}$$

$$B_c = \begin{bmatrix} \frac{1}{C_{p1}} & 0 \\ 0 & \frac{1}{C_{p2}} \end{bmatrix}, u(t) = \begin{bmatrix} Q_{h1} \\ Q_{h2} \end{bmatrix}, w(t) = \begin{bmatrix} T_{sa1} \\ T_{sa2} \\ T_a \\ Q_{sg1} \\ Q_{sg2} \\ Q_{ig1} \\ Q_{ig2} \end{bmatrix}, C_c = [1 \quad 0]$$

$$E_c = \begin{bmatrix} \frac{m_{sa1}c_{pa1}}{C_{p1}} & 0 & \frac{UA_1 + m_{inf1}\,c_{pa1}}{C_{p1}} & \frac{1}{C_{p1}} & 0 & \frac{1}{C_{p1}} & 0 \\ 0 & \frac{m_{sa2}c_{pa2}}{C_{p2}} & \frac{UA_2 + m_{inf2}\,c_{pa2}}{C_{p2}} & 0 & \frac{1}{C_{p2}} & 0 & \frac{1}{C_{p2}} \end{bmatrix}$$

We separate the controlled input with uncontrolled inputs for easier formulation of the objective function, which will be discussed soon. We input the same parameters in TRNSYS and Matlab; then we validate whether Matlab gives the same results as TRNSYS. Figure 4.4 shows the free-floating room temperatures of the two zones from the controller model in Matlab and the system model in TRNSYS for the first two days (ventilation rate is assumed to be 0). We can see that both models give exactly identical outputs (Matlab results are hidden by TRNSYS). Identical results for a longer duration under different weather conditions are omitted here.

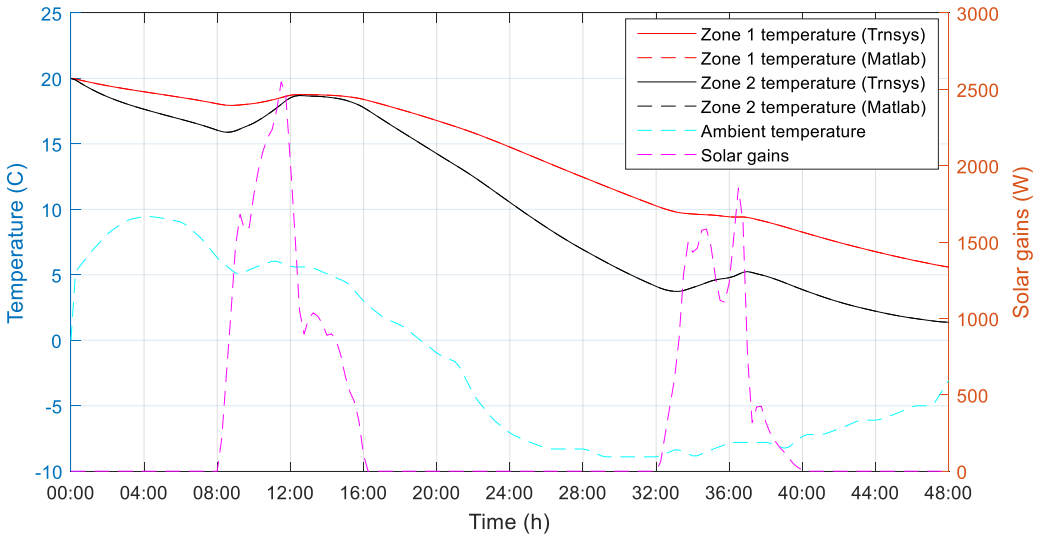

Figure 4.4: Validation of the controller model in Matlab

In order to get the same results, we need to pay attention to the TNRSYS outputs, where all values are averaged within each time step to perform better energy balance. Therefore we also need to calculate the average solutions of the differential state equation in Matlab. Details about the average solutions can be found in Appendix A.

4.3.2 Objective function formulation

Our MPC approach is divided into two steps: deriving predictive output and then finding the optimal control trajectory. The predictive output is intuitive to obtain by using a discretized state

equation. The Appendix A includes how to formulate the predictive output with unspecified prediction and control horizon. The predictive output can be formulated in the following equation

$$Y(t) = A_p T(t) + B_p U(t) + E_p W(t) \tag{4.4}$$

$Y(t)$ is the vector of predictive outputs; A_p, B_p, E_p are the predictive matrices; $T(t)$ is the feedback state; $U(t)$ is the vector of future controlled input; $W(t)$ is the forecast of disturbances.

The optimization toolbox in Matlab generally takes three types of constraints: inequality and equality equations, as well as upper and lower bounds for the optimization variables. In our optimization problem, the predictive output should stay within the variable comfort range $[Y_{min}, Y_{max}]$; that is

$$Y_{min} \leq A_p T(t) + B_p U(t) + E_p W(t) \leq Y_{max} \tag{4.5}$$

We transform the above inequalities as an expression of our optimization variable $U(t)$ as below:

$$A_{ineq} U(t) \leq b_{ineq} \tag{4.6}$$

With $A_{ineq} = \left[-B_p; B_p\right]$, $b_{ineq} = [-Y_{min} + A_p T(t) + E_p W; Y_{max} - A_p T(t) - E_p W]$

The bounds for the controlled input are the physical range of the input. It should be noted that the constraints applied here are quite stringent for the optimization. Cases with looser constraints would be easier to converge for the optimization algorithm.

The control objective is to reduce power cost with time-of-use price, thus we can formulate the objective function as a function of the optimization variable $U(t)$, the vector of future controlled input. A simple objective function can be written in a linear form as

$$J = f^T U(t) \tag{4.7}$$

f is a vector of power prices in the control horizon. Other forms of objective function can also be formulated such as the commonly-used quadratic function which guarantees convexity. The function “fmincon” in Matlab optimization library allows free-form nonlinear objective function and constraints. In our case here, the linear programming function “linprog” is selected to solve the problem because of its simplicity and efficiency. The linear programming solves optimization

problems whose objective function, equality and inequality constraints are all linear. These linear requirements may not be applicable for many cases but suitable for the demonstrative purpose here.

There are three algorithms available for the “linprog” function in Matlab, in which the “interior-point” is chosen for the study. This method searches solutions in the interior of the feasible region. A barrier parameter is adapted in each iteration to approach the minimum of the objective function. The algorithm may yield slightly less accurate solutions compared with other algorithms, but it is capable to solve both large-scale and small-scale problems efficiently (Nocedal & Wright, 2006).

4.3.3 Optimal control solution

The parameters for the lumped-capacitance model are obtained from the BESTEST Cases report; the overall heat loss coefficients and capacitances are derived by summing the construction properties. As mentioned previously, only Zone 1 is controlled with idealized heating. Zone 2 is not controlled without any heating system. If our MPC method works well, we can anticipate that more power will be used to preheat the building during off-peak periods so that less power will be needed during peak times.

Figure 4.5 shows the optimal control results for one day. We can see that the system temperatures of the two zones (represented by TRNSYS) are exactly the same as the temperatures from the controller (represented by Matlab) due to identical modelling. The optimal setpoint for Zone 1 is not included in the Figure because it is the same as the room temperature. During the off-peak time, the heating power is kept minimum until the last moment for preheating; then maximum heating power is used until the arrival of peak time. Zero heating power is used during the two peak periods. From 20:30 to 22:00, the necessary heating power is provided to maintain the room temperature at the lower bound of the thermal comfort. We have thus confirmed that the control signal (setpoint temperature) determined by our MPC method is optimal, where no extra heat is used to further increase the room temperature, as higher room temperature would lead to higher heat losses.

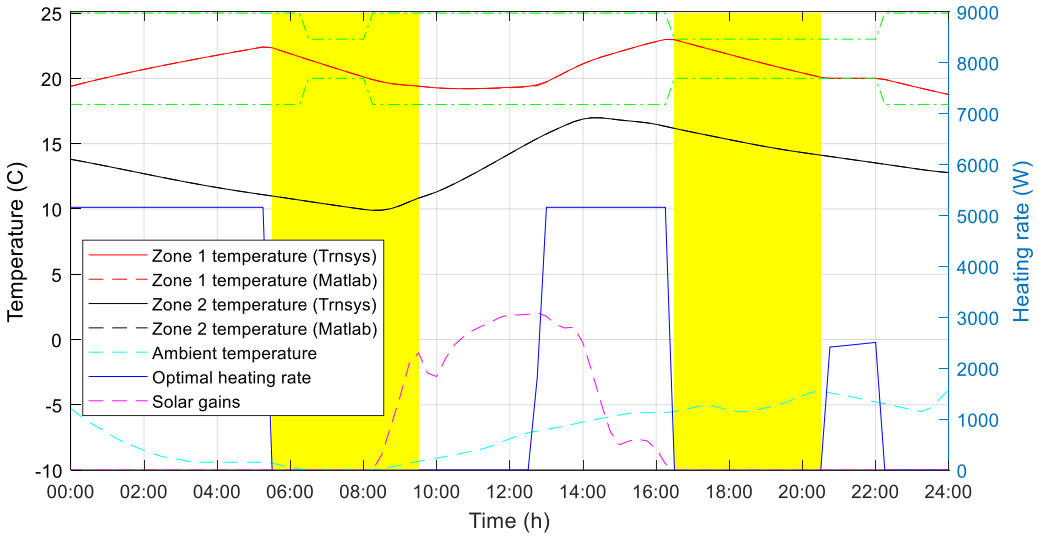

Figure 4.5: MPC results without model mismatch

4.3.4 Receding horizon control

MPC is a type of receding horizon control. At each time step, the controller predicts future outputs within the prediction window, sends optimal signals to the system and receives feedback from the system; then this process moves forward to a next iteration. This mechanism gives the phenomenon of a receding horizon. Figure 4.6 clearly represents this phenomenon, which shows the predictive temperature profiles from 4:00 to 18:00 with a 12-hour prediction horizon. The temperatures before 15:00 predicted at different time steps are actually identical to each other. They are spread out in the figure for better visualization. We can find that as the prediction horizon approaches the peak time at 16:30, the controller starts to correct the predictive temperatures from 4:45 on and this correction continues as time moves closer and closer to the critical periods. In such a manner, the optimal setpoint temperature is found out by the algorithm along a receding horizon. This prediction and correction process perfectly present the main advantage of the modelled-based optimal control.

The results shown in the above two figures have validated our proposed MPC approach. The co-simulation shows a fast convergence of the selected algorithm. The approach delivers exactly the optimal control trajectories when no model mismatch exists between the system and the controller model. This can help us to assess the MPC with a model mismatch in the following sections.

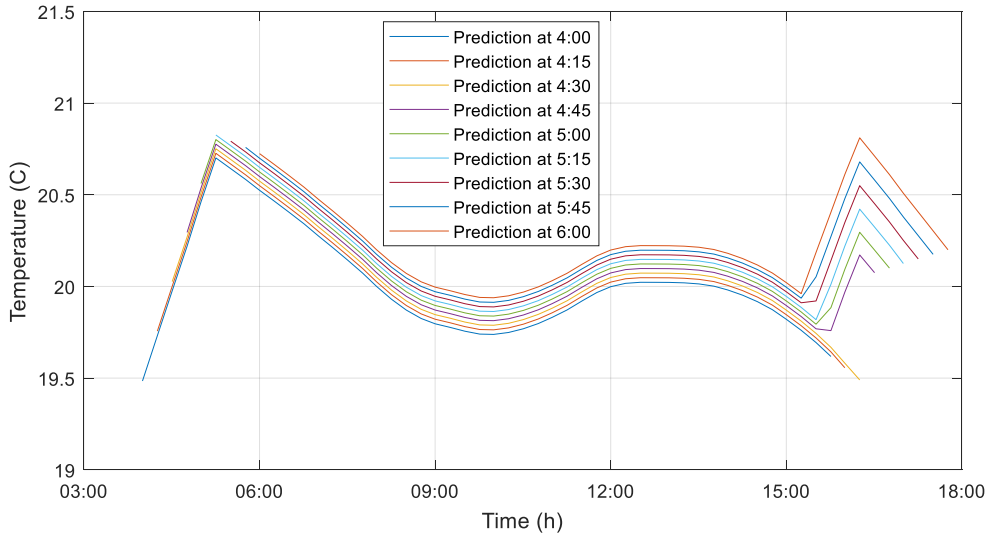

Figure 4.6: The predictive temperature at each time step (15 min)

4.4 MPC with online parameter identification

Parameter estimation or system identification in the literature generally deals with offline identification (Žáčeková, Váňa, & Cigler, 2014). Offline identification has the advantage of collecting a large amount of data beforehand and adopting computationally-intensive and time-consuming algorithms, which is commonly seen in the machine learning functions. In this offline process, iterative try and error can be employed until reasonable parameters or models are obtained.

In this section, we present a method to implement online parameter identification, which uses a simple approach called recursive least squares. It does not require a lot of data nor time for the training or learning process, and the parameters can be identified very quickly with acceptable accuracy. With the co-simulation structure to represent online control as described previously, the method is particularly suitable.

For the virtual building in TRNSYS, we build a detailed two-zone building model using Type 56. Unlike the lumped-capacitance model Type 660 used in Section 4.3, the building model in Type 56 constructs all the layers of walls, floors, and ceilings with their physical properties such as density, conductivity and specific capacitance as well as detailed window models. The outputs from this model are used as “measured” data for parameter identification in Matlab.

4.4.1 Parameterization of the state equation

To implement the online parameter identification, we first need to discretize and parameterize the state equation (4.1) into the following form:

$$T_1(t+1) - T_1(t) = \left\{ \frac{UA_1 + m_{inf1}\, c_{pa1}}{C_{p1}} [T_a(t) - T_1(t)] + \frac{m_{sa1} c_{pa1}}{C_{p1}} [T_{sa1}(t) - T_1(t)] + \frac{U_p}{C_{p1}} [T_2(t) - T_1(t)] + \frac{\alpha_1}{C_{p1}} Q_{sr1}(t) + \frac{1}{C_{p1}} [Q_{ig1}(t) + Q_{h1}(t)] \right\} dt \quad (4.8)$$

Equation (4.8) is a discretized form of Equation (4.1) using the forward Euler method. The parameter α_1 is introduced as a coefficient for the total (beam and diffuse) solar radiation incident on the window surface. We can rewrite the equation (4.8) as

$$y_1(t) = \Phi_1(t-1)\theta_1 \quad (4.9)$$

with $y_1(t) = T_1(t) - T_1(t-1)$, $\Phi_1{}^T(t-1) = \begin{bmatrix} [T_a(t-1) - T_1(t-1)]dt \\ [T_{sa1}(t-1) - T_1(t-1)]dt \\ [T_2(t-1) - T_1(t-1)]dt \\ Q_{sg1}(t-1)dt \\ [Q_{ig1}(t-1) + Q_{h1}(t-1)]dt \end{bmatrix}$ and $\theta_1{}^T = \begin{bmatrix} \frac{UA_1 + m_{inf1}\, c_{pa1}}{C_{p1}} & \frac{m_{sa1} c_{pa1}}{C_{p1}} & \frac{U_p}{C_{p1}} & \frac{\alpha}{C_{p1}} & \frac{1}{C_{p1}} \end{bmatrix}$.

θ_1 is the parameter vector and we assume it is constant. The vector $\Phi_1(t)$ is called regressor and we can find that the variables in the regressor and the output $y_1(t)$ are all measurable. Using the least squares method, we can solve the parameter vector as

$$\theta_1 = R_1(t)^{-1} S_1(t) \quad (4.10)$$

With $S_1(t) = \sum_{t=1}^{N} \Phi_1(t-1) y_1(t)$ and $R_1(t) = \sum_{t=1}^{N} \Phi_1(t-1)^T \Phi_1(t-1)$. $S_1(t)$ is the summation of cross-correlation between past inputs and outputs during N series and $R_1(t)$ is the summation of the auto-correlation of the past inputs. Details about how the parameter vector is solved can be found in the Appendix A. And we can similarly estimate the parameters for Zone 2. The function “recursiveLS” in Matlab is a handy function to use to estimate the parameters. The most important parameter of the function is the number of parameters to estimate. It includes a

white noise term in the regression model to compensate for disturbances such as measurement errors. The function also provides several algorithms as options, each of which derives the parameter vector in a robust way by ensuring the covariance matrix to be positive-definite during the updating process. The default algorithm is called “forgetting factor” with a value of 1, which corresponds to “no forgetting” for all the past inputs and outputs. It is suitable for estimating constant parameters of a model.

4.4.2 MPC with identified parameters

After a two-day identification process, the parameters are subsequently used in the model for control. The predictive output and objective function are formulated in the same manner as discussed in Section 4.3.

Figure 4.7 presents the optimal setpoint temperature for Zone 1 shown by the red solid curve. We can see that the controller tries to preheat the building before the peak times by increasing the setpoint. Then during the peak periods, the setpoint drops to the lower bound of thermal comfort. The controller uses the maximum power before the peak times and no power during peak periods based on its own model shown by the blue dotted curve. Instead, the virtual building does not provide maximum power before the arrival of peak time and certain power is still used during the peak periods to maintain the setpoint temperature (see blue solid curve), due to the model discrepancy from the controller.

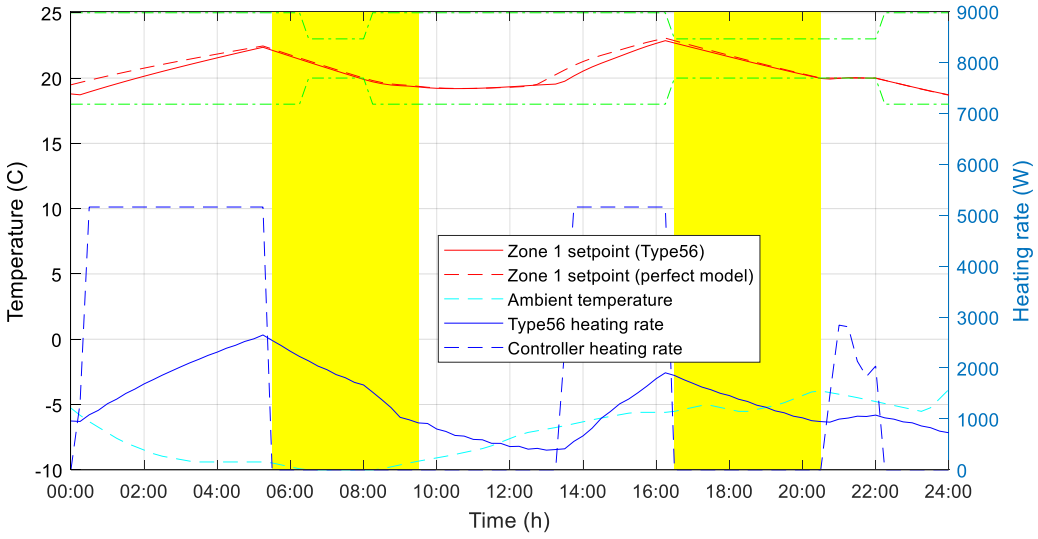

Figure 4.7: MPC results with parameter estimation (Zone 1)

If we compare the optimal setpoint temperature with the case of no model mismatch discussed in Section 4.3 (shown by red dotted curve), we can find that the two optimal setpoint profile are quite close to each other. This shows that the controller has proposed a near-optimal result based on its model with estimated parameters.

Checking the temperature of Zone 2 further proves that the controller model predicts the zone temperature fairly well. Figure 4.8 shows the estimated temperature of Zone 2 in Matlab and the "measured" temperature in TRNSYS on the same day as shown previously. The maximum discrepancy between the two temperatures is within 1 °C, which is mainly caused by the underestimation of solar gains. This relatively good performance of our controller is associated with its structure. Firstly, the controller updates its prediction at each time step by taking the feedback temperature from the virtual building. Secondly, the formulation of parameters and regressors in the identification process is taking the zone temperatures as outputs. Therefore, it can predict the temperatures better than the heating rate. If the heating rate is also taken as one of the outputs, the controller model would be more likely to deliver a better estimation.

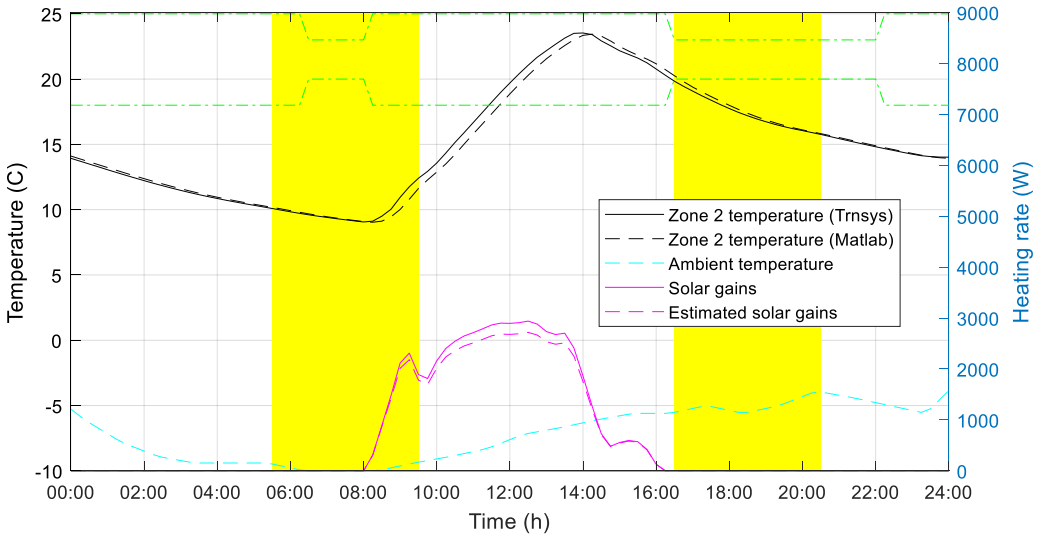

Figure 4.8: MPC results with parameter estimation (Zone 2)

Note that this result is based on an online parameter estimator with identification data of only two days. If more data is used for the identification process, or we take the approach of offline system identification, we could get a better model for the controller. However, this can be an independent study and is beyond the scope of this work.

4.5 MPC with state estimation

State estimation is not uncommon in the design of model predictive controllers because not all states are always available or measurable, for instance, the wall temperature can be an important state in some situations, but not necessarily measured or measurable. Other times, measuring all the states is just not a good solution when there are too many, which may be costly or difficult to manage. In those cases, we can design a model predictive controller with a state estimator.

4.5.1 State estimator

In this example case, the output is again the Zone 1 temperature while the Zone 2 temperature is the unmeasured state that we are supposed to estimate. The estimator we adopt is called Luenberger observer. In the implementation, we estimate the temperatures of both zones in the observer in Matlab, but Zone 1 has a state feedback while Zone 2 does not. This approach is called the full-order Luenberger observer. A reduced-order observer that eliminates the known state (Zone 1 temperature) can be found in (Wu & Duan, 2004).

The idea of this simple observer is to place the poles of the observer where it can converge faster than the original system. We need to find the system poles, which are the eigenvalues of the matrix A_c in the state space representation. After getting the system poles, we can place the observer poles where they converge faster. In general, the faster the observer poles converge, the bigger errors the observer give at the beginning (peaking phenomenon) and the more sensitive to disturbances it will be.

There are many advanced observers to reduce the peaking phenomenon, such as sliding mode control. The family of the Kalman filter is another common type of state estimator which has more attractive noise resilience property. This work adopts the Luenberger observer by considering its simplicity and ease of explanation.

4.5.2 State estimation predictive control

The controller model used for the state estimation in this section is the same as the identified model obtained in Section 4.4. After formulating the state estimator, we then use the same approach to formulate the predictive controller. Figure 4.9 shows the setpoint profile for Zone 1 with state estimation of Zone 2 temperature. It can be found that the shape of the setpoint profile

proposed by the observer-controller (red solid curve) is fairly similar to the optimal setpoint profile without any model mismatch between the system and the controller (red dotted curve). However, the virtual building still requires heating in the peak periods according to setpoint signals sent by the observer-controller, while the controller model case does not need any heating during peak times by maximizing the heating power before the peaks.

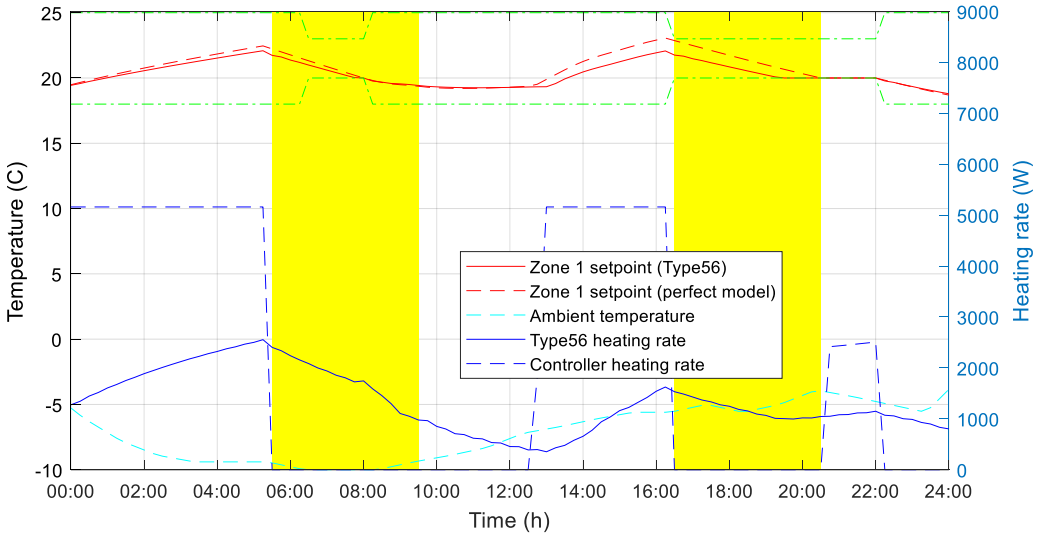

Figure 4.9: MPC results with state estimation (Zone 1)

Figure 4.10 presents the state estimation results for Zone 2. It can be easily seen that the deviation of the state estimation can be high when the solar gains are strong. The largest difference between the measured and estimated temperature of Zone 2 is around 7 degrees at 14:00 when the solar gains approach the maximum. This temperature difference remains until the evening because part of the heat is stored in the thermal mass. If we compare the solar gains with the heating rate of Zone 1, we find that their maximum power is of the same magnitude at around 3 kW. This shows that the impact of solar gains presents the highest disturbance in this example. Since Zone 2 has no heating system, a slight estimation error results in a large deviation. However, the impact of this gap does not impact the control of Zone 1 as shown in Figure 4.9.

As can be seen, the solar gains play an important role in the examples for both state and parameter estimation. This is because the two adopted BESTEST cases were initially designed to test the performance of BPS tools; therefore they are especially sensitive to weather conditions. Meanwhile, we also find that the observer presents a good performance for the control purpose.

This is due to the effect of state feedback control. And the performance can be further improved by tuning the design parameters of the observer if necessary.

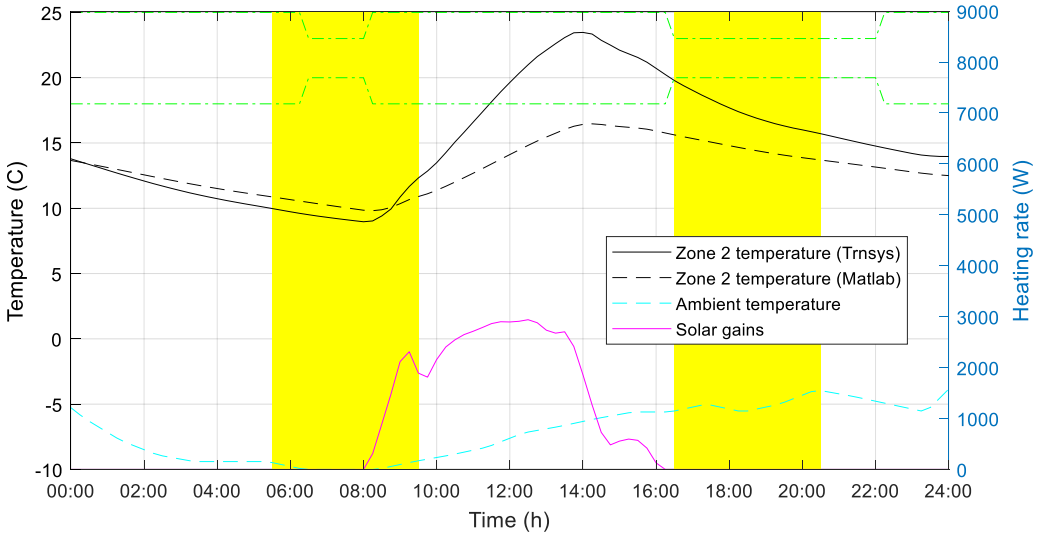

Figure 4.10: MPC results with state estimation (Zone 2)

4.6 Discussions

This chapter described an MPC framework for supervisory control. The MPC approach is especially suitable for building systems, and the chapter aims at explaining the MPC approach pedagogically for building energy modellers who are not yet familiar with this control method. Although this framework is only applied to the example buildings at the zone level, it can be applied to more complex building systems or to district-level energy systems.

Three different scenarios were investigated in this work. The first scenario “MPC without model mismatch” addressed the optimal control method theoretically. Since the identical model is used for the controller and the controlled system, it is easy to identify the potential error occurring in the optimization process. Simple optimization function from Matlab was used in order to better examine the optimization results and interpret them physically. This often becomes difficult as increasingly complicated optimization or machine learning algorithms are applied in the research.

The online parameter identification method showcased the capability of the MPC framework without accurate models or lack of data to identify models offline. The latter can be a problem for data-driven models. The last scenario discussed a state estimator coupled with the MPC method.

State estimation may be useful for state space models and state feedback systems. Each scenario comes with simple examples and the results are analyzed.

The same MPC framework is applied on the CCHT house in Chapter 6.

CHAPTER 5 MODEL PREDICTIVE CONTROL WITH DETAILED MODEL

The present chapter investigates the Model Predictive Control (MPC) method using a detailed building model as the controller model. The MPC potential for energy flexibility is presented for two separate scenarios: independent single Demand Response (DR) event and two consecutive DR events. Heuristic MPC methods are explored in order to save computation cost associated with optimizing the detailed building model.

5.1 Introduction

5.1.1 Literature review

Among the research issues in MPC on buildings, the foremost is the choice of building models, which determines the effectiveness and efficiency of control strategies. The main building models utilized by researchers can be divided into three categories: white box, grey box, and black box. Note that this nomenclature does not necessarily reflect its corresponding literal meaning, nor should they be confused with that used in the domain of system identification.

The first model type, often referred to as physical models, can be built by Building Performance Simulation programs such as EnergyPlus, TRNSYS, and ESP-r. The second type is often represented by RC network models, which go in between the white-box and black-box models. It is simpler than the white-box models and may be able to be physically interpreted to a certain degree. The third type is also called a data-driven model. It mainly relies on data to construct models whose parameters cannot be explained from the building physics perspective. Machine learning models are typically black-box. This section reviews papers with white-box or physical models; the other two types are included in Section 6.1.

The white-box model describes a building in details based on first principles of building physics. Based on physical parameters and thermodynamic laws familiar to building engineers, the white-box model is a very intuitive representation of buildings, for example, information about geometry and materials of building construction are required for this type of model. Thus it allows building engineers easily to use, understand, analyze or even redevelop them. However, because of a large amount of input information, it suffers from the complexity of model

construction (Privara et al., 2013; Prívara, Váňa, Žáčeková, & Cigler, 2012). In addition, it causes difficulty in real-time control application due to its high computation cost and difficulty of state estimation and parameter identification.

Because of their complexity and high-computation requirement, the white-box models are mostly used for offline predictive control with other optimization tools, e.g. GenOpt (Wetter, 2001). Several studies explored the "offline" control application based on the white-box model. Coffey et al. (2010) proposed a model predictive control strategy using a detailed TRNSYS building model in the controller for the purpose of peak shaving. A software framework was outlined, where the optimization work was executed externally by GenOpt with a genetic algorithm. The optimal decision was handled in another organization layer, where optimal outputs were sent to the building energy management system. May-Ostendorp et al. (2011) developed a model of a small office building in EnergyPlus, which was used for extraction of supervisory building control rules.

Besides offline control application, the white-box model is more often used to generate a synthetic database, which is further employed for system identification and validation of simplified models. Examples of this type of application are included in Section 6.1.

5.1.2 Objective

For building engineers and researchers, modelling building systems using BPS tools is a common practice. It can be interesting and convenient to test MPC with BPS tools, especially when the detailed models are already available. Although optimizing these types of models are computationally-intensive, computation services that are getting less expensive make it promising in the future. In addition, the optimization time is not that significant compared with machine learning algorithms.

The goal of this chapter is to investigate MPC based on detailed models. In this case, there is no modelling error in the controller, as the same model is used for the controlled system. Energy flexibility results based on KPIs described before are reported for this approach.

5.2 Methodology

5.2.1 KPIs adapted to MPC

Due to the anticipative capability of MPC, the KPIs for the energy flexibility may need to be adjusted. Figure 5.1 presents a theoretical downward flexibility case with the MPC strategy assuming the system knows the occurrence of the demand response event in advance. It shows that the MPC preheats the building before the event, uses energy as least as possible during the event and reheats the building to an acceptable comfort level after the event. The notations in the figure are the same as discussed in Figure 3.1 in Chapter 3.

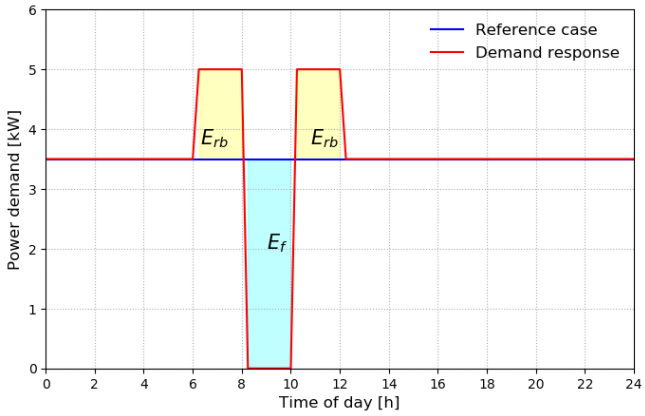

Figure 5.1: Flexible energy demand of buildings with MPC (downward flexibility)

The flexible energy E_f remains identical as Equation (3.1). The rebound energy E_{rb} needs to be adjusted to include the preconditioning energy as shown in the equation below. The flexible energy efficiency η and maximum flexible power P_{fmax} remain the same.

$$\boldsymbol{E_{rb}} = \int_{t_{dr}}^{t_{\infty}} (P_{dr} - P_{ref})dt + \int_{t_{-\infty}}^{t_{dr}} (P_{dr} - P_{ref})dt \tag{5.1}$$

The first part of Equation (6.1) is the same as Equation (3.1) indicating the possible rebound after the DR event; the second part of the equation indicates the energy consumed during the preconditioning period. The $-\infty$ is used similarly as the ∞ to denote the rebound horizon. When calculating E_{rb}, $-\infty$ can be several hours or longer depending on the preconditioning response of the MPC strategy.

5.2.2 Cost function

The optimization objective is to reduce power demand during peak hours. The cost function, in equation (5.2), represents a measure of the total power demand during the optimization horizon. The measure can be monetary cost of electricity or power for the electricity users if the time-of-use (TOU) electricity rates are used or cost for players in the electricity market if associated price signal is used.

$$J = \sum R_k U_k + \mu \left| T_k - T_{b,k} \right| \tag{5.2}$$

In this equation, the first term represents the power demand costs, where U_k denotes the power at time k. R_k denotes the price signal. This is expressed as a linear function as in Equation (4.7) in Chapter 4 but as discussed before, any other forms can be used e.g. quadratic and nonlinear form if deemed necessary.

The second term of the cost function is a penalty function which indicates certain constraints should not be jeopardized in the optimization process. In the building case, it normally means the desired temperature comfort levels. T_k denotes the zone temperature here and $T_{b,k}$ represents the thermal comfort bounds for the zone at time k. μ is the weighting factor which scales the penalty function to a close dimension of the first term. The penalty function is evaluated as zero when the room temperature is within the defined intervals but becomes much larger when the temperature does not fall within the comfort limits.

The penalty function term is described as inequality constraints in Equation (4.5) in Chapter 4. It is expressed in such a fashion here because it is easier to implement in the selected program GenOpt which is introduced in the following section.

5.2.3 Implementation

To test MPC with detailed building models, we need an easy-to-use optimization tool. In this work, we adopt the optimization program GenOpt with detailed models in TRNSYS. GenOpt is a generic program developed mainly for building system optimization with an extended library of optimization algorithms and can be used with any text-based simulation program. It is especially

useful for derivative-free optimization and does not require any specific form for the objective or cost function.

Figure 5.2 shows the interaction between TRNSYS and GenOpt in the optimization process (Quintana & Kummert, 2015). Before launching the optimization in GenOpt, templates of input and output files have been created in TRNSYS. In each optimization, GenOpt updates the variables, i.e. setpoints in this case, in the templates. GenOpt then searches for the minimal cost function value among all the optimization results.

In this study, the "Hybrid Generalized Pattern Search (GPS) Algorithm with Particle Swarm Optimization (PSO)" algorithm is employed. This algorithm first starts a global optimization using the PSO algorithm for the user-defined generations (10 generations in our case). Afterward, the hybrid algorithm launches the GPS algorithm starting from the set of variables with the lowest cost function value obtained from the PSO. The optimization process terminates when the cost function value does not further decrease on the mesh points as well as on the mesh points with reduced distance in iterations.

In this structure, the cost function is calculated inside of TRNSYS, as well as penalty function and all other constraints so that GenOpt only needs to read the designated parameters in corresponding files.

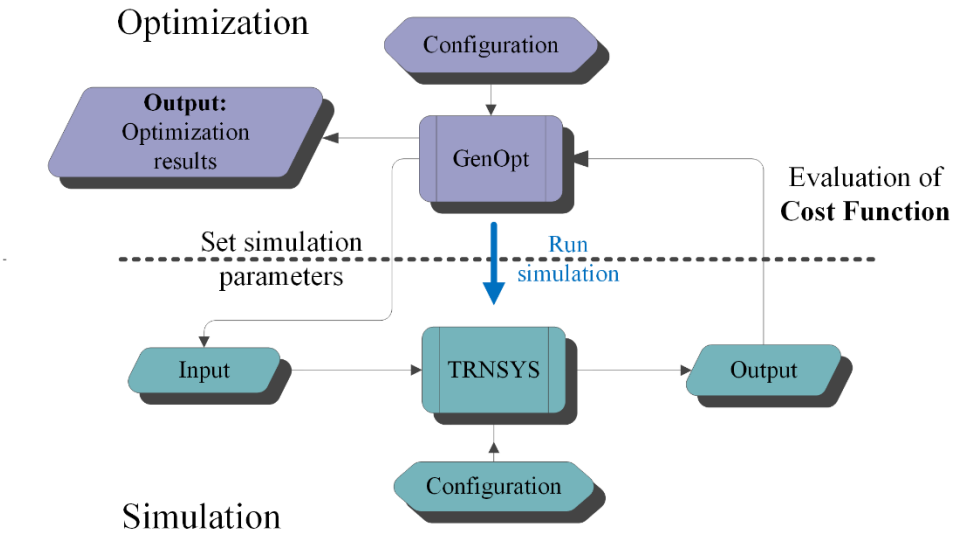

Figure 5.2: MPC scheme with TRNSYS and GenOpt (Quintana & Kummert, 2015)

The following steps detail the implementation path for the MPC strategy.

- Define optimization objectives, parameters to be optimized, constraints, assumptions for the optimization problem;
- Define the cost function that includes on-peak/off-peak electricity cost and penalties for constraints violation;
- Build a detailed model of the selected building that is used to investigate control strategies if there is not one already;
- Configure GenOpt and TRNSYS (or other BTS tools); couple the two programs for test runs so that syntactic errors can be identified;
- Check the optimization results to see if the algorithm works correctly; if not, recheck the configuration and cost function definition;
- Assess control strategies based on a reference case and compute evaluation metrics.

5.3 Results of a single DR event

The MPC results of a single downward flexibility event happening between 7 AM and 9 AM is presented in Figure 5.3 with a 15-minute time step in the simulation.

The reference setpoint in the zone is 21 °C showing by the dashed curve. The reference heating power drops suddenly at around 19 h because the dishwasher (1.7 kW) and dryer (8.1 kW) are turned on at this moment, generating thermal gains in the building. Other drops are due to one or more zones overheating because of internal or solar gains.

The thermal comfort range is assumed to be within 2 °C of the reference case for the optimal controller, the same assumption as used for the rule-based temperature modulation in Section 3.2. It is observed that the controller increases the setpoint in the zones before the event to preheat the building, as shown by the black dashed curve. The setpoint ramps up until the upper temperature bound 23 °C and stays there for half an hour; then it drops immediately during the peak periods and keeps at the minimum temperature bound of 21 °C. In result, we observe a power demand increase before the event, a dramatic power reduction during the event and a power rebound after the event. The zone temperature of the first floor, shown by the purple curve, follows the setpoint increase and decrease but is never outside the defined thermal comfort range.

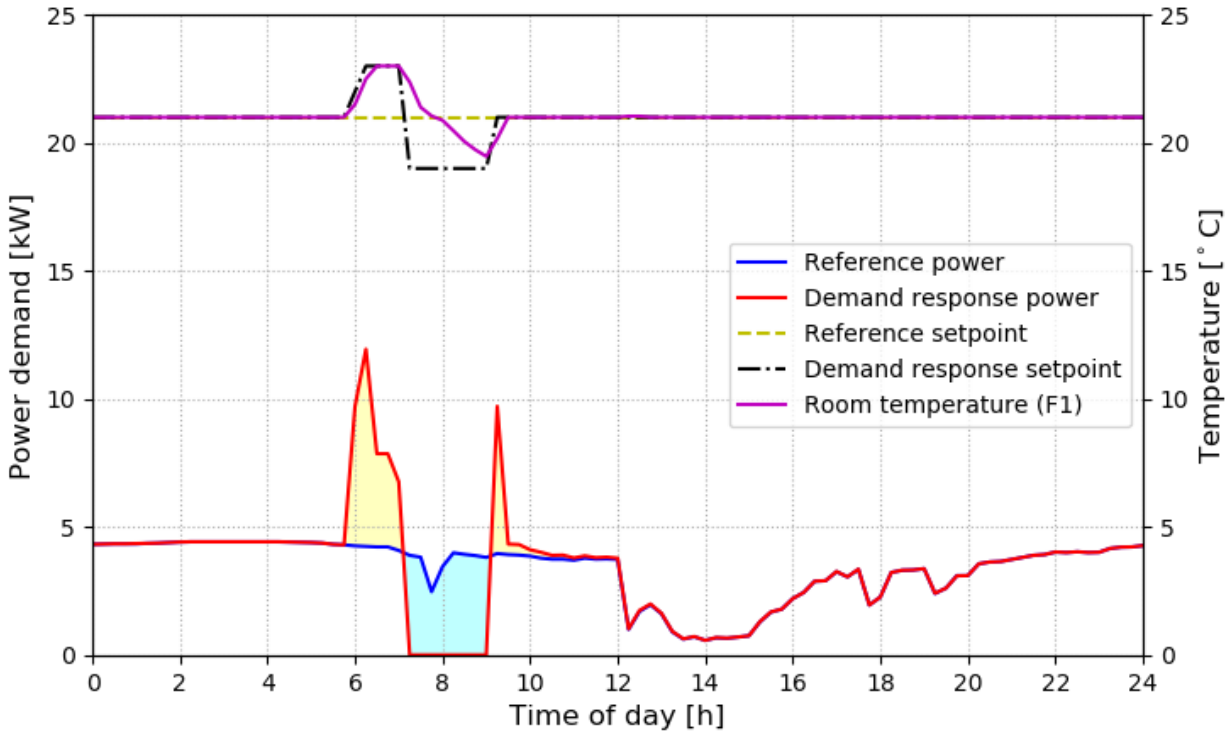

Figure 5.3: MPC results for a downward flexibility event

Table 5.1 presents the results of the flexibility indicators for both the MPC method and the rule-based control method. The RBC method modulates the setpoint temperature by 2 °C during the DR event as assumed in Chapter 3. We find that the MPC method delivers 16% more flexible energy. This shows that the anticipative capability of the MPC method is effective, given that the thermal comfort limit is the same in both cases. On the other hand, the rebound energy of MPC is also higher due to the same anticipation effect. The resulting flexible efficiency of MPC is lower than that of RBC. The maximum flexible power is identical for both methods, which reach the maximum potential.

Table 5.1: Flexibility results of MPC for a single DR event (downward flexibility)

	MPC	**RBC**
Flexible energy [kWh]	7.3	6.3
Rebound energy [kWh]	7.8	5.0
Flexible efficiency [-]	0.84	1.19
Maximum flexible power [kW]	4.0	4.0

Comparing the resulting MPC profiles of downward flexibility with those of the general upward flexibility, we find that they are quite similar in terms of variations: using more energy during the first period and saving energy in a next period. They are however two different types of DR events and the price signals in these two scenarios are very different.

5.4 Results with occupancy constraint

The MPC strategy for a signal DR event presented in the above section is a simple case. This section discusses a more realistic scenario taking into account the occupancy in the building. Two consecutive peak periods in the same day are also investigated.

The two peak periods are defined from 5:30 to 9:30 and from 16:30 to 20:30 respectively, which are typical winter daily peaks for the electric utility of Quebec (Hydro-Quebec, 2013). Here a much larger price signal is imposed for the peak periods because we try to assess the potential of peak savings for a utility, not to optimize a customer's electrical bill with a realistic TOU tariff. Electricity is not considered to be free outside of these on-peak periods but its value is significantly reduced. This price contrast is depicted in Figure 1.1 for the IESO daily power demand and price.

It is assumed that the thermostat setpoint can be adjusted between 20 °C and 23 °C when the rooms are occupied; between 18 °C and 23 °C when they are not occupied. Occupancy in the living area and basement is assumed to be the same, during a morning period (6:30 AM to 8:00 AM after the occupant wake up and before they leave the house) and an evening period (4:30 PM to 10 PM after the occupants return from school/work and before they go to their bedrooms). It is assumed that the control system is allowed to modify the setpoints in the basement and the living area of the house, but not in the bedrooms (which are also electrically heated). These assumptions for occupancy and peak durations are identical as applied in Chapter 4.

Only one day is considered in the optimization study, January 12th. The simulation is run from January 1st to January 12th to allow for building preheating, as the multizone building model Type 56 is initialized with unrealistic temperature profiles (uniform temperature across zones and building envelope) at the start of the simulation.

Uncontrolled disturbances such as weather variables (e.g. temperature, solar radiation) and internal gains (from occupants, lighting, and appliances) are considered to be known to the

optimization process (perfect forecasts). This will provide a higher bound for the performance of the MPC method and isolate the differences attributable to different models from other influences.

5.4.1 Brute-force optimization

The setpoint profile obtained by MPC with GenOpt is shown in Figure 5.4. The two bars in the figure indicate the peak demand durations and the green dashed curves indicate the thermal comfort bounds. We can see that the optimal control strategy reduces the heating setpoint during unoccupied periods and ramps up the setpoint to the maximum allowed value before the on-peak periods so that the building is preheated before the critical periods. The preheating time in the early morning is around 4 hours, while it is 1 hour shorter in the afternoon. However, the rebound effect for the second peak period is more obvious due to the narrower thermal comfort band of occupied time in the evening. It can also be more cost-efficient to increase then decrease the setpoint seen by the optimization algorithm as discussed in Figure 5.3.

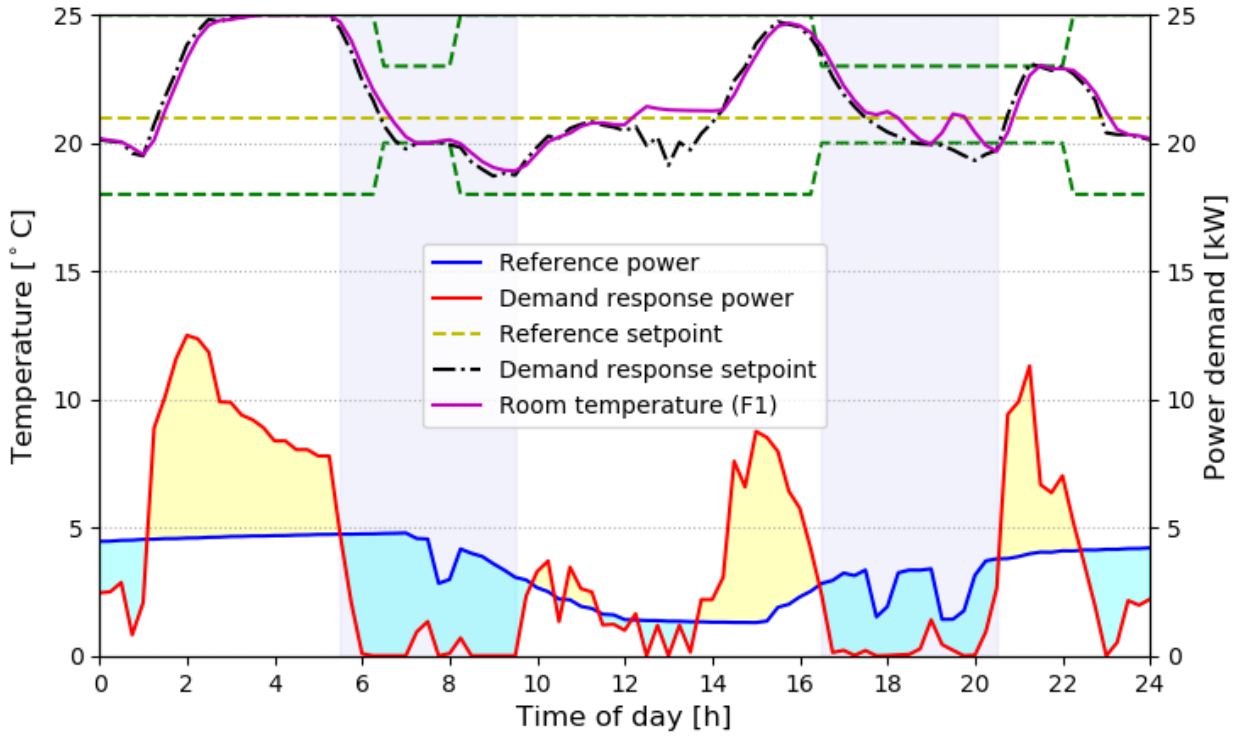

Figure 5.4: MPC results for two consecutive DR events

It is interesting to see that at around noon the building is left free-floating until it cools down to the lower setpoint limit, showing by the jagged profile. This period of the unsmooth signal may be due to a lack of feedback of the optimization scheme: when the setpoint drops at a faster rate than the building cools down naturally, there is no difference in the cost function until the setpoint reaches some constraints. Secondly, GenOpt algorithms are sensitive to numerical noise in the cost function and building simulation programs often result in noisy numerical results. The optimization process was also found to be sensitive to initial values discussed which will be discussed in section 5.4.3. The setpoint drifts below the thermal comfort limit at around 19:30 but the room temperatures are still within the comfort bound due to the internal thermal gains in the building. When the peak demand ends at 20:30, the setpoint ramps up to add more heat to the zones because the occupancy time lasts until 22:00.

This MPC result with two consecutive long peak periods and constricted occupancy proves that the preheating time does not need to be very long, in this case not longer than the peak duration. The evening peak period even requires less preheating time because the ambient temperature and solar radiation help to reduce the thermal losses when the building is being charged with heat.

The figure also shows that the power reduction during the two peak periods is very effective for the utility. The power demand during the peak hours remains zero for most of the time or close to zero if not. The rebound effect before or after the events is also quite pronounced.

Table 5.2 summarizes the flexibility metrics for this MPC approach. We can see that the delivered flexible energy is very impressive. The flexible efficiency is not very high with rebound energy higher than the flexible energy for both events. The maximum flexible power for both periods reaches the maximum potential.

Table 5.2: Flexibility results of MPC for two consecutive DR events

	Event 1 (morning)	**Event 2 (afternoon)**
Flexible energy [kWh]	15.1	9.5
Rebound energy [kWh]	21.0	18.2
Flexible efficiency [-]	0.72	0.52
Maximum flexible power [kW]	4.8	3.3

5.4.2 Heuristic optimization

The computing time of the Brute-force MPC method is fairly significant, with a 12-day simulation (with a 1-day optimization) taking more than 16 h of computing time on an i7-4770 CPU (3.5 GHz) – the same simulation with a constant setpoint profile takes about 20 seconds. Hence, several heuristic MPC approaches are explored to reduce the computation time. Heuristic MPC methods are conceived to limit the maximum power demand during the peak times and to decrease the computational requirements of the complex optimization process.

The heuristic methods are inspired from the papers by (Coffey et al., 2010; Lee & Braun, 2008a). The general idea is to reduce the number of optimization variables to save computation cost. For the three off-peak periods, a constant setpoint temperature for each period is assumed. For the on-peak periods, there are different numbers of variables depending on various methods.

Figure 5.5 illustrates the results for the “Jump” profile for optimal setpoints. In this case, higher constant temperatures are assumed for the three off-peak periods with two lower constant temperatures for the on-peak times. The setpoint jumps from a high value to a low value at the beginning of the peaks, showing by the black dot-dashed curve in Figure 5.5. In result, only 5 free parameters for the setpoint values need to be optimized, while the Brute-force MPC need to optimize 96 different variables for one-day optimization with a 15-minute timestep. Note that all the heuristic strategies respect the thermal comfort constraints presented previously.

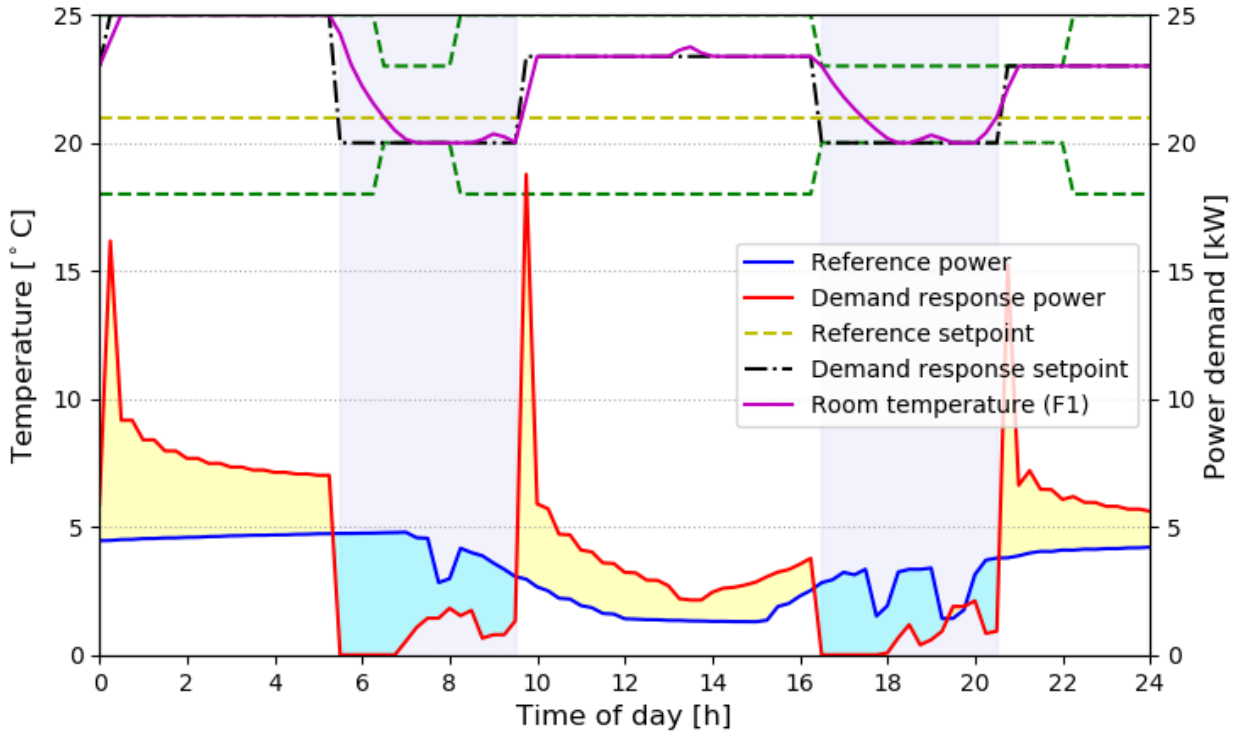

Figure 5.5: Heuristic MPC with an optimal Jump setpoint profile

We can see that the peak power reduction is quite effective for both peak durations from Figure 5.5. This method delivers similar power reduction capabilities as the Brute-force optimization with a much reduced computational time (20 minutes vs. 16 hours). The steep power increase after the peaks is as impressive, which is however expected since the setpoint is allowed to increase abruptly within one timestep after the peaks. Curtailment strategy can be implemented, for example, increasing the setpoint linearly within a period of time, if this after-peak power increase is of concern.

Instead of changing the setpoint within one timestep as with the case of Jump strategy, another method called “Linear” setpoint profile was examined, which allows the setpoint to drop linearly during each stretch of 4h peak period depicted by the dot-dashed curve in Figure 5.6. The peak power reduction is quite significant as well but less effective than the Jump method. On the other hand, the zone temperature is higher than the latter. Therefore, it can be considered as a less aggressive demand reduction strategy with better thermal comfort results.

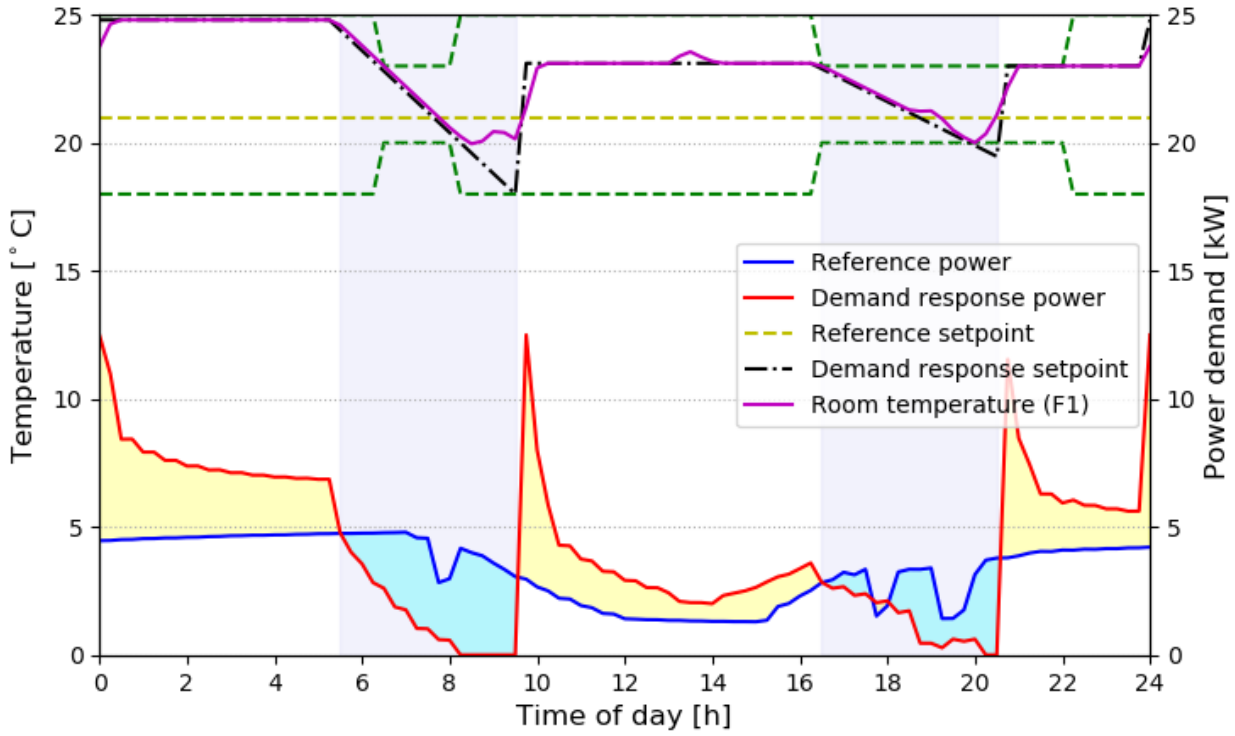

Figure 5.6: Heuristic MPC with an optimal Linear setpoint profile

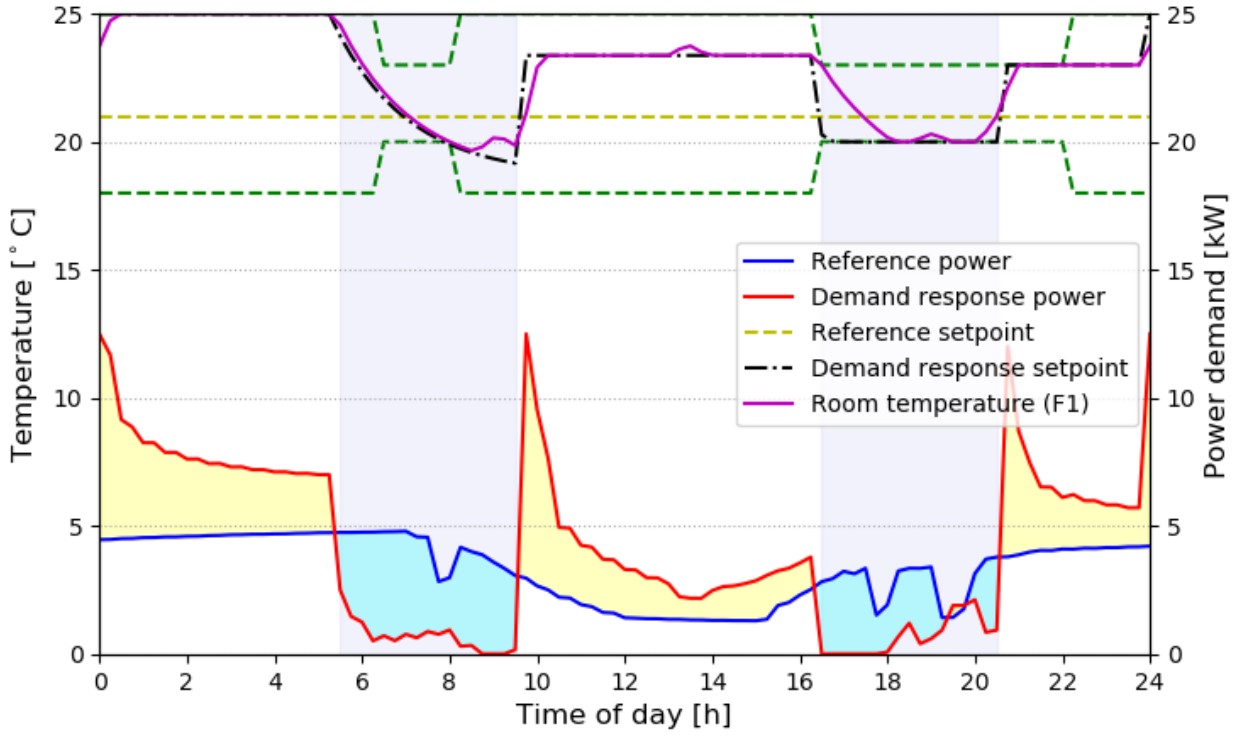

Figure 5.7: Heuristic MPC with an optimal Exponential setpoint profile

Figure 5.7 shows the results with “Exponential” setpoint profile which guides the setpoint to decrease exponentially during the peak times. The resulting shape of the two exponential drops is different because two different time constants are assumed for the two on-peak periods. The exponential profile delivers a similar power decrease capability as the Jump method.

The last heuristic method considered is to find the lowest power demand during the peak time. This may be interesting from the perspective of a utility company, which allows a given power usage to selected customers during peak events. The optimization strategy for this method is different from the other methods: it optimizes the maximum peak demand value instead of minimizing the overall power cost in the optimization horizon. Figure 5.8 illustrates the results of this approach. The average power usage during on-peak periods is slightly higher than that of the other optimization results, but the maximum power requested at any 15-min timestep by the building is the lowest of all, at 4 kW (vs. 5 to 8 kW for the other results).

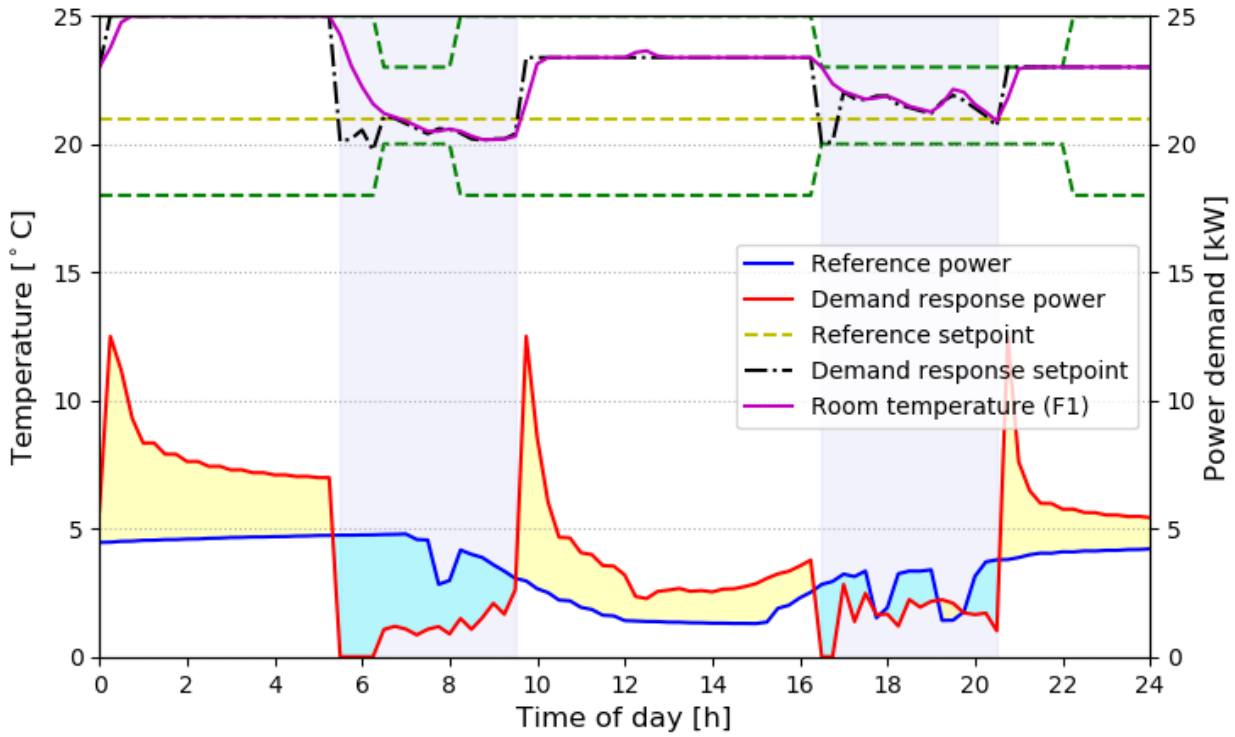

Figure 5.8: Heuristic MPC with Minimum Power at peak time

A night setback case is also tested, which can be considered as a heuristic optimization since building occupants often adopt this “manually optimal” strategy to save energy. In this case, the setback periods are chosen by trial and error so that the temperature can reach the thermal

comfort requirement just when the living room is occupied. This is often referred to as an "optimal start" scenario in the literature. The resulting setback setpoint profile shown in Figure 5.9 is very close to the case in reality, where the setpoint is set back between 7:45 and 16:00, and between 21:30 and 6:00. As we can see, it leads to a large increase in the heating power at the end of the 2 setback periods, resulting in a higher power demand at the beginning of the morning on-peak period. Since the setback period starts within the on-peak period, the overall performance is marginally worse than that of the constant setpoint scenario.

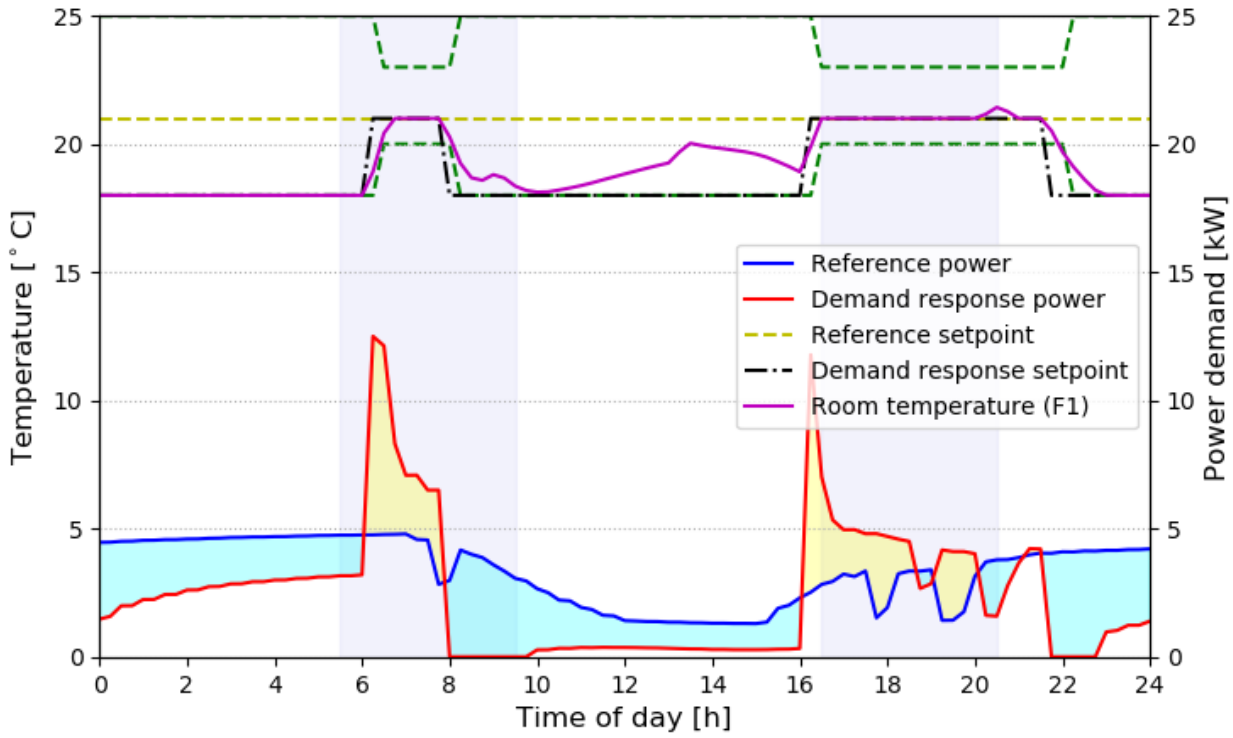

Figure 5.9: Night setback profile

The figures above show that the heating power profile during off-peak is affected by different strategies, with large peaks at the beginning of the preheating periods. These large peaks would also be present with conventional setbacks strategies, but not with a constant setpoint as shown by the reference case. The impact on overall system efficiency, capital or maintenance cost is probably negligible for electric baseboard heating, as considered in this study. However, this impact needs to be taken into account if other heating system types were considered, e.g. hydraulic heating with a boiler or heat pump.

Table 5.3 presents the peak power demand results from all the scenarios discussed in this chapter. The computation time is included in the Table given that it is an important factor for the MPC approach with detailed models. The indicative CPU Time is the time taken to run a 12-day simulation including the optimization process.

From the Table, we can see that the Exponential profile shows near-optimal results compared with the Brute-force MPC, while its computational time is much less. The Jump method also delivers very close power reduction to the exponential profile; the Linear method is less effective in terms of power demand reduction. The Minimum Power method requires the lowest maximum power demand during peak periods, which is just over 4kW. The Night Setback approach shows the highest maximum power demand, which is also part of the reason why the grid experiences peak demand.

Table 5.3: Power demand reduction and computation time

	Average Power Demand (peak) [kW]	**Max Power Demand (peak) [kW]**	**Indicative CPU Time[-]**
Constant	6.0	8.1	16 sec
Night Setback	6.6	15.9	19 sec
Brute-force MPC	2.6	5.6	16.3 h
Jump	3.0	4.9	18 min
Linear	3.6	7.7	25 min
Exponential	2.9	5.4	21 min
Minimum Power	3.5	4.2	6.7 h

Table 5.4 summarizes the energy flexibility characteristics of the Brute-force MPC and the heuristic approaches discussed above for the first or morning peak period. The Brute-force MPC method delivers the highest flexible energy and its rebound energy is also the largest. Similarly, the Exponential setpoint profile results in the closest amount of flexible energy as that of the Brute-force MPC and its flexible efficiency is the even higher than the latter. However, in terms of Maximum flexible power, the Exponential method is not as good as the Jump and Minimum Power methods, both of which deliver the same magnitude of power reduction as the Brute-force MPC.

Table 5.5 presents the flexible characteristics for the afternoon peak case. The overall results are similar to the morning peak case (Event 1), except that the Minimum Power method gives the lowest flexible energy and maximum flexible power.

Table 5.4: Summary of flexible results of MPC and heuristic approaches (morning peak)

	Flexible energy [kWh]	**Rebound energy [kWh]**	**Flexible efficiency [-]**	**Maximum flexible power P_{fmax} [kW]**
Brute-force MPC	15.1	21.0	0.72	4.8
Jump	13.1	17.2	0.76	4.8
Linear	11.4	17.2	0.67	4.2
Exponential	14.1	18.1	0.78	4.3
Minimum Power	11.9	16.5	0.72	4.8

Table 5.5: Summary of flexible results of MPC and heuristic approaches (afternoon peak)

	Flexible energy [kWh]	**Rebound energy [kWh]**	**Flexible efficiency [-]**	**Maximum flexible power P_{fmax} [kW]**
Brute-force MPC	9.5	18.2	0.52	3.3
Jump	8.3	20.8	0.40	3.3
Linear	6.0	18.4	0.32	3.8
Exponential	8.3	20.8	0.40	3.3
Minimum Power	4.2	18.7	0.22	2.9

5.4.3 Sensitivity of optimization

Different initial conditions of the Brute-force MPC approach were tested with the same algorithm Hybrid Generalized Pattern Search with Particle Swarm Optimization. The PSO algorithm always starts the global search using the initial values given by users; then a random number generator is used to uniformly spread the particles or sets of solutions. In the process, it is found that a set of well-initialized solution helps facilitate the optimization. Therefore, the optimal setpoint profiles from previous iterations were used for later optimizations until the cost function value was not further decreased.

If initial values are set to 21 °C for the whole day, the optimization process reaches a very different solution with large oscillations as shown in Figure 5.10. Even though the difference in cost function (power used during the on-peak periods) is only marginally affected, the solution is

clearly less desirable than the one obtained with “informed” initial values. The computational time is also affected (more than doubled).

Very large oscillations can be observed on setpoint temperatures and heating power. This can be partly explained by the fact that the exact value of the setpoint has no impact on the building behaviour once it is above the temperature that could be reached with full power or once it is below the temperature that would be reached in free-floating, without heating. So there is no impact on the cost function when GenOpt tries very different values of setpoint. To illustrate this phenomenon, consider the situation at 11 AM. GenOpt reduces the setpoint drastically, which results in no heating power being required. The building reaches a temperature close to 23.5 °C in free-floating, while the setpoint is at 20 °C. For that particular time step, the results and the cost function would be exactly the same for any setpoint below 22.5 °C. So the value of 20 °C is somewhat arbitrary and affected by numerical artifacts. One possible workaround to avoid such behaviour would be to impose an additional penalty on rapid changes in the setpoint.

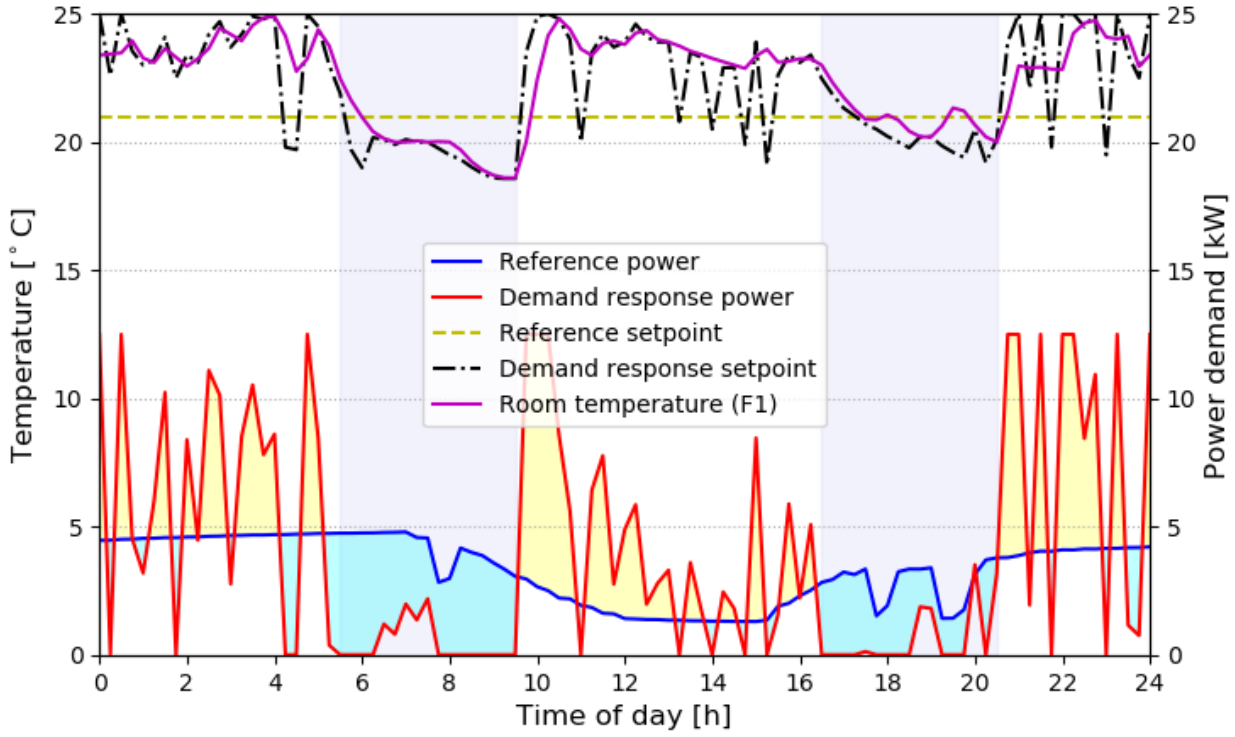

Figure 5.10: Brute-force MPC with poor initial values

5.5 Discussions

This chapter applied the MPC framework using detailed building models in BPS tools. This method is easy to use for building engineers and also convenient if building models are already available.

Two scenarios of DR events were discussed, i.e., a single event and two consecutive events within one day. It is found that the MPC method delivers higher flexible energy than the RBC method. The flexible efficiency of the MPC strategy is however not as high because the rebound effect is very pronounced; in other words, the preheating energy before the event (and rebound energy after if there is any) is larger than the flexible energy. The power demand reduction during the event is very effective, which reaches the maximum potential that is possible. It is also found that the preheating time is not longer than the peak duration. This indicates that the building has enough thermal storage capability to handle consecutive DR events as long as the interval between the two events is not shorter than the coming DR event.

The case study only optimized one day of the simulated period because this approach is rather computationally-intensive. To reduce computation time, different heuristic MPC strategies were studied, which restrict the possible setpoint profiles to predefined shapes. Heuristic methods were shown to deliver near-optimal performance in terms of flexible energy and maximum flexible power during on-peak periods, while significantly reduce the computation time (simulation time increased by a factor of 60 to 80 compared to the base MPC case). The flexible efficiency is also as promising even though there is an abrupt rebound power after the peaks.

A different set of electricity price signals was investigated instead of the time-of-use rates adopted in the last chapter. This proved that the cost function of the MPC framework can apply to different market contexts. A performance evaluation and comparison on a longer period can be possible as well.

Two main simplifications were made in this study in developing predictive control strategies. First, perfect forecasting was assumed for internal gains, occupancy and weather. Second, there is no model mismatch between the system and the controller. The obtained profiles are sensitive to optimization parameters (cost function and initial values) and to numerical noise. Further work needs to investigate the sensitivity of optimization methods and alternative implementations.

CHAPTER 6 MODEL PREDICTIVE CONTROL WITH SIMPLIFIED MODEL

This chapter applies the Model Predictive Control (MPC) method based on simplified building models presented in Chapter 4 to the case study building. Energy flexibility results are analyzed and compared with the rule-based control strategy and with the MPC method using the detailed controller model.

6.1 Introduction

6.1.1 Literature review

A building model in the literature can be categorized into three groups: white-box, grey-box, and black-box as discussed in Section 5.1.1. This section dedicates to the literature review on grey-box and black-box models.

The grey-box model describes a building using resistors and capacitors based on an electric analog of building Resistance and Capacitance (RC), hence it is also called the RC network model. A node of the network represents a space or a layer of wall/floor with a homogeneous temperature; the thermal mass of the space or construction is represented by a capacitor. Figure 6.1 shows examples of RC network representation of a wall (left), a house with radiators (middle) and with a floor heating system (right) (Masy, Georges, Verhelst, Lemort, & André, 2015). Chapter 1This type of model is the most widely applied in the literature by far.

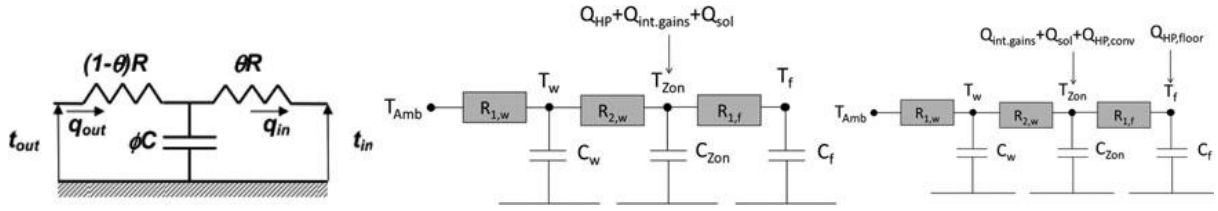

Figure 6.1: RC network representation of a building wall using different nodes

The RC network model is termed grey-box because the identified parameters such as the building resistance and capacitance could be physically interpreted. Research findings on electric RC networks can be transplanted to the building system too. For instance, the number of capacitors determines the order of the dynamic system, whose time constant can be analyzed for the

building system in a similar way. Observations and findings could be pursued, which may also be helpful for the controller design.

Candanedo et al., (2013) analyzed the capacitance ratio of the central zone and perimeter zone of an office building after the parameter identification of an RC model. It was observed that the central zone, due to larger capacitance, showed slower temperature variation than the perimeter zone. According to Madsen & Holst (1995), an RC model may or may not describe the long-term dynamics of a building, depending on the number of time constants of the corresponding RC network. They suggested using at least two time constants for a single-storey building because the physical building system is nonlinear, while the RC network approximates it using the linear system. To what extent an RC network represents well enough a building system was further investigated (Bacher & Madsen, 2011). Different scenarios of envelope, heater and sensor combinations were examined and discussed and the final selected model was composed of 1 node for each of the following components: the envelope, heater, internal space, and sensor.

Comparing with the white-box physical model, the grey-box model is much simpler. It requires much less computation power and can be easily implemented in the real-time control application. However, some researchers questioned the accuracy of the grey-box model and proposed some in-between models. In the study of Wang & Xu (2006), a model was created by combining functions based on thermodynamics laws with the grey-box model. Then the parameter identification technique was applied with operation data to obtain the model. Besides the dynamics of different thermal zones, the model also took into account the dynamics of internal mass and multilayer external walls and roof.

Unlike the grey-box model, the black-box model cannot necessarily be understood from the physical point of view. They are often pure mathematical models, deriving from data based on different machine learning algorithms, such as polynomial models (e.g. Autoregressive Moving Average (ARMA) models) and Artificial Neural Network (ANN).

Jiménez, Madsen, & Andersen (2008) presented a detail guidance on how to identify an ARMA with Exogenous terms (ARMAX) model for the building using the Matlab system identification toolbox. The relationship between the RC network and the polynomial models (or parametric models) were also explored. Huang, Chen, & Hu, (2014) developed an ANN model based on the model structure of nonlinear Autoregressive with Exogenous terms (ARX). A three-layer

Multilayer Perceptions was chosen and the Levenburg-Marquardt algorithm was used as the training algorithm to minimize the mean square errors between the predicted and measured data. In the study, an RC-network model was also created and compared; results showed that the ANN model gave slightly better predictions. A study showed that the ANN model could perform better even than the white-box model (Ruano, Crispim, Conceição, & Lúcio, 2006). However, choosing the correct orders or layers of the ANN model is challenging. The ANN model structure is complicated, which could result in a non-convex optimization problem that is difficult to solve. Dong & Lam (2014) examined the feasibility and applicability of the support vector machine (SVM) algorithm in building load forecasting. Results showed that coefficients of variance and the percentage errors of all prediction results are within 5%.

The advantage of the black-box model is their flexibility of model structure, compared with the grey-box model. Jiménez et al. (2008) showed that the RC network model is just one special type of the polynomial models. However, since the polynomial model is more flexible in its parameters and structure, the original physical meaning of the RC network model cannot be retained in the expansion of parameters and structure. As for other machine learning algorithms, the choices can be abundant, but each of them has its own limitations too.

Black-box and grey-box models are generally simpler than white-box models, so they are more widely applied for real-time control in practice. However, the former two types rely heavily on measurement data, which could remain an obstacle in reality. In the literature, one common approach is using the white-box model built in BPS programs to generate a synthetic database for system or parameter identification for the simplified models. This approach diminishes the potential problems existing in system identification using real measurements, such as sampling rates selection, satisfaction of excitation condition and data duration requirement etc. Moreover, the simplified models can also be validated with the white-box model (Ma, Qin, & Salsbury, 2014)

In a study by Ma, Qin, Salsbury, & Xu (2012), the Building Controls Virtual Test Bed environment was utilized to integrate EnergyPlus and Matlab. The input-output information of the EnergyPlus model was used to identify the ARX model in Matlab. This simplified model was used in the MPC to provide optimal cooling setpoints for a five-zone building (see Figure 6.2).

The study from Garnier, Eynard, Caussanel, & Grieu (2015) created a complex building model in EnergyPlus, and an ANN model was then identified based on the input-output data generated by EnergyPlus. The optimal network topology was identified with 18-24 hidden neurons using a dataset of 2 months.

Although different types of model exist, each of them has its own advantages and disadvantages as well as its field of applications. Finding the right model and tool to solve one's own problem is perhaps more critical than showing one model structure is better than the other. And conclusions drawn from one case study are very likely to be reversed under different conditions.

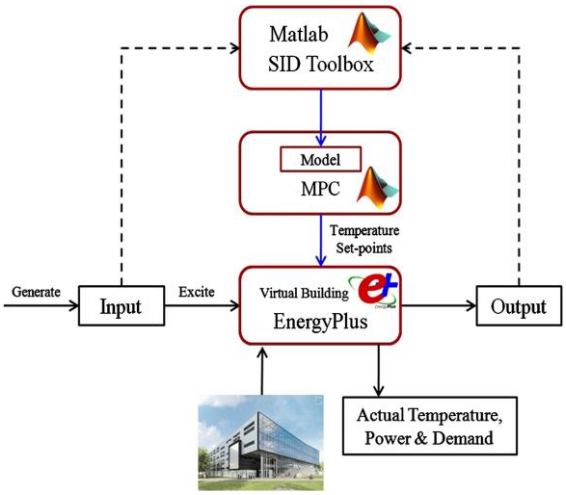

Figure 6.2: Co-simulation in BCVTB with Matlab and EnergyPlus (Ma. et al., 2012)

6.1.2 Objective

The aim of this chapter is to apply the MPC framework discussed in Chapter 4 to the case of the studied building: CCHT houses. A simplified model of the building system is first obtained through parameter identification technique. The identification data is generated from the calibrated detailed model presented in Chapter 2.

The simplified model is then employed as the controller model for the MPC method. The same online co-simulation structure is adopted using TRNSYS Type 155. The energy flexibility results are analyzed and compared with the rule-based control as well as with the MPC method with detailed modelling.

6.2 Methodology

6.2.1 Simplified model construction

As discussed in the literature review, there are quite many ways to build simplified models. In this work, we use the RC network to formulate our building model. More specifically, we use 1 resistance and 1 capacitance to represent 1 thermal zone. This choice of 1R1C to represent 1 thermal zone has been proved to be able to model the dynamics of the thermal zone (Bacher & Madsen, 2011). This approach results in lumped parameters for the resistances and capacitances. Based on those assumptions, we can draw a network of six resistances and three capacitances for the CCHT house as shown in Figure 6.3.

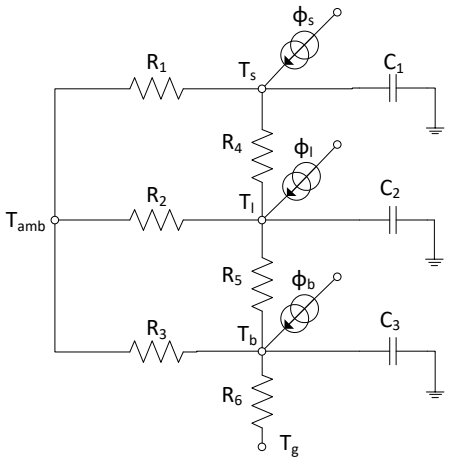

Figure 6.3: RC model schematic

There is a thermal resistance between every two nodes, and a resistance between nodes and the ambient and ground temperature respectively. The solar radiation injects heat directly into the thermal zones. For simplicity, ϕ_s, ϕ_l and ϕ_b in the figure denote the overall heat injected into the three zones (respectively sleeping room, living room and basement), including the heating power, internal heat gains and solar radiation.

Concretely, we can write the following state space equation to represent the system. The output equation is omitted because our concerned outputs are the same as the states. The input vector is separated into two vectors U and W. U is the controlled inputs while W is uncontrolled but measured inputs.

$$\dot{x} = A_c\, x + B_c U + E_c W \tag{6.1}$$

The vector $x = [T_s \quad T_l \quad T_b]^T$ denotes the state matrix of the system: temperatures of the sleeping room, living room and basement. $U = [U_s \quad U_l \quad U_b]^T$ denotes the heating powers in each zone, and $W = [\phi_{IG_s} \quad \phi_{IG_l} \quad \phi_{IG_b} \quad \phi_{sol} \quad T_{amb} \quad T_g]$ represents the disturbance inputs where ϕ_{IG_s}, ϕ_{IG_l} and ϕ_{IG_b} denote the internal gains to each zone; ϕ_{sol} denotes the incident solar radiation; T_{amb} denotes the ambient temperature and T_g the ground temperature. The triple (A_c, B_c, E_c) is obtained with only parameters to be identified as follows.

$$A_c = \begin{bmatrix} -(\frac{1}{R_4C_1} + \frac{1}{R_1C_1}) & \frac{1}{R_4C_1} & 0 \\ \frac{1}{R_4C_2} & -(\frac{1}{R_4C_2} + \frac{1}{R_2C_2} + \frac{1}{R_5C_2}) & \frac{1}{R_5C_2} \\ 0 & \frac{1}{R_5C_3} & -(\frac{1}{R_3C_3} + \frac{1}{R_5C_3} + \frac{1}{R_6C_3}) \end{bmatrix}$$

$$B_c = \begin{bmatrix} \frac{1}{C_1} & 0 & 0 \\ 0 & \frac{1}{C_2} & 0 \\ 0 & 0 & \frac{1}{C_3} \end{bmatrix} \quad E_c = \begin{bmatrix} \frac{1}{C_1} & 0 & 0 & \frac{\alpha_1}{C_1} & \frac{1}{R_1C_1} & 0 \\ 0 & \frac{1}{C_2} & 0 & \frac{\alpha_2}{C_2} & \frac{1}{R_2C_2} & 0 \\ 0 & 0 & \frac{1}{C_3} & \frac{\alpha_3}{C_3} & \frac{1}{R_3C_3} & \frac{1}{R_6C_3} \end{bmatrix}$$

Where α_1, α_2 and α_3 denote multiplication coefficients applied to the solar radiation for each thermal zone.

6.2.2 Parameter identification

When the symbolic model is ready, we then fit the model to input-output data to obtain the unknown parameters. The data can be from measurements, or from BPS simulation. The data from the latter approach is sometimes termed synthetic data. The benefit of using synthetic data is the availability of the information about the states, control inputs, disturbance inputs, and outputs. Some of those data may not be measured or measurable in real experiments. In our case, we obtain the data from the calibrated TRNSYS model. Note that the offline parameter estimation approach is employed in this chapter, unlike the online parameter identification method used in Chapter 4. This choice was made to improve the simplified model performance.

We discretize the state equation (6.1) for the purpose of parameter identification as well as for MPC. The discrete-time form of the state equation can be written as equation (6.2):

$$x(k+1) = Ax(k) + BU(k) + EW(k) \tag{6.2}$$

The triple $(A, B, E) \in R^{3\times3\times6}$ denotes the discretized form of (A_c, B_c, E_c). Based on the data, we estimate the parameter values that result in the minimal error between the predictions and true values by solving the following problem:

Given $x(k), U(k)$ and $W(k)$ for $k = 0,1, \dots, K \dots, N-1$, find the matrices A, B and E that minimize the error function J_E:

$$J_E = \sum_{k=0}^{N-1} [\hat{x}(k+1) - x(k+1)]^T [\hat{x}(k+1) - x(k+1)] \tag{6.3}$$

N denotes the number of training samples; the period of time selected for training is N/f_s hours, where f_s is the sampling frequency or timestep.

$\hat{x}(k)$ denotes the predicted model state at time k, which depends on the 12 parameters, namely $[R_1 \quad R_2 \quad R_3 \quad R_4 \quad R_5 \quad R_6 \quad C_1 \quad C_2 \quad C_3 \quad \alpha_1 \quad \alpha_2 \quad \alpha_3]$.

$$\hat{x}(k+1) = Ax(k) + BU(k) + EW(k) \quad \text{for} \quad k = 0,1, \dots, K \dots, N-1 \tag{6.4}$$

The training period for the identification process is 12 days with a 15-minute sampling frequency or $N = 1152$ samples for each variable. The GenOpt optimal setpoint profiles were used as one of the main inputs for the training data. The corresponding outputs, i.e., the zone temperatures are collected along with the disturbance inputs $W(k)$. This choice was made to ensure excitation in the input/output training data. Using randomly generated input signals is a common practice to ensure the excitation requirement. The large oscillation of setpoint temperatures from GenOpt optimization was proved to enable the parameter identification. Note that all of the states of the system are measurable due to the model structure; therefore there is no need to observe the states.

The predicted outputs are formulated based on current system states, the current control input, current disturbance inputs, and the unknown parameter matrices (A, B, E) based on Equation (6.4). The prediction error minimization problem with the objective function (6.3) is then solved using the "fmincon" function in Matlab Optimization Toolbox, yielding results for the matrices (A, B, E). The algorithm "interior-point" is employed from the options provided by the function. This algorithm was also selected for the "linprog" function as described in Chapter 3.

When the parameters were identified, the model was validated with a new set of data. The results are shown in Figure 6.4. We can observe that the one-step-ahead prediction is really close to the "measured" temperatures for each zone during this day. The RMSE between the measured outputs and the one-step-ahead predicted outputs of the three zones are 0.08, 0.4 and 0.5 °C respectively for the sleeping room, living room and basement. The 1-day ahead (96 steps ahead) prediction gives worse results than the 1-step ahead prediction; however the RMSE for the 1-day ahead predictions are acceptable, which are 0.7, 1.15 and 2.05 °C for the sleeping room, living room and basement separately.

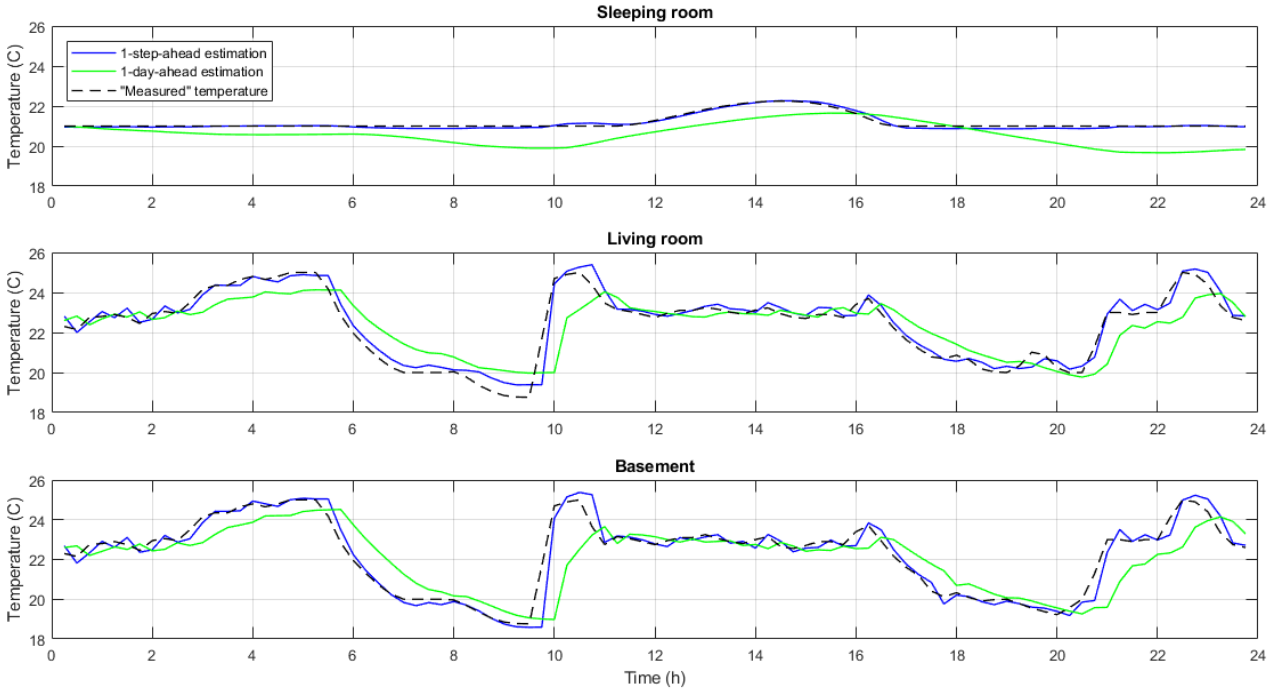

Figure 6.4: Validation results of the RC model

6.2.3 MPC formulation

The identified model is in discrete-time form, therefore the predicted states (or outputs) over the prediction horizon can be obtained intuitively as:

$$x(k+i+1|k) = Ax(k+i|k) + BU(k+i|k) + EW(k+i|k) \qquad (6.5)$$

In the equation, $i = 0, 1, \dots, K, \dots, P-1$, where P indicates the prediction horizon. The predicted information is then used to calculate the future controlling input (heating system in the building). The optimal control signal is obtained by solving an optimization problem. The objective of the

controller is to reduce power demand during the peak hours; thus we formulate the objective function as follows:

$$J(k) = \sum_{i=0}^{P-1} U^T(k+i|k)\, R(k+i)\, U(k+i|k) \tag{6.6}$$

$U(k+i|k)$ is the future controlling input vector corresponding to the time instant $k+i$ for $i = 0,1,\dots K,\dots P-1$, while $R(k+i)$ denotes a positive definite matrix representing the changing price signal. The cost function $J(k)$ is minimized given the current state $x(k)$ and the predicted disturbance $\{W(k), W(k+1),\dots W(k+P-1)\}$. The solution is the optimal input sequence $\{U(k|k), U(k+1|k),\dots, U(k+P-1|k)\}$, where only the first signal is applied in the feedback loop. Note that this objective function is formed as a quadratic function, instead of the linear form used in Chapter 4. The quadratic form shows better convergence performance in this case here.

The objective function is also subjected to constraints of the physical system, and without loss of generality, we can express the constraints as equations below:

$$\begin{cases} S(k+i)U(k+i|k) \le s(k+i) \\ G(k+i)x(k+i+1|k) \le g(k+i) \\ G_{eq}x(k+i+1|k) = g_{eq}(k+i) \end{cases} \tag{6.7}$$

The first inequality represents the constraints on inputs, for example, the minimum and maximum boundary of the heating capacity, while the second inequality represents the set of state constraints at each time instant $k+i+1$ for $i = 0,1,\dots K,\dots P-1$, i.e., the lower and upper temperature limits for thermal comfort. They are expressed as a function of time because they may change when the room is occupied or non-occupied. The last equation represents the equality constraint on zone temperatures which obeys the governing equation of the building system.

6.3 MPC results

Based on the MPC formulation discussed in the last section, the optimization problem was solved using the “fmincon” function in MATLAB, the same as used in parameter estimation in section 6.2.2. This function was selected because it delivers more robust results than the “linprog” used

in Chapter 4 for this case study. The “fmincon” function also provides more algorithm options and its objective function can be any form.

The algorithm “active-set” was chosen through trial and error for this problem, which delivered the best results. The algorithm is termed active set because it determines the active constraints which influence the final optimization results in each iteration. For instance, the equality constraints are always active until an iteration violates them. The algorithm can take large steps, which may however result in intermediate errors for some problems in the optimization process (Wong, 2011).

The prediction and control horizon are both set at 4 hours; tests show that longer horizons only improve the results slightly yet require much longer simulation time. A receding horizon is applied to the control process: the optimal setpoint from the controller is sent to TRNSYS, whose temperatures are fed back to the controller. This feedback loop is repeated at each time step.

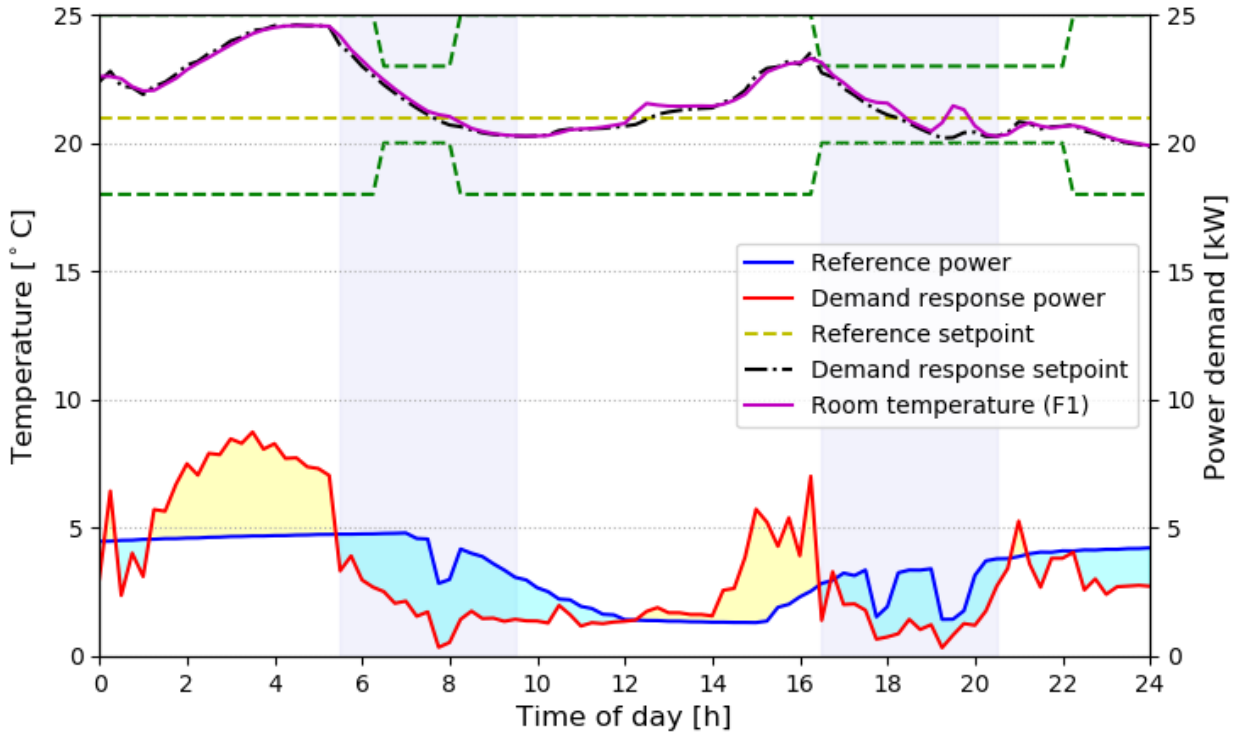

Figure 6.5: MPC with RC network model

Figure 6.5 shows the MPC results with the simplified controller model. The same occupancy constraints and peak durations are applied as in the Brute-force MPC with the detailed model discussed in section 5.4.1. A similar preheating phenomenon before the occurrences of peaks can

be observed in the Figure. The controller decides to preheat the building around 1 AM, several hours before the first peak starts. Preheating is employed again before the second on-peak period, although the maximum available power is not used.

The preheating effect is less significant than the Brute-force MPC with the detailed model as shown in Figure 5.4. The average power demand during on-peak periods, which is not as impressive as the Brute-force MPC either, results in about 4 kW. From the optimal setpoint profile, it is clear that the setpoint has the potential to further go down during the peak periods to yield higher flexible energy. Since the simplified controller model cannot give 100% accurate prediction, it is reasonable that the optimal setpoint change is less aggressive than the Brute-force MPC which has no modelling error.

A significant peak power reduction can still be observed for the MPC with the simplified model compared to the reference case. The computing time is very efficient, with the 12-day simulation taking about 20 seconds, which is the same magnitude as the reference scenario but substantially faster than the Brute-force MPC approach (20 s vs. 16.3 h).

6.4 Sensitivity analysis

As presented in Section 6.2, the RC network was employed to construct the simplified model structure and then parameter identification technique was used to obtain the model parameters. Another system identification approach called “ssest” is tried to get the simplified model. The advantage of this method is that it reduces the two-step approach of the RC model to one step.

This approach first estimates a state-space model using the subspace method. Both time-domain or frequency-domain input-output data can be utilized. The estimated parameters are then improved through minimizing the prediction error (Ljung, 1999). The general model structure is presented as follows:

$$\begin{cases} \dot{x}(t) = Ax(t) + Bu(t) + Ke(t) \\ y(t) = Cx(t) + e(t) \end{cases} \tag{6.8}$$

The state-space representation in equation (6.8) is typical, except that the last term $e(t)$ is additional. It denotes the error term or “disturbance”, a terminology commonly used in control system analysis. The function provides the option to set the K matrix to zero or to estimate this

parameter. In our case, the K matrix is not estimated since the input-output data is synthetic from the calibrated detailed model. The other important free parameter in this function is the order of the system. Results show that setting the order to 1 is sufficient to represent the controller model in our case. After the system identification, the state-space model is used in the same fashion as the RC model for the control and optimization process.

Figure 6.6 presents the MPC results with the estimated state-space model. We can see that this model delivers similar profiles as the RC network model that it preheats the building before the peaks and reduce setpoints during the peaks. Although the results are not as good as the RC network model (which can also be improved), fine-tuning the model can definitely improve the performance. This demonstrates that the optimal controller is not very sensitive to the modelling approach. Even if the model sometimes does not give accurate predictions, the feedback scheme allows the model to correct its errors promptly.

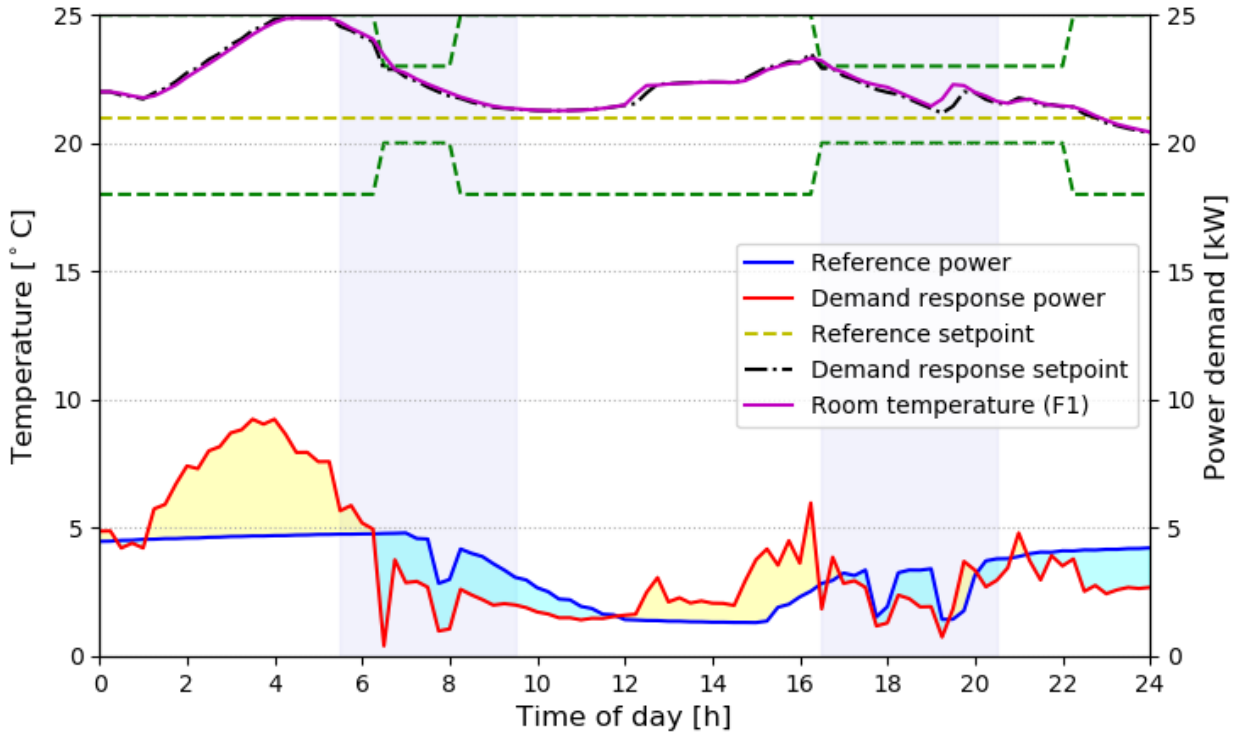

Figure 6.6: MPC results with state-space model

6.5 Comparison between MPC and RBC

Chapter 3 investigated the energy flexibility based on the Rule-Based Control, which modulates the setpoint by 2 °C in a period of 2 hours. It was intended to study the general scenario of the energy flexibility; peak durations were therefore not specified. To make a fair comparison, the same constraints for occupancy and peak times imposed on the MPC approach was implemented on the RBC method discussed in this section.

Figure 6.7 shows the results of one possible RBC strategy. The setpoint temperature remains at 21°C before the morning peak; it then decreases by 1 °C from 5:30 to 8:30. When the occupants leave the building, the setpoint reduces another 2 °C until the end of the morning peak. The setpoint change from 5:30 to 6:30 is 1 °C instead of 2 °C or 3 °C to the thermal comfort lower bound, because 2 °C setpoint change would result in power rebound larger than the reference power at 6:30, when the setpoint comes back to 20 °C required by the thermal comfort limit. This power rebound during the peak time is what we should avoid. For the afternoon peak, the setpoint drops only 1 °C for the whole duration, because that is what the thermal comfort constraints allow.

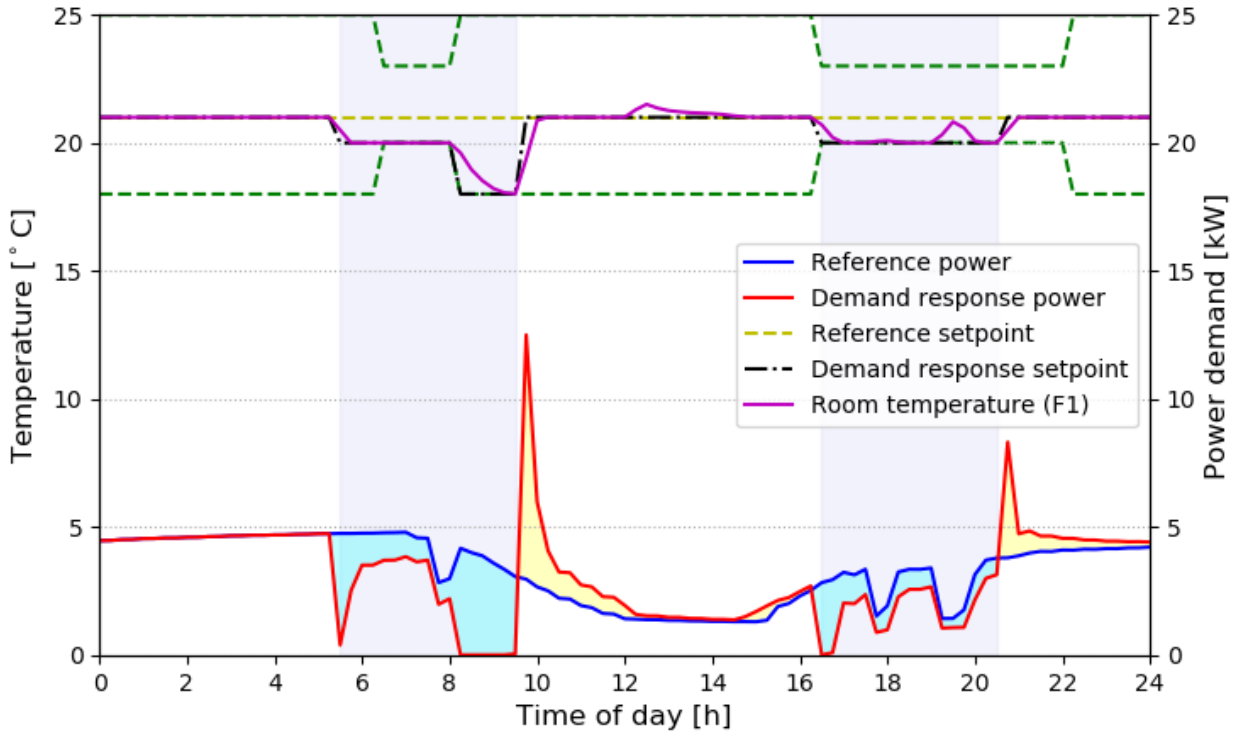

Figure 6.7: Rule-based control strategy with occupancy constraint

Table 6.1 summarizes the results of the two MPC approaches as well as the RBC strategy. Comparing the two MPC methods, the simplified model provides less flexible energy than the detailed model. Meanwhile, it has also less rebound energy. The resulting flexible efficiency with the simplified model is higher than with the detailed model, especially for the afternoon peak. The maximum flexible power of the simplified model is only slightly lower than the detailed model.

Table 6.1: Flexibility characteristics comparison between MPC and RBC

	Event 1 (morning)			**Event 2 (afternoon)**		
Modeling	MPC (detailed)	MPC (simplified)	RBC	MPC (detailed)	MPC (simplified)	RBC
Flexible energy [kWh]	15.1	9.1	7.3	9.5	5.4	3.7
Rebound energy [kWh]	21.0	11.7	4.7	18.2	6.8	2.6
Flexible efficiency [-]	0.72	0.78	1.55	0.52	0.79	1.4
Max flexible power [kW]	4.8	4.5	4.0	3.3	2.8	2.8

Comparing the MPC methods with RBC, it is clear that MPC provides higher flexible energy than RBC; this phenomenon is more obvious for the afternoon peak event. The MPC method with the detailed model has more than twice flexible energy than RBC for the morning peak event and more than three times flexible energy for the afternoon peak event. It should be noted that the RBC method has been refined by trial and error, so it represents a well-tuned conventional controller.

The MPC methods provide more flexible energy but their rebound effect is also more pronounced. The rebound energy in both MPC methods is larger than the flexible energy, resulting in flexible efficiency lower than 1. On the other hand, the RBC method has much lower rebound energy and its flexible efficiency is about 1.5 for both events, around twice as efficient as the MPC methods.

The maximum flexible power of MPC is higher than that of RBC, but the difference is not as significant as the flexible energy shows for the two strategies.

6.6 Discussions

In this chapter, the model predictive control framework presented in Chapter 3 was applied to a model of a real building, the same case study of a typical Canadian house employed in Chapter 5.

The MPC approach of this chapter differs from the last chapter in that a simplified model was used in the optimal controller instead of a detailed controller model. Data used for parameter identification and model validation of the simplified model were obtained from the detailed model.

The optimal controller was further co-simulated with the detailed building model in TRNSYS to emulate the online control scheme. Perfect forecasts were assumed for the weather and occupancy.

Energy flexibility of the MPC methods was discussed. It is found that both MPC methods deliver a significant flexible energy during the on-peak periods. The MPC with the detailed model delivers larger flexible energy at the cost of a very high computational effort, while the simplified model delivers less impressive performance but at a much more reasonable computational cost (its simulation time is the same magnitude as the reference case).

A rule-based control strategy was also investigated for the same day with the same occupancy and thermal comfort constraints. Results show that both MPC methods provide more flexible energy than the RBC method; however, their rebound effect is also more pronounced. The resulting RBC flexible efficiency is around twice of MPC. The MPC methods also deliver higher maximum flexible power than RBC, although the maximum flexible power difference is not as significant as that of flexible energy.

CHAPTER 7 CONCLUSION AND RECOMMENDATIONS

7.1 Summary

Buildings with their energy storage capability can be beneficial for the electric grid to balance its supply and demand. This capability allows buildings to operate in an energy-flexible way while preserving the indoor thermal comfort requirement. The aim of this research was to characterize the energy flexibility in buildings in a quantitative way and to assess the impact of supervisory control strategies on this flexibility through simulation studies.

A good model of the studied system is the basis of a valid simulation work; therefore, modelling composed an important part of this thesis. At first, a detailed physical model of the case study building was built using TRNSYS, a state-of-the-art dynamic building performance simulation tool. This model was further calibrated using monthly and hourly measured data from experiments of the real building. The calibration work included evaluation of both energy usage and indoor conditions. The indoor conditions calibration was not required according to the ASHRAE guideline 14 but was essential for our study because the calibrated model was further used for control study. Results in Chapter 2 showed that the calibrated model could capture the dynamic behaviour of the space heating and cooling system as well as satisfy the criteria for integrated energy.

This detailed model was further employed in three different ways.

First, it was used to examine a methodology to quantify the building energy flexibility. This general methodology was proposed with a set of Key Performance Indicators (KPIs) intended for a variety of systems, e.g. passive or active energy storage, different Heating, Ventilation and Air-Conditioning (HVAC) systems, on-site energy generation, and associated control strategies. Chapter 3 applied the methodology to assess the energy flexibility potential of building thermal mass based on simple setpoint modulation. It was shown that the energy flexibility provided by the thermal mass was significant: a median downward flexible energy at around 6 kWh and a median upward flexible energy at around 7.5 kWh for 2-h Demand Response (DR) events. The setpoint change in the DR events was 2 °C, which was assumed to be acceptable within the thermal comfort limit. A sensitivity analysis of the KPIs showed that the flexibility was subject to the weather condition, DR duration, setpoint change magnitude etc.

Second, the detailed building model was adopted to generate synthetic data for parameter identification of a simplified model, which was employed in a supervisory Model Predictive Control (MPC) framework. The general MPC framework, detailed in Chapter 4, explained an online co-simulation method from the perspective of building energy modellers. This method could be helpful for those modellers who are unfamiliar with but interested in MPC. Three common issues related to MPC application on buildings were discussed, which are respectively modelling errors, parameter identification and state estimation.

Last, the detailed building model was tested as the controller model of MPC. This approach optimized a set of variables from the detailed model, which required a large computation power. Several heuristic MPC methods were explored to reduce the computation cost. Results in Chapter 5 presented that the heuristic methods delivered near-optimal performance with much less computation time.

Since the control method has a high impact on the amount of the energy flexibility, the Rule-Based Control (RBC) strategy was compared with the MPC strategy. Comparison results in Chapter 6 showed that MPC delivered higher flexible energy and larger maximum flexible power than RBC, where MPC with the detailed model delivered the highest flexible energy, twice or three times of RBC depending on the hour of the DR event. MPC with the simplified model showed less flexible energy than that with the detailed model, but its computation time is in the same magnitude as the RBC method in seconds. On the other hand, the rebound effect of the MPC methods was more pronounced, resulting in lower flexible efficiency than RBC.

7.2 Conclusions

To conclude, buildings possess the high potential to provide energy flexibility services to the grid, even for typical Canadian residential buildings with a low thermal mass. In other words, buildings can become an asset in the grid system instead of being passive “customers”. The impact of control strategies on the available energy flexibility is significant. Predictive strategies have the potential to increase the flexibility but also present a risk of increasing the rebound effect, where “rebound” includes the period before a DR event. MPC is demonstrated as a good candidate for supervisory control to improve the energy flexibility. The proposed framework offers a method for building and HVAC scientists to pursue the application and analysis of MPC strategies.

The thesis includes the following contributions:

- A whole building performance model is calibrated using measured data. The calibrated model satisfies the criteria by ASHRAE guideline 14 in terms of monthly and hourly energy use. In addition, the model can capture the dynamics of the indoor temperature variations and the power demand of the HVAC system.
- A general methodology with performance indicators is investigated to characterize the energy flexibility of building systems. This methodology can be applied to different energy storage and generation systems, as well as to different levels of buildings from a cluster of buildings to district energy systems.
- An MPC framework is proposed for online supervisory control based on co-simulation. The framework offers a simple method for the MPC application on building simulations.
- The impact of control strategies on building energy flexibility is quantified and analysed. The proposed MPC method is compared with an RBC strategy. Advantages and disadvantages of both control strategies are analyzed.

7.3 Further studies

The general methodology proposed to quantify energy flexibility only applied to the building thermal mass in this work. Other energy storage systems such as hot water tank, ice water tank, and electrical storage systems can be examined with the same methodology. In addition, the integrated effect of different storage systems in one building can be investigated.

The methodology can also be applied to various HVAC systems and associated control strategies. Different HVAC systems produce different demand profiles, which may result in different flexibility characteristics. Other types of buildings (e.g. commercial, office, and institutional buildings), a cluster of buildings and district energy systems can also adopt the general methodology to quantify their energy flexibility potential.

The supervisory MPC framework proposed in this thesis can be extended to different levels of systems such as district energy systems. Experiments on the RBC and MPC methods can be carried out to investigate their applicability in the real world.

BIBLIOGRAPHY

Aggarwal, S., & Orvis, R. (2016). *Grid flexibility: methods for modernizing the power grid*. San Francisco, CA: Energy Innovation Policy & Technology LLC.

ASHRAE. (2014). *ASHRAE Guideline 14-2014 Measurement of Energy, Demand and Water Savings*. Atlanta, GA: American Society of Heating Refrigeration and Air-Conditioning Engineers, Inc.

ASHRAE. (2017). *ASHRAE Handbook: Fundamentals*. Atlanta, GA: American Society of Heating Refrigeration and Air-Conditioning Engineers, Inc.

Bacher, P., & Madsen, H. (2011). Identifying suitable models for the heat dynamics of buildings. *Energy and Buildings*, *43*(7), 1511–1522. https://doi.org/10.1016/j.enbuild.2011.02.005

Bemporad, A., Morari, M., & Ricker, N. L. (2015). *Model Predictive Control Toolbox User's Guide*. Natick, MA: The MathWorks, Inc.

Braun, J. E. (1990). Reducing Energy Costs and Peak Electrical Demand through Optimal Control of Building Thermal Storage. *ASHRAE Transactions*, *96*(2), 876–888.

Braun, J. E. (2003). Load Control Using Building Thermal Mass. *Transactions of the ASME*, *125*, 292–301. https://doi.org/10.1115/1.1592184

Braun, J. E., & Chaturvedi, N. (2002). An Inverse Gray-Box Model for Transient Building Load Prediction. *HVAC&R Research*, *8*(1), 73–99. https://doi.org/10.1080/10789669.2002.10391290

Braun, J. E., & Lee, K. (2006). Assessment of Demand Limiting Using Building Thermal Mass in Small Commercial Buildings. *ASHRAE Transactions*, *112*, 1–12.

California ISO. (2017). *Impacts of renewable energy on grid operations*. Folsom, CA: California Independent System Operator.

Camacho, E. F., & Bordons, C. (2007). *Model Predictive Control*. London: Springer-Verlag London Limited.

Candanedo, J. A., Dehkordi, V. R., Saberi-Derakhtenjani, A., & Athienitis, A. K. (2015). Near-optimal transition between temperature setpoints for peak load reduction in small buildings.

Energy and Buildings, *87*, 123–133. https://doi.org/10.1016/j.enbuild.2014.11.021

Candanedo, J., Dehkordi, V., & Lopez, P. (2013). A control-oriented simplified building modelling strategy. *Proceedings of BS2013: 13th Conference of International Building Performance Simulation Association, Chambery, France, Aug. 26-28*, 3682–3689.

Clarke, J., Strachan, P. A., & Pernot, C. (1993). An approach to the calibration of building energy simulation models. *ASHRAE Transactions*, *99*(2), 917–927.

Clauß, J., Finck, C., Vogler-finck, P., & Beagon, P. (2017). Control strategies for building energy systems to unlock demand side flexibility – A review. In *Proceedings of the 15th IBPSA Conference, San Francisco, CA, USA, Aug. 7-9, 2017* (pp. 611–620).

Coakley, D., Raftery, P., & Keane, M. (2014). A review of methods to match building energy simulation models to measured data. *Renewable and Sustainable Energy Reviews*, *37*, 123–141. https://doi.org/10.1016/j.rser.2014.05.007

Coakley, D., Raftery, P., & Molloy, P. (2012). Detailed Case Study of a Naturally Ventilated Building Using. In *First Building Simulation and Optimization Conference, Loughborough, UK, 10-11 September* (pp. 57–64).

Coffey, B. (2013). Approximating model predictive control with existing building simulation tools and offline optimization. *Journal of Building Performance Simulation*, *6*(3), 220–235. https://doi.org/10.1080/19401493.2012.737834

Coffey, B., Haghighat, F., Morofsky, E., & Kutrowski, E. (2010). A software framework for model predictive control with GenOpt. *Energy and Buildings*, *42*(7), 1084–1092. https://doi.org/10.1016/j.enbuild.2010.01.022

Corbin, C. D., Henze, G. P., & May-Ostendorp, P. (2013). A model predictive control optimization environment for real-time commercial building application. *Journal of Building Performance Simulation*, *6*(3), 159–174. https://doi.org/10.1080/19401493.2011.648343

Date, J., Athienitis, A. K., & Fournier, M. (2015). A Study of Temperature Set Point Strategies for Peak Power Reduction in Residential Buildings. *Energy Procedia*, *78*, 2130–2135. https://doi.org/10.1016/j.egypro.2015.11.289

Davito, B., Tai, H., & Uhlaner, R. (2010). *The smart grid and the promise of demand-side management*. San Francisco, CA: McKinsey & Company.

De Coninck, R., & Helsen, L. (2016). Quantification of flexibility in buildings by cost curves - Methodology and application. *Applied Energy*, *162*, 653–665. https://doi.org/10.1016/j.apenergy.2015.10.114

Denholm, P., O'Connell, M., Brinkman, G., & Jorgenson, J. (2015). *Overgeneration from Solar Energy in California: A Field Guide to the Duck Chart*. Golden, CO: National Renewable Energy Laboratory. https://doi.org/10.2172/1226167

Dong, B., & Lam, K. P. (2014). A real-time model predictive control for building heating and cooling systems based on the occupancy behavior pattern detection and local weather forecasting. *Building Simulation*, *7*(1), 89–106. https://doi.org/10.1007/s12273-013-0142-7

Fabrizio, E., & Monetti, V. (2015). Methodologies and advancements in the calibration of building energy models. *Energies*, *8*(4), 2548–2574. https://doi.org/10.3390/en8042548

Finck, C., Clauß, J., Vogler-Finck, P., Beagon, P., Zhang, K., & Kazmi, H. (2018). *Review of applied and tested control possibilities for energy flexibility in buildings Review of applied and tested control possibilities for energy flexibility in buildings*. https://doi.org/10.13140/RG.2.2.28740.73609

Fournier, M., Leduc, M.-A., & Sansregret, S. (2018). DSM with Line Voltage Communicating Thermostats : a Real Life Experiment Hydro-Québec. In *2018 Canmet Demand Response workshop* (pp. 1–18).

Fournier, M., & Leduc, M. (2014). Study of Electrical Heating Setpoint Modulation Strategies for Residential Demand Response. In *eSim 2014 Conference, Ottawa, Canada, May 7-10* (pp. 1–14).

Garnier, A., Eynard, J., Caussanel, M., & Grieu, S. (2015). Predictive control of multizone heating, ventilation and air-conditioning systems in non-residential buildings. *Applied Soft Computing Journal*, *37*, 847–862. https://doi.org/10.1016/j.asoc.2015.09.022

Henninger, R. H., & Witte, M. J. (2004). *EnergyPlus testing with ANSI/ASHRAE standard 140-2001 (BESTEST)*. Washington, D.C.: U.S. Department of Energy.

Henze, G. P. (2013). Model predictive control for buildings: a quantum leap? *Journal of Building Performance Simulation*, *6*(3), 157–158. https://doi.org/10.1080/19401493.2013.778519

Henze, G. P., Felsmann, C., & Knabe, G. (2004). Evaluation of optimal control for active and passive building thermal storage. *International Journal of Thermal Sciences*, *43*(2), 173–183. https://doi.org/10.1016/j.ijthermalsci.2003.06.001

Henze, G. P., Kalz, D. E., Simeng, L., Felsmann, C., Liu, S., & Felsmann, C. (2005). Experimental analysis of model-based predictive optimal control for active and passive building thermal storage inventory. *HVAC&R Research*, *11*(2), 189–213. https://doi.org/10.1080/10789669.2005.10391134

Huang, H., Chen, L., & Hu, E. (2014). Model Predictive Control for Energy-Efficient Buildings : An Airport Terminal Building Study. In *2014 11th IEEE International Conference on Control & Automation* (pp. 1025–1030).

Hydro-Quebec. (2013). Demystifying peak electricity demand. Retrieved August 17, 2018, from http://news.hydroquebec.com/en/news/119/demystifying-peak-electricity-demand/

Hydro One. (2003). *Electricity Demand in Ontario Submitted to the Ontario Energy Board regarding RP-2003-0144*. Toronto, ON: Hydro One Networks & Hydro One Brampton.

IEA EBC Annex 67. (2014). Energy Flexible Buildings. Retrieved from IEA EBC Annex 67 project www.iea-ebc.org/projects/ongoing-projects/ebc-annex-67/

IESO. (2016). Independent Electricity System Operator power data. Retrieved from http://www.ieso.ca/power-data

Jensen, S. Ø., Henrik, M., Lopes, R., Junker, R. G., Aelenei, D., Li, R., … Pasut, W. (2017). Annex 67: Energy Flexible Buildings - Energy Flexibility as a key asset in a smart building future. Retrieved from http://annex67.org/media/1470/position-paper-energy-flexibility-as-a-key-asset-i-a-smart-building-future.pdf

Jensen, S. Ø., Marszal-Pomianowska, A., Lollini, R., Pasut, W., Knotzer, A., Engelmann, P., … Reynders, G. (2017). IEA EBC Annex 67 Energy Flexible Buildings. *Energy and Buildings*, *155*, 25–34. https://doi.org/10.1016/j.enbuild.2017.08.044

Jiménez, M. J., Madsen, H., & Andersen, K. K. (2008). Identification of the main thermal

characteristics of building components using MATLAB. *Building and Environment*, *43*(2), 170–180. https://doi.org/10.1016/j.buildenv.2006.10.030

Johnson, N. (2017). *Building Energy Model Calibration for Retrofit Decision Making*. Portland State University. https://doi.org/10.15760/etd.3369

Kelly, G. E. (1988). Control system simulation in North America. *Energy and Buildings*, *10*(3), 193–202. https://doi.org/10.1016/0378-7788(88)90005-9

Kummert, M., Leduc, M., & Moreau, A. (2011). Using MPC to reduce the peak demand associated with electric heating. In *Model predictive control in buildings workshop, Montreal, Canada. June 24-25*.

Laurencelle, F., & Moreau, A. (2018). Impact of voluntary demand response actions taken by customers with a non-electric secondary heating system. In *2018 Canmet Demand Response workshop* (pp. 1–11).

Le Dréau, J., & Heiselberg, P. (2016). Energy flexibility of residential buildings using short term heat storage in the thermal mass. *Energy*, *111*(1), 1–5. https://doi.org/10.1016/j.energy.2016.05.076

Leduc, M.-A., Daoud, A., & Le Bel, C. (2011). Developing winter residential demand response strategies for electric space heating. In *Proceedings of Building Simulation 2011: 12th Conference of International Building Performance Simulation Association, Sydney, Nov. 14-16* (pp. 1111–1118).

Lee, K., & Braun, J. E. (2006a). An experimental evaluation of demand limiting using building thermal mass in a small commercial building. *ASHRAE Transactions*, *112 PART 1*, 559–571.

Lee, K., & Braun, J. E. (2006b). Development of Methods for Determining Demand-Limiting Setpoint Trajectories in Commercial Buildings Using Short-Term Data Analysis. In *Second National IBPSA-USA Conference, Cambridge, MA, Aug. 2-4* (pp. 99–106).

Lee, K., & Braun, J. E. (2006c). Evaluation of Methods for Determining Set-point Trajectories in Commercial Buildings Using Short-Term Data Analysis. In *SimBuild 2006 IBPSA-USA National Conference, Cambridge, MA, Aug. 2-4* (pp. 107–114).

Lee, K., & Braun, J. E. (2008a). Evaluation of methods for determining demand-limiting setpoint trajectories in buildings using short-term measurements. *Building and Environment*, *43*(10), 1769–1783. https://doi.org/10.1016/j.buildenv.2007.11.003

Lee, K., & Braun, J. E. (2008b). Model-based demand-limiting control of building thermal mass. *Building and Environment*, *43*(10), 1633–1646. https://doi.org/10.1016/j.buildenv.2007.10.009

Li, R., Dane, G., Finck, C., & Zeiler, W. (2017). Are building users prepared for energy flexible buildings?—A large-scale survey in the Netherlands. *Applied Energy*, *203*, 623–634. https://doi.org/10.1016/j.apenergy.2017.06.067

Ljung, L. (1999). *System Identification: Theory for the User*. Upper Saddle River, NJ: Prentice Hall PTR.

Ma, J., Qin, J., Salsbury, T., & Xu, P. (2012). Demand reduction in building energy systems based on economic model predictive control. *Chemical Engineering Science*, *67*(1), 92–100. https://doi.org/10.1016/j.ces.2011.07.052

Ma, J., Qin, S. J., & Salsbury, T. (2014). Application of economic MPC to the energy and demand minimization of a commercial building. *Journal of Process Control*, *24*(8), 1282–1291. https://doi.org/10.1016/j.jprocont.2014.06.011

Ma, Y., Borrelli, F., Hencey, B., Packard, A., & Bortoff, S. (2009). Model Predictive Control of Thermal Energy Storage in Building Cooling Systems. In *48th IEEE Conference on Decision and Control and 28th Chinese Control Conference, Shanghai, P.R.China, Dec. 16-18* (pp. 392–397).

Madsen, H., & Holst, J. (1995). Estimation of continuous-time models for the heat dynamics of a building. *Energy and Buildings*, *22*(1), 67–79. https://doi.org/10.1016/0378-7788(94)00904-X

Manning, M. M., Swinton, M. C., Szadkowski, F., Gusdorf, J., & Ruest, K. (2007). The Effects of thermostat setting on seasonal energy consumption at the CCHT Twin House Facility. *ASHRAE Transactions*, *113*(1), 1–12.

Masy, G., Georges, E., Verhelst, C., Lemort, V., & André, P. (2015). Smart grid energy flexible buildings through the use of heat pumps and building thermal mass as energy storage in the

Belgian context. *Science and Technology for the Built Environment*, *21*(6), 800–811. https://doi.org/10.1080/23744731.2015.1035590

May-Ostendorp, P., Henze, G. P., Corbin, C. D., Rajagopalan, B., & Felsmann, C. (2011). Model-predictive control of mixed-mode buildings with rule extraction. *Building and Environment*, *46*(2), 428–437. https://doi.org/10.1016/j.buildenv.2010.08.004

Morari, M., & Lee, J. H. (1999). Model predictive control: past, present and future. *Computers & Chemical Engineering*, *23*(4–5), 667–682. https://doi.org/10.1016/S0098-1354(98)00301-9

Nassif, N., Kajl, S., & Sabourin, R. (2005a). Optimization of HVAC Control System Strategy Using Two-Objective Genetic Algorithm. *HVAC&R Research*, *11*(3), 459–486. https://doi.org/10.1080/10789669.2005.10391148

Nassif, N., Kajl, S., & Sabourin, R. (2005b). Simplified Model-based Optimal Control of VAV Air-conditioning System. In *Ninth International IBPSA Conference, Montreal, Canada, Aug. 15-18* (pp. 823–830).

Natural Resources Canada. (2012). *2012 R-2000 Standard*. Ottawa, ON: Natural Resources Canada's Office of Energy Efficiency.

New Buildings Institute. (2018). The GridOptimal Initiative. Retrieved August 17, 2018, from https://newbuildings.org/wp-content/uploads/2018/01/NBI_USGBC_GridOptimalInitiative010918_PresentationSlides.pdf

Nocedal, J., & Wright, S. J. (2006). *Numerical Optimization*. NewYork, NY: Springer-Verlag London Limited. https://doi.org/10.1007/0-387-33477-7

Numerical Logics. (1999). *Canadian Weather for Energy Calculations, User's Manual and CD-ROM*. Downsview, Ontario: Environment Canada.

Palensky, P., & Dietrich, D. (2011). Demand side management: Demand response, intelligent energy systems, and smart loads. *IEEE Transactions on Industrial Informatics*, *7*(3), 381–388. https://doi.org/10.1109/TII.2011.2158841

Palomo, E., Marco, J., & Madsem, H. (1997). Method to compare measurements and simulations. In *Proceedings of the 5th International Conference of the International Building*

Performance Simulation Association, Prague, Czech Republic, September 8-10 (pp. 570–577).

Privara, S., Cigler, J., Vana, Z., Oldewurtel, F., Sagerschnig, C., & Zacekova, E. (2013). Building modeling as a crucial part for building predictive control. *Energy and Buildings*, *56*, 8–22. https://doi.org/10.1016/j.enbuild.2012.10.024

Prívara, S., Váňa, Z., Žáčeková, E., & Cigler, J. (2012). Building modeling: Selection of the most appropriate model for predictive control. *Energy and Buildings*, *55*, 341–350. https://doi.org/10.1016/j.enbuild.2012.08.040

Quintana, H. J., & Kummert, M. M. (2015). Optimized control strategies for solar district heating systems. *Journal of Building Performance Simulation*, *8*(2), 79–96. https://doi.org/10.1080/19401493.2013.876448

Raftery, P., Keane, M., & O'Donnell, J. (2011). Calibrating whole building energy models: An evidence-based methodology. *Energy and Buildings*, *43*(9), 2356–2364. https://doi.org/10.1016/j.enbuild.2011.05.020

Rawlings, J. B., & Mayne, D. Q. (2012). *Model Predictive Control : Theory and Design*. Madison, Wisconsin: Nob Hill Publishing, LLC.

Reddy, T. A. (2006). Literature review on calibration of building energy simulation programs: Uses, problems, procedures, uncertainty, and tools. *ASHRAE Transactions*, *112*(1), 226–240. https://doi.org/Article

Reddy, T. A., Maor, I. H., & Panjapornpon, C. (2007a). Calibrating detailed building energy simulation programs with measured data - Part II: Application to three case study office buildings (RP-1051). *HVAC and R Research*, *13*(2), 243–265.

Reddy, T. A., Maor, I., & Panjapornpon, C. (2007b). Calibrating detailed building energy simulation programs with measured data - Part I: General methodology (RP-1051). *HVAC and R Research*, *13*(2), 221–241. https://doi.org/Article

Reynders, G., Diriken, J., & Saelens, D. (2015). A generic quantification method for the active demand response potential of structural storage in buildings. In *14th International Conference of the International Building Performance Simulation Association (IBPSA), Hyderabad, India, Dec. 7-9, 2015* (pp. 1986–1993).

Reynders, G., Diriken, J., & Saelens, D. (2017). Generic characterization method for energy flexibility: Applied to structural thermal storage in residential buildings. *Applied Energy*, *198*, 192–202. https://doi.org/10.1016/j.apenergy.2017.04.061

Rossiter, J. A. (2003). *Model-Based Predictive Control: A Practical Approach*. Boca Raton, Florida: CRC Press.

Royapoor, M., & Roskilly, T. (2015). Building model calibration using energy and environmental data. *Energy and Buildings*, *94*, 109–120. https://doi.org/10.1016/j.enbuild.2015.02.050

Ruano, A. E., Crispim, E. M., Conceição, E. Z. E., & Lúcio, M. M. J. R. (2006). Prediction of building's temperature using neural networks models. *Energy and Buildings*, *38*(6), 682–694. https://doi.org/10.1016/j.enbuild.2005.09.007

Schwarz, H., & Cai, X. (2017). Integration of renewable energies, flexible loads and storages into the German power grid: Actual situation in German change of power system. *Frontiers in Energy*, *11*(2), 107–118. https://doi.org/10.1007/s11708-017-0470-x

Seem, J. E. (1987). *Modeling of heat transfer in buildings*. University of Wisconsin-Madison.

Seem, J. E., Klein, S. A., Beckman, W. A., & Mitchell, J. W. (1989). Transfer Functions for Efficient Calculation of Multidimensional Transient Heat Transfer. *Journal of Heat Transfer*, *111*(5), 5–12. https://doi.org/10.1115/1.3250659

Sourbron, M., Verhelst, C., & Helsen, L. (2012). Building models for model predictive control of office buildings with concrete core activation. *Journal of Building Performance Simulation*, (October 2014), 1–24. https://doi.org/10.1080/19401493.2012.680497

Sun, J., & Reddy, T. A. (2006). Calibration of Building Energy Simulation Programs Using the Analytic Optimization Approach. *HVAC&R Research*, *12*(1).

Swinton, M. C., Moussa, H., & Marchand, R. G. (2001). Commissioning twin houses for assessing the performance of energy conserving technologies. In *Proceedings of Performance of Exterior Envelopes of Whole Buildings VIII: Integration of Building Envelopes, Clearwater Beach, Florida. Dec. 2-7* (pp. 925–931). Clearwater Beach, FL, USA. https://doi.org/10.1016/j.enbuld.2004.03.004

Thermal Energy System Specialists LLC. (2018). TRNSYS. Retrieved August 28, 2018, from

http://www.trnsys.com/

Thornton, J. W., Bradley, D. E., McDowell, T. P., Blair, N. J., Duffy, M. J., LaHam, N. D., & Naik, A. V. (2018). *TESS Basement Model Input File*. TRNSYS manual.

Ulbig, A., Borsche, T. S., & Andersson, G. (2014). Impact of low rotational inertia on power system stability and operation. *IFAC Proceedings Volumes (IFAC-PapersOnline)*, *19*, 7290–7297. https://doi.org/10.3182/20140824-6-ZA-1003.02615

Venmar. (2018). Vermar AVS 1.8 HE specification. Retrieved from https://www.venmar.ca/DATA/DOCUMENT/46_3_en~v~specification-sheet.pdf

Vito NV. (2018). *Developing a smart readiness indicator for buildings*. Boeretang: European Commission DG Energy.

Walker, I. S., & Wilson, D. J. (1998). Field validation of algebraic equations for stack and wind driven air infiltration calculations. *ASHRAE Transactions*, *104*(2), 118. https://doi.org/10.1080/10789669.1998.10391395

Wang, S., & Jin, X. (2000). Model-based optimal control of VAV air-conditioning system using genetic algorithm. *Building and Environment*, *35*(6), 471–487. https://doi.org/10.1016/S0360-1323(99)00032-3

Wang, S., & Xu, X. (2006). Simplified building model for transient thermal performance estimation using GA-based parameter identification. *International Journal of Thermal Sciences*, *45*(4), 419–432. https://doi.org/10.1016/j.ijthermalsci.2005.06.009

Wetter, M. (2001). GenOpt - A Generic Optimization Program. In *Proceedings of IBPSA's Building Simulation 2001 Conference, Rio de Janeiro, August 13-15* (pp. 601–608).

Wetter, M. (2011). Co-simulation of building energy and control systems with the building controls virtual test bed. *Journal of Building Performance Simulation*, *4*(3), 185–203. https://doi.org/10.1080/19401493.2010.518631

WhiteBox Technologies. (2018). WhiteBox Technologies. Retrieved from http://weather.whiteboxtechnologies.com/

Wong, E. (2011). *Active-set methods for quadratic programming*. University of California, San Diego.

Wu, Y., & Duan, G. (2004). Reduced-order Observer Design for Matrix Second-order Linear Systems. In *Proceedings of the 5th World Congress on Intelligent Control and Automation, Hangzhou, P.R.China, June 15-19* (pp. 28–31).

Yin, R., Kara, E. C., Li, Y., DeForest, N., Wang, K., Yong, T., & Stadler, M. (2016). Quantifying flexibility of commercial and residential loads for demand response using setpoint changes. *Applied Energy*, *177*, 149–164. https://doi.org/10.1016/j.apenergy.2016.05.090

Žáčeková, E., Váňa, Z., & Cigler, J. (2014). Towards the real-life implementation of MPC for an office building: Identification issues. *Applied Energy*, *135*, 53–62. https://doi.org/10.1016/j.apenergy.2014.08.004

Zirnhelt, H. E. (2013). *Using Calibrated Simulation to Quantify the Energy Savings From Residential Passive Solar Design in Canada*. Ryerson University, Toronto, ON, Canada.

APPENDIX A

A.1 State equation solutions

The state-space model can be easily discretized and solved in Matlab; however, when the sampling rate is too big, it can result in errors. To eliminate the discrepancies between Matlab and TRNSYS, it is necessary to use the same approach as TRNSYS to solve differential equations in Matlab.

Unlike Matlab, TRNSYS takes the exact solution of discrete differential equations for internal iteration while outputs the average value during each time step to perform better energy balance. Therefore, we need to hard-code the instantaneous and average solutions of state-space models in Matlab, so that we can achieve a true model match. In general, the discrete state equation solution, in our case, the discrete instantaneous solution $T(t)$ can be written as follows

$$T(t) = A_d T(t-1) + B_d u(t-1)$$

With $A_d = e^{A_c \Delta t}$, $B_d = {A_c}^{-1}(e^{A_c \Delta t} - I_n)B_c$. Note that the parameters A_c, B_c are matrices; I_n is the same size as A_c.

By using the definition of average values over one time step period, we can derive the average solution $\bar{T}(t)$ as

$$\bar{T}(t) = A_{da} T(t-1) + B_{da} u(t-1)$$

With $A_{da} = (A_c \Delta t)^{-1}(e^{A_c \Delta t} - I_n)$, $B_{da} = (A_c \Delta t)^{-1} {A_c}^{-1}(e^{A_c \Delta t} - I_n)B_c - {A_c}^{-1} B_c$.

By outputting the average solution of the state equation while iterating using instantaneous solution, we can get exactly identical results in Matlab as TRNSYS.

A.2 Predictive output formulation

The general discrete-time state-space equations for linear systems can be written as:

$$\begin{cases} x(k+1) = Ax(k) + Bu(k) \\ y(k) = Cx(k) \end{cases}$$

Suppose the control horizon is N_c; then the future control input U at time k is

$$U[N_c \times 1] = [u(k+1|k) \quad u(k+2|k) \quad u(k+3|k) \quad \dots \quad u(k+N_c-1|k)]^T;$$

Suppose the prediction horizon is N_p ($N_p \geq N_c$); then the output prediction Y at time k is

$$Y[N_p \times 1] = [y(k+1|k) \quad y(k+2|k) \quad y(k+3|k) \quad \dots \quad y(k+N_p-1|k)]^T.$$

We then formulate each one-step-ahead output based on the state equation as follows until the prediction horizon.

$$y(k+1|k) = Cx(k+1|k) = CAx(k) + CBu(k)$$

$$x(k+2|k) = Ax(k+1|k) + Bu(k+1|k) = A[Ax(k) + Bu(k)] + Bu(k+1|k)$$
$$= A^2x(k) + ABu(k) + Bu(k+1|k)$$

$$y(k+2|k) = Cx(k+2|k) = CA^2x(k) + CABu(k) + CBu((k+1|k)$$

... ...

$$x(k+N_p|k) = A^{N_p}x(k) + A^{N_p-1}Bu(k) + \cdots + A^{N_p-N_c}Bu(k+N_c-1|k)$$

$$y(k+N_p|k) = CA^{N_p}x(k) + CA^{N_p-1}Bu(k) + CA^{N_p-2}Bu(k) + \cdots + CA^{N_p-N_c}Bu(k+N_c-1|k)$$

Let

$$F[N_p \times 1] = [CA \quad CA^2 \quad CA^3 \quad \dots \quad CA^{N_p}]^T$$

and

$$\Phi[N_p \times N_c] = \begin{bmatrix} CB & 0 & 0 & \dots & 0 \\ CAB & CB & 0 & \dots & 0 \\ CA^2B & CAB & CB & \dots & 0 \\ \dots & \dots & \dots & \dots & \dots \\ CA^{N_p-1}B & CA^{N_p-2}B & CA^{N_p-2}B & \dots & CA^{N_p-N_c}B \end{bmatrix}$$

Then we have

$$Y = Fx(k) + \Phi U$$

A.3 Least squares estimation

The parameterized regression model, in general, can be written as $y(t) = \Phi(t-1)\theta$. We let $e(t,\theta) = y(t) - \Phi(t-1)\theta$ and set the objective function as

$$J(t,\theta) = \frac{1}{2}\sum_{t=1}^{N} e(t,\theta)^2$$

The minimal result can be found when the first derivative of the objective function equals 0.

$$\frac{\partial J(t,\theta)}{\partial \theta} = -\Phi(t-1)\sum_{t=1}^{N} e(t,\theta) = 0$$

$$\Phi(t-1)\sum_{t=1}^{N}[y(t) - \Phi(t-1)\theta] = 0$$

$$\sum_{t=1}^{N}\Phi(t-1)y(t) = \theta\sum_{t=1}^{N}\Phi(t-1)^T\Phi(t-1)$$

We can notice that the left-hand side of the equation is the summation of cross-correlation between the inputs and outputs and the right-hand side is the summation of the auto-correlation of the inputs.

Let $S(t) = \sum_{t=1}^{N}\Phi(t-1)y(t)$ and $R(t) = \sum_{t=1}^{N}\Phi(t-1)^T\Phi(t-1)$, then

$$\theta = R(t)^{-1}S(t)$$

Note that the term ${\Phi_{N-1}}^T\Phi_{N-1}$ should be nonsingular for the convergence of this method.